INVERSE SCATTERING AND TOMOGRAPHY, DELAY DIFFERENTIAL EQUATIONS IN CYBER-PHYSICAL SYSTEMS

by

Siamak RabieniaHaratbar

A Dissertation

Submitted to the Faculty of Purdue University

In Partial Fulfillment of the Requirements for the Degree of

Doctor of Philosophy

Department of Mathematics

West Lafayette, Indiana

May 2020

THE PURDUE UNIVERSITY GRADUATE SCHOOL
STATEMENT OF COMMITTEE APPROVAL

Prof. Plamen D Stefanov, Chair

Department of Mathematics

Prof. Shirley J Dyke

Mechanical Engineering and Civil Engineering

Prof. Antonio Sa Barreto

Department of Mathematics

Prof. Kiril Datchev

Department of Mathematics

Approved by:

Prof. Plamen D Stefanov

Associate Head for Graduate Studies, Department of Mathematics

To my mom Zarbanou, My dad Rouhollah

My sisters Samaneh and Sanaz

My fiancé Natalie.

ACKNOWLEDGMENTS

I would like to express my heartfelt appreciation to my advisor Plamen Stefanov for his support, patience, and guidance throughout my doctoral program. It has been an honor learning from him during my Ph.D. study at Purdue.

I would like to thank my thesis defense committee, Shirley J Dyke, Antonio Sa Barreto, Kiril Datchev, and Plamen Stefanov for their insightful comments during my defense and their important remarks about my dissertation.

During my Ph.D. I had the opportunity to attend to different conferences thanks to the financial support of different people and institutions. I would like to express my deep gratitude especially to Gunther Uhlmann, Todd Quinto, and my advisor Plamen Stefanov.

I am in debt with Dean Hamid Rassoul for his support at Florida Institute of Technology. I want to express my gratitude to my former advisors Mahmoud Hesaaraki and Farhad Khellat for introducing me to the field of Partial Differential Equations and Inverse Problems during my graduate and undergraduate studies at Sharif University of Technology and Shahid Beheshti University.

Last but not certainly the least, I would like to express my sincerest gratitudes to my family and fiancé; my friends. Those who believed in me and supported me by their love during my academic endeavor.

TABLE OF CONTENTS

LIST OF TABLES

LIST OF FIGURES

LIST OF ABBREVIATIONS

tr	Trace
Vol	Volume
grad	Gradient
supp	Support
Ker	Kernel
Coker	Co-Kernel
WF	Wave Front Set
WFA	Analytic Wave Front Set
curl	Curl
codim	Co-dimension
Arg	Argument
neigh	neighborhood
ext	Exterior
const	Constant

ABSTRACT

This dissertation concludes three mathematical works in Inverse Problems as well as an engineering work in Cyber-Physical Systems. Our mathematical works are in the area of Inverse Problems and Scattering Theory where the main focuses are on Support theorem of Vectorial Light-ray transform in Minkowski Spaces, Dynamical X-ray Tomography, and Inverse Scattering of the biharmonic operator.

For the first project, we prove a support theorem for vector fields whose integral lines vanish on an open set of light-like lines. In this work, we employ the method of microlocal analysis and Pseudo Differential Operators. We illustrate the application of our results for the inverse recovery of the hyperbolic Dirichlet-to-Neumann map through various examples.

The second project is motivated by an inverse problem arising from medical imaging where we investigate a dynamic operator, $\mathscr{A}$, integrating over a family of level curves when the object changes between the measurements. Microlocal analysis is used to determine which singularities can be recovered by the data-set. We prove that not all singularities can be recovered, depending on the particular movement of the object compare to the X-ray source. We then find sufficient conditions under which the reconstruction is possible. We also show that one can establish stability estimates and injectivity results under the Visibility, the Local and Semi-global Bolker conditions. We illustrate the implementation of our results in Fan-beam geometry.

In the final project, we consider a perturbed biharmonic operator and study the inverse scattering problem for this operator by investigating the recovery process of the magnetic field $\mathbf{A}$ and the potential field V. Using the high-frequency asymptotic of the scattering amplitude of the biharmonic operator, we prove the unique recovery of **curl A** and $V - \frac{1}{2}\nabla \cdot \mathbf{A}$. By investigating the near-field scattering, we show that the high-frequency asymptotic expansion up to an error $\mathscr{O}(\lambda^{-4})$ (where λ is the frequency or the spectral parameter) recovers the same above quantities but does not provide any additional information about the magnetic and the potential fields. We also establish stability estimates for **curl A** and $V - \frac{1}{2}\nabla \cdot \mathbf{A}$.

Our engineering work is in the area of Cyber-Physical systems where we study Real-time hybrid simulation (RTHS). By the use of RTHS, which is an efficient technique that investigate cyber-physical system in a cost-effective way, we introduce powerful indicators to examine the structural behavior and seismic resilience of a structure through various settings.

INTRODUCTION

1.1 Inverse Problems

In mathematics and statistics, given a complete set of observation associated with a physical model, one can utilize the existing theories to make predication on the outcome of system. The process of predicting the system's output from the given input is called *Forward* or *Direct Problem*. If "x" and "y" denote the input and output of a physical model, respectively, the mathematical interpretation of the forward problem is to estimate the output $y = F(x)$ given the input x. In contrast, the *Inverse Problem* is the problem of predicating the system's input x while the output of the system y is given. To be more precise, to define an inverse problem one needs to fully understand the forward operator F which maps objects of interest, parameters which provide information about objects of interest, and data or measurements. The objective of the inverse problem is to estimate the input x that cannot be obtained using direct measurements for various reasons due to the loss of data in an experiment or due the fact that the data is never being measured precisely in the first place. The below schematic diagram shows the relation between a forward and an inverse problem. Many real-world applications are in fact Inverse problems, for instance Computed Tomography (CT), source reconstruction using acoustic waves, or estimating the Earth's internal structures from travel-time of seismic waves.

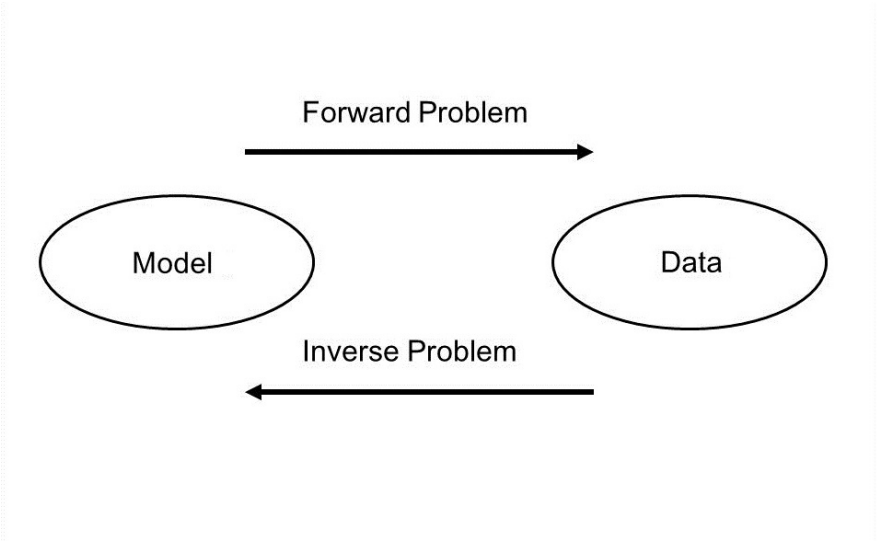

Figure 1.1. Forward and Inverse Problems.

The main goal of the theory of inverse problem is to study the forward operator and infer the values of the parameters which characterize the physical model by extracting all possible information from the available measurements. In this regard, the following features are of practical importance in the study of inverse problems:

(I) Uniqueness: What information about the object x can we recover?
Under what circumstances one can uniquely determine the model's unknown parameters utilizing the known measurements (data)?

(II) Stability: How do errors in the available measurements translate into reconstructions errors? What are the methods to quantify and characterize reconstruction errors?

(III) Inversion: What are the reconstruction methods? Is there any explicit way to formulate the inverse operator?

(IV) Partial Data: Can we still reconstruct the object in the Region-of-Interest (ROI) if the data-set is incomplete?

All above questions have pratical applications. Uniqueness and inversion can be considered as the theoretical aspect of inverse problem theory which provides meaningful insights regarding a specific problem. On the other hand, question of stability and reconstruction will have practical applications, for example, in medical imaging to investigate features of interest (like singularities). In some applications, there are no uniqueness results as one may modify the parameters of interest by considering any arbitrary diffeomorphism while the measured data will remain the same. Thus, stability plays a crucial role in reconstruction due to available errors in the measurements. In Electrical Impedance Tomography (EIT) problems, for example, one can only be hope for to reconstruct the object x up to a *gauge transform*. In another instance, real-world CT scans are done only within the ROI which means only radiating a part of body (like the heart) instead of the whole body. In this type of problems, it has been shown that the measurements within the ROI is not sufficient for the reconstruction process, (Stefanov-Uhlmann). However, one practical way to reconstruct the object within the ROI, is to recover the singularities of the object. In this regard, microlocal analysis is a very well-suited method that can be used to study above questions, in particular the stability. Questions of stability are often tied with the notion of ellipticity which can be utilized in theory of Pseudo Differential Operators and Fourier Integral Operators to study features of interest, in particular recovery of singularities. This thesis studies above questions in the following three inverse problems: RabieniaHaratbar (2018); Rabieniaharatbar (2019); RabieniaHaratbar (2019) :

1- Vectorial Light-Ray Transform of Vector Fields: The first problem is in the area of Integral geometry where functions, vector fields, and tensor fields can be studied from their integral over geodesics (lines) rather than local (differential) properties. The study investigates the geodesic light-ray transform of a vector field in Minkowski spaces and obtains a support theorem when the available light-rays are limited to an open set.

2- Dynamic X-ray Tomography: The Second problem can be considered in the area of Dynamic Inverse Problems where the object of interest is no longer stationary. The goal of this study is to generalize the existing results on dynamic operators to a more integral geometry problems using microlocal analysis techniques.

3- Inverse Scattering the Biharmonic Operator: The third problem is in the area of scattering and inverse scattering theory motivated by existing results on Schrödinger operators.

1.2 Cyber-Physical Systems

Cities and communities around the world and in particular in the U.S. are entering a new era of transformational change, in which their inhabitants, the surrounding built, and natural environments are increasingly connected by smart technologies, leading to new opportunities for innovation, improved services, and enhanced quality of life. Experimental dynamic assessment of structural units is critical in structural engineering and provides structural engineers a better understanding of structural integrity at both component and system levels. Taking the cost and availability of experimental resources into consideration, full-scale experimental evaluation of structures is a challenging proposition. Therefore, creating inexpensive and trustworthy methods of measuring structural performance, stability and resilience therefore presents economic benefits in the form of reduced US federal spending. In chapter 5, we investigate the Real-Time Hybrid Simulation (RTHS), a cyber-physical technique used to examine the global behavior of structural systems subjected to earthquake loads that are too large or complex to test in a laboratory.

Utilizing RTHS and Time-Delay Differential Equations, we quantify the sensitivity of different partitioning choices to de-synchronization at the interface. RTHS is interdisciplinary and requires deep expertise in vibrations, control, signal processing, and computer engineering. Most of the past experiments conducted using RTHS have been based on trial and error. In other words, after selecting a structure and partitioning it into physical and computational components, the hope is that an actuator controller can be designed to enable the testing to proceed without considering the global behavior or the potential for instabilities in the experimental feedback loop. Maghareh, Dyke, Rabieniaharatbar, and Prakash (2017)

1.3 Preliminaries from Integral Geometry and Microlocal Analysis

Often Inverse Problems describe a phenomenon that arises from a physical system which can be modeled by a Partial Differential Equation (PDE). Therefore, the objective of an inverse problem would be to recover the coefficients of the PDE associated to the physical situation. Inverse Problems are generally ill-posed and highly non-linear even if the corresponding forward problems are well-defined. By Hadamard's definition, in a well-posed forward problem, the goal is to obtain infinite-precision data $F(x)$, for the given input x. In contrast, in an ill-posed problem, given a noisy data $y = F(x) + \varepsilon$, the objective is to reconstruct x. The full reconstruction, however, might not be of practical importance in real world application. For instance in medical imaging, often the image reconstruction of an organ like the heart or the lunge will be of interest compare to full body reconstruction. Therefore, one needs to acquire tools where an object can be studied locally.

In this respect, *Integral Geometry* and *Microlocal Analysis* provides necessary techniques to investigate an object locally. Integral Geometry is an area of mathematics where functions, vector fields, and tensor fields need to be recovered from their integral over geodesics (lines) rather than local (differential) properties. The main object of study in integral geometry is an *Integral Transform* that can be used to do the reconstruction of an object (represented by a function for instance) from knowledge of integral quantities of the object along lines or planes. On the other hand, Microlocal Analysis helps us to investigate the discontinuities (singularities) of functions (all points where their graphs are not smooth curves) in an inverse problem by utilizing the notion of the *Wavefront Set*. The Wavefront Set is a classifier that determines the set of points and directions where the singularities occur (see Figure 1.2). We mainly follow the general approach in Hörmander (1983b, 1985); Sjöstrand (1982); Taylor (1981); Trèves (1980) to briefly introduce the necessary techniques and details in microlocal anlysis and in particular the *Real-Analytic Theory*.

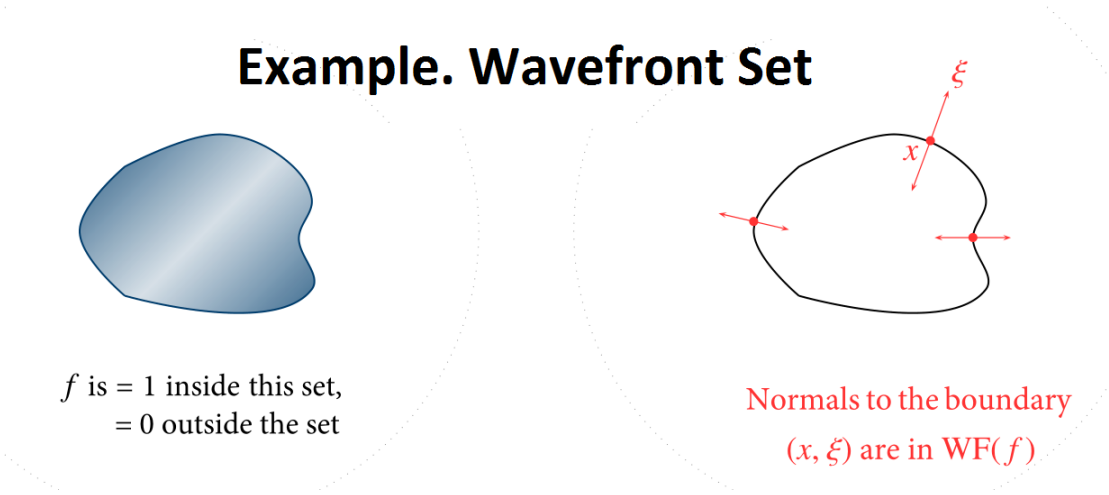

Figure 1.2. Wavefront Set.

In the following sections, the main integral transforms will be introduced.

1.3.1 X-ray Transforms

X-ray Transform is one of the most important integral transforms which has many real world applications specifically in medical imaging. To formulate the X-ray transform, let I_0 be the number of X-ray photons impinge on a homogeneous material of thickness $\Delta x \approx 0$ and I be the expected number of photons that pass through the material (along a line with length l) without interacting. By Beer's Law, we have

$$\Delta I = I - I_0 = -\sigma(x)\Delta x,$$

where ΔI is the (negative of the) expected number of photons that interact and are removed from the X-ray beam and σ is the linear attenuation coefficient or the absorption of the body. Then the differential form of the Beer's law will take the following form

$$\frac{dI}{I} = -\sigma(x)dx.$$

Solving the above ODE, one has

$$\log(\frac{I_0}{I}) = \int_0^l \sigma(x)dx.$$

Therefore, by Beer's law we have all line integrals of σ (Measurements). In general, note that each line $L \in \mathbf{R}^n$ can be represented by a point $x \in \mathbf{R}^n$ and a direction $\theta \in S^{n-1}$. Therefore, the intensity I of the X-rays depends on the $(x,\theta) \in \mathbf{R}^n \times S^{n-1}$, and solves the transport equation

$$(\theta \cdot \nabla_x + \sigma(x))I(x,\theta) = 0, \tag{1.1}$$

with the following initial and boundary conditions:

$$\lim_{s\to-\infty} I(x+s\theta,\theta) = I_0, \quad \lim_{s\to\infty} I(x+s\theta,\theta) = I_1.$$

Here I_0 is the source intensity and I_1 is the measurement outside the object. If the function σ is compactly supported, then the transport equation (1.1) has the following explicit solution

$$I(x,\theta) = I_0\, \mathbf{e}^{\int_{-\infty}^0 \sigma(x+s\theta)ds}.$$

Using the above initial and boundary condition, we have

$$\log(\frac{I_1}{I_0}) = \int_{\mathbf{R}} \sigma(x+s\theta)ds.$$

We now formally define the X-ray transform of a function $f \in \mathbf{R}^n$ as its line integrals

$$Xf(L) = \int f(L)ds \quad \text{or} \quad Xf(x,\theta) = \int_{\mathbf{R}} f(x+s\theta)ds, \quad (x,\theta) \in \mathbf{R}^n \times S^{n-1}.$$

Here ds is the unit length measure along the line L parametrized by a point $x \in \mathbf{R}^n$ and a direction $\theta \in S^{n-1}$.

In what we showed above, the transport equation (1.1) is considered as a forward problem and the X-ray transform is an explicit solution of our forward problem. Therefore, the inverse problem would be the recovery of the function f from its X-ray transform. In the context of scattering theory, the recovery process of the function f will be an inverse scattering problem if we consider $\frac{I}{I_0}$ as the scattering information corresponding to the transport equation (1.1).

1.3.2 Radon Transforms

In the previous section, we defined the X-ray transform of a function as its line integrals. For a given function one may also think of its integral along all possible planes. This motivates us to define the *Radon Transform* of a function $f \in \mathbf{R}^n$ as its integral over all hyperplanes $\Pi \in \mathbf{R}^n$ as follows:

$$Rf(\Pi) = \int_{\Pi} f dS,$$

where each plane Π is a hyperplane (i.e. $(n-1)D$ plane) and dS is the Euclidean surface measure on each plane Π. Since each hyperplane Π can be parametrized by following representation ed by the following written in exactly two different ways in the form

$$\Pi = \{x \cdot \omega = p\} = \{x \cdot (-\omega) = -p\}$$

with $(p, \omega) \in \mathbf{R} \times S^{n-1}$, we have

$$Rf(p, \omega) = \int_{x \cdot \omega = p} f dS_x.$$

Note that, in two dimension the X-ray and Radon transforms are the same, see Figure 1.3.

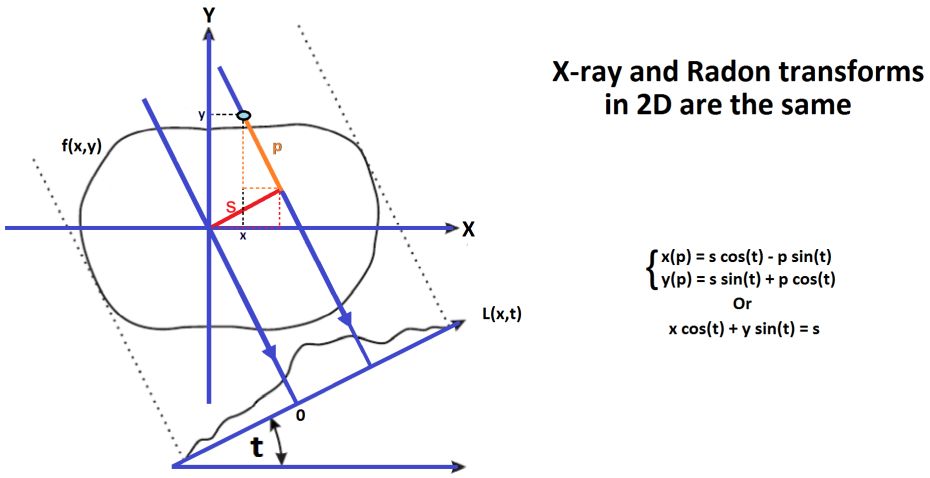

Figure 1.3. Parametrization.

Next we define a generalized X-ray and Radon transforms with more general curves and weights that can be studied, for example, in X-rays of tensor fields of order one (1-forms), Light-ray Transforms over Minkowski Spaces and Lorentzian manifolds, and Dynamical Operators. We refer to some of results in Beylkin (1984); Frigyik, Stefanov, and Uhlmann (2008); Guillemin (1985); Guillemin and Sternberg (1977); B. N. Hahn and Quinto (2016); Homan and Zhou (2017).

1.3.3 Generalized Radon Transforms

Consider the map

$$x = (x^1, x^2) \longrightarrow \phi(t,x),$$

where the function ϕ can be an analytic real-valued function. We define the level curves of function ϕ as follows:

$$H(s,t) = \{x \in X : s = \phi(t,x)\}, \quad s \in \mathbf{R},\ t \in \mathbf{R}.$$

The Generalized Radon Transform is defined by

$$\mathscr{A}f(s,t) = \int_{\phi(t,x)=s} \mu(t,x) f(x) \mathrm{d}S_{s,t}, \tag{1.2}$$

where μ is a new positive and real analytic weight and $dS_{s,t}$ is the Euclidean measure of the level curves of function ϕ. We use this operator to study dynamical X-ray tomography problems arising from field of medical imaging and non-destructive testings. (See Chapter 3.)

1.3.4 Fourier and Inverse Fourier Transforms

In this section, we briefly recall the Fourier transform and its basic properties. In what follows, we will use the notation $\langle x\rangle = (1+|x|^2)^{\frac{1}{2}}$, known as the Japanese bracket, for $x \in \mathbf{R}^n$.

Definition 1.3.1 Let $f \in C^\infty(R^n)$ be an smooth function in $\mathbf{R}^n$. The Schwartz space $\mathscr{S} = \mathscr{S}(\mathbf{R}^n)$ is the set of all smooth functions f so that, for all $\alpha = (\alpha_1, \alpha_2, \ldots, \alpha_n) \in N^n$ and all $m \geq 0$,

$$|\partial_x^\alpha f(x)| \leq C_{\alpha m}\langle x\rangle^{-m}, \quad x \in \mathbf{R}^n.$$

The natural topology of $\mathscr{S}$ is given by the following seminorms:

$$\max_{|\alpha \leq m|} \sup_{\mathbf{R}^n} \langle x\rangle^m |\partial_x^\alpha f(x)|.$$

Definition 1.3.2 For $f \in \mathscr{S}$, we define the *Fourier Transforms* and *Inverse Fourier Transforms* of the f on $\mathbf{R}^n$ as follows

$$\hat{f}(\xi) = \int e^{-\mathrm{i}x\cdot\xi} f(x)dx,$$

and

$$f(x) = (2\pi)^{-n} \int e^{\mathrm{i}x\cdot\xi} \hat{f}(\xi)d\xi.$$

Here x represent a point in $\mathbf{R}^n$ and ξ represent the direction in the dual space. In engineering in frequency domain ... It can be shown that the Fourier transform of f decays faster than any polynomial as $|\xi| \to \infty$. Therefore, a faster decay for the Fourier transform is the consequence of a higher regularity.

1.3.5 Symbol Classes

Consider the following differential operator P and the corresponding polynomial, p, in ξ with x dependent coefficients

$$P = \Sigma_{|\alpha|\leq m} a_\alpha(x) D^\alpha, \quad p(x,\xi) = \Sigma_{|\alpha|\leq m} a_\alpha(x)\xi^\alpha,$$

where $D = (D_1, D_2, \ldots, D_m)$ with $D_j = \frac{1}{\mathrm{i}}\partial_j$. Clearly

$$D^\alpha f(x) = (2\pi)^{-n} \int e^{\mathrm{i}x\cdot\xi}\xi^\alpha \hat{f}(\xi) d\xi.$$

Using the above property and $p(x,\xi)$, we have

$$Pf(x) = \Sigma_{|\alpha|\leq m} a_\alpha(x) D^\alpha f(x) = \Sigma_{|\alpha|\leq m} a_\alpha(x)(2\pi)^{-n} \int e^{\mathrm{i}x\cdot\xi}\xi^\alpha \hat{f}(\xi) d\xi$$

$$= \Sigma_{|\alpha|\leq m}(2\pi)^{-n} \int e^{\mathrm{i}x\cdot\xi} a_\alpha(x)\xi^\alpha \hat{f}(\xi) d\xi = (2\pi)^{-n} \int e^{\mathrm{i}x\cdot\xi} a_\alpha(x) p(x,\xi)\hat{f}(\xi) d\xi.$$

We call the function p with above property the *Full Symbol* associated to the operator P and show it by $\sigma(P) = p$. We now formally define the symbol in this context.

Definition 1.3.3 For $m, \eta \in \mathbf{R}$, the *Symbol Class* $S^{\eta,m} = S^{\eta,m}(\mathbf{R}^n \times \mathbf{R}^n)$ is the set of all smooth functions $p : \mathbf{R}^{2n} \to C$ so that, for all natural multi-index α, β,

$$|\partial_x^\alpha \partial_\xi^\beta p(x,\xi)| \leq C_{\alpha\beta} \langle x\rangle^\eta \langle\xi\rangle^{m-\beta}, \quad x, \xi \in \mathbf{R}^n.$$

We simply denote $S^m = S^{0,m}$ when $\eta = 0$. Often

Definition 1.3.4 Let P be an operator with corresponding symbol of class $S^m(\Omega)$. The *Principal Symbol* of the opeator P, $\sigma_p(P)$, is defined by any representative of the equivalence class $[\sigma(P)] \in \frac{S^m(\Omega)}{S^{m-1}(\Omega)}$.

Similar to Schwartz classes, by introducing the following natural semi-norms

$$\max_{|\alpha+\beta\leq N|} \sup_{\mathbf{R}^n} \langle x\rangle^{-\eta} \langle\xi\rangle^{-m+|\beta|} |\partial_x^\alpha \partial_\xi^\beta f(x,\xi)|,$$

pseudo-differential operators form a class operators which is closed under adjunction and composition.

Another subtle definition is the ellipticity of a symbol.

Definition 1.3.5 We say the symbol $p \in S^m$ is *Elliptic* if

$$|p(x,\xi)| \geq c\langle\xi\rangle^m, \quad |\xi| \gg 1$$

for $m \in \mathbf{R}^n$ and some $c > 0$. It can be shown, if $p \in S^m$ then $\frac{1}{p} \in S^{-m}$.

1.3.6 Pseudo Differential Operators (ΨDOs)

In theory, a pseudo-differential operator generalizes the concept of differential operators.

Definition 1.3.6 Let $\Omega \in \mathbf{R}^n$, $f \in \mathscr{S}(\Omega)$ and $p \in S^{\eta,m}(\Omega)$. We define the *Pseudo-Differential Operator* $p(x,D)$ corresponding the symbol of symbol p as by

$$p(x,D)f(x) = (2\pi)^{-n} \int_{\mathbf{R}^n} e^{\mathrm{i}x\cdot\xi} a_\alpha(x) p(x,\xi) \hat{f}(\xi) d\xi.$$

Definition 1.3.7 We say the operator $p(x,D)$ is an *Elliptic Pseudo-Differential Operator* if the symbol $p(x,\xi)$ is elliptic.

Definition 1.3.8 Let $P = p(x,D)$ be a ΨDO with corresponding symbol p. We say P is an *Smoothing Operator* if

$$p \in S^{-\infty} = \cap_{m=1}^{\infty} S^m.$$

It can be shown that smoothing operators map $\mathscr{D}'(\mathbf{R}^n) \to C^\infty(\mathbf{R}^n)$. Next we define the Schwartz Kernel of the ΨDO with corresponding symbol $p \in S^m(\Omega)$ and call an integral operator a smoothing operator if its Schwartz kernel is smooth.

Definition 1.3.9 Let $p(x,D)$ be a ΨDO associated with the symbol $p \in S^m(\Omega)$. The *Schwartz Kernel* K_p of the operator $p(x,D)$ is a distribution $\mathscr{D}(\Omega \times \Omega)$ defined by the following oscillatory integral

$$K_p(x,y) = (2\pi)^{-n} \int_{\mathbf{R}^n} e^{\mathrm{i}(x-y)\cdot\xi} p(x,\xi) d\xi.$$

One can show that $K_p(x,y)$ is singular on the diagonal of $\Omega \times \Omega$. We say s Schwartz kernel is *properly supported* if for any compact subset K of Ω,

$$\operatorname{supp} K_p \cap (K \times \Omega) \quad \text{and} \quad \operatorname{supp} K_p \cap (\Omega \times K)$$

are both compact.

Now consider the cut-off function $\chi \in C_0^\infty(\mathbf{R})$ which one in a neighborhood of zero. For $\chi \in C_0^\infty(\mathbf{R})$, it can be shown that, up to a smoothing operator, every ΨDO has a properly supported Schwartz kernel. In fact, any Schwartz kernel can be written as

$$K_p(x,y)\chi(|x-y|^2) + K_p(x,y)(1-\chi(|x-y|^2)),$$

where the first term is a properly supported kernel, while the second term is a smooth kernel. ΨDOs with proper support maps $C^\infty(\Omega) \to C^\infty(\Omega)$ and they are continuous with $L^2(\Omega)$–adjoint that are also ΨDOs of the same class seeTheorem II.4.1, Taylor (1981).

Definition 1.3.10 Let $f \in \mathscr{D}'(\mathbf{R}^n)$. We say that $x_0 \notin \operatorname{sing\,supp} f$ if there exists $\phi \in C_0^\infty(\mathbf{R}^n)$ such that $\phi(x_0) \neq 0$ and $\phi f \in C^\infty(\mathbf{R}^n)$.

One can conclude the elliptic regularity results for a ΨDo, by using the following lemma *Pseudolocal Property*.

Lemma 1.3.1 *Let $f \in \mathscr{E}'(X)$. Then for any ΨDO P we have*

$$\operatorname{sing\,supp} Pf \subset \operatorname{sing\,supp} f.$$

Lemma 1.3.2 *(Elliptic Regularity) Let $f \in \mathscr{E}'(X)$. Then for any elliptic ΨDO P we have*

$$\operatorname{sing\,supp} Pf = \operatorname{sing\,supp} f.$$

An elliptic ΨDO is of practical importance as one can construct the corresponding inverse operator. In fact, let P be a properly supported elliptic ΨDO with corresponding symbol $p \in S^m(\Omega)$. Then there exists an operator Q with corresponding symbol $q \in S^{-m}$ so that

$$PQ = I + R, \quad R \in S^{-\infty}.$$

The operator Q is called a pseudo-inverse of P. [Theorem III.1.3-Taylor (1981)]

As we mentioned earlier, one of the main goals throughout this thesis is to establish Stability Estimates which is one of the most important features of interests in microlocal analysis. As we pointed out earlier, stability estimates quantify how error in measurements translate to errors in reconstruction process. In this study, we follow functional analysis arguments similar to Theorem V.3.1-Taylor (1981) to establish stability estimates that are in nature similar to the following lemma.

Lemma 1.3.3 *Let P be a properly supported elliptic ΨDO with corresponding symbol $p \in S^m(\Omega)$, and $K \subset \Omega$ compact. Then for every $f \in H^m = H^m(\Omega)$ with $\operatorname{supp} f \subset K$, there exists a constant $C > 0$ so that for all $s > 0$ and corresponding constant $C_s > 0$, one has*

$$\| f \|_{H^m} \leq C \| Pf \|_{L^2} + C_s \| f \|_{H^{-s}} .$$

Moreover, if the operator P is injective, then there exists a constant $C_0 > 0$ such that

$$\| f \|_{H^m} \leq C_0 \| Pf \|_{L^2} .$$

In the next section, we introduce the notion of general oscillatory integrals.

1.3.7 Oscillatory Integrals

Consider the n-dimensional Radon transform

$$Rf(p, \omega) = \int_{x \cdot \omega = p} f dS_x, \quad (p, \omega) \in \mathbf{R} \times S^{n-1}.$$

It can be shown the Radon transform can be written in terms of delta function as follows

$$Rf(p,\omega) = \int_{\mathbf{R}^n} \delta(p - x\cdot\omega) f(x) dx.$$

Note that since the delta function is one-dimensional, one has

$$\delta(p) = (2\pi)^{-1} \int_{\mathbf{R}} e^{\mathrm{i}\lambda p} dp,$$

where λ is the dual variable corresponding p. Setting $\varphi(p,\omega,x,\lambda) = \delta(p - x\cdot\omega)$ and $a(p,\omega,x,\lambda) = (2\pi)^{-1}$, we have

$$Rf(p,\omega) = \int e^{\mathrm{i}\varphi(p,\omega,x,\lambda)} a(p,\omega,x,\lambda) f(x) dp dx.$$

The function φ is the *Phase* and the function a is called the *Amplitude.* The integral representation on the r.h.s above equation is the motivation to define general oscillatory integral operators. To formally define these operators we first need to define the phase function, Hörmander (1983a).

Definition 1.3.11 Phase A function $\varphi(x,\theta) \in C^\infty(\Omega \times \mathbf{R}^n)$ is called a phase function, if for all $(x,\theta) \in \Omega \times \mathbf{R}^n$, the following non-degeneracy conditions are satisfied:
$(i) \mathscr{I}\varphi(x,\theta) \geq 0$, i.e. $|e^{\mathrm{i}\varphi(x,\theta)}| \leq 1$,
$(ii) \varphi(x,\sigma\theta) = \sigma\varphi(x,\theta)$ for all $\sigma > 0$, i.e. φ is a positively homogeneous function of degree one,
$(iii) |\varphi_x^{'}|^2 + |\theta|^2 |\varphi_\theta^{'}|^2 > 0$, i.e. $d_{x,\theta}\varphi = \varphi_x^{'} dx + \varphi_\theta^{'} d\theta \neq 0$ on $\Omega \times \mathbf{R}^n$,
(iv) If $d_\theta \varphi = 0$, then the forms

$$d_{x,\theta}\left(\frac{\partial\varphi}{\partial\theta_j}\right), \quad j = 1,2,\ldots,n,$$

are linearly independent.

Given the phase function $\varphi \in \Omega \times \mathbf{R}^n$ and the amplitude (symbol) $a \in S^m(\Omega \times \mathbf{R}^n)$, an *Oscillatory Integral Operator* is defined by:

$$I_{a,\varphi}(x) = \int e^{\mathrm{i}\varphi(x,\theta)} a(x,\theta) d\theta.$$

Theorem 1.3.1 *Let $f \in C_0^\infty(\mathbf{R}^n)$. For the phase function $\varphi \in \Omega \times \mathbf{R}^n$ and the amplitude $a \in S^m(\Omega \times \mathbf{R}^n)$,*

$$\langle I_{a,\varphi}(x), f\rangle = \iint_{\Omega\times\mathbf{R}^n} e^{\mathrm{i}\varphi(x,\theta)} a(x,\theta) f(x) dx d\theta$$

is a distribution on Ω for any k with $m-k<-n$. In addition, the map $a \to I_{a,\varphi}$ is continuous from S^m to $D^{'(k)}(\Omega)$, (see Theorem 7.8.2, Hörmander (1983a)).

1.3.8 Fourier Integral Operators (FIOs)

We now are ready to introduced the local theory of *Fourier Differential Operators* (FIOs) which are a particular case of Oscillatory Integrals. We refer to Duistermaat (1996); Hörmander (1983a) for details and definitions. Let $\Omega = X \times Y \subset \mathbf{R}^{n_1} \times \mathbf{R}^{n_2}$, $\varphi(x,y,\theta)$ be a non-degenerate phase function defined on $\Omega \times \mathbf{R}^n$. Let $a(x,y,\theta) \in S^M(\Omega \times \mathbf{R}^n)$ be a local symbol which is a smooth function with support in a closed and conic subset of $\Omega \times \mathbf{R}^n$ and $M = m - \frac{n}{2} + \frac{n_1+n_2}{4}$.

Definition 1.3.12 (Local) We say the operator $\mathscr{A}$ is a Fourier Integral Operator, if its Schwartz kernel is an oscillatory integral. That is

$$\mathscr{A}f(x) = \int e^{\mathrm{i}\varphi(x,y,\theta)} a(x,y,\theta) f(y) dy d\theta, \quad \text{for } f \in C_0^\infty(Y).$$

Remark 1.3.1 Note that if $\varphi(x,y,\theta) = (x-y)\cdot\theta$ and $n_1 = n_2 = n$, we simply have a pseudo differential operator. We also remark that an FIO is invariantly defined with respect to the phase function φ.

In theory of microlocal analysis, often we need to analyze the regularity of the Schwartz kernel of an FIO $\mathscr{A}$ defined by the phase function φ and the amplitude a. This, in fact, leads to find necessary conditions under which $\mathscr{A}f$ is C^∞ in a neighborhood of $x \in X$ while f is not C^∞.

Definition 1.3.13 Let $\mathscr{A}$ be an FIO associated with the phase function φ and the amplitude a. We define the *Critical Set* of the phase function φ in $\Omega \times \mathbf{R}^n$ by

$$C_\varphi = \{(x,y,\theta) \in \Omega \times \mathbf{R}^n | d_\theta \varphi = 0\}.$$

Note that C_φ is a *Coinc* set, that is, $(x,\theta) \in C_\varphi \Rightarrow (x, r\theta) \in C_\varphi$ for $r > 0$. In the context of FIO, C_φ is also called *Characteristic Manifold*.

Remark 1.3.2 Since the phase function is non-degenerate, the map $T : C_\varphi \to T^*(X \times Y) \setminus 0$ with

$$T(x,y,\theta) = (x,\xi,y,\eta) := (x, d_x\varphi(x,y,\theta), y, d_y\varphi(x,y,\theta)) \in T^*(X \times Y) \setminus 0$$

is an immersion.

Definition 1.3.14 Let φ be a phase function. A conic Lagrangian manifold Λ_φ is defined by

$$\Lambda_\varphi = \{(x,\xi,y,\eta) | \xi = d_x\varphi(x,y,\theta), \eta = d_y\varphi(x,y,\theta)\}.$$

The Canonical Relation associated to the phase function φ and the FIO $\mathscr{A}$ is the twisted Λ_φ defined by

$$\Lambda_\varphi^{'} = \{(x,\xi,y,\eta) | (x,\xi,y,-\eta) \in \Lambda_\varphi\}.$$

Above we represented an FIO locally. To see the global theory of an FIO we refer to Hörmander (1983a); Taylor (1981).

Consider the microlocal version of double fibration:

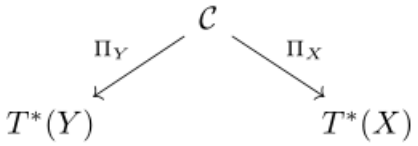

where

$$\Pi_X(x,y,\theta) = (x,\varphi_x'), \quad \Pi_Y(x,y,\theta) = (y,-\varphi_y').$$

Definition 1.3.15 We say a local FIO is a graph type if $\Lambda_\varphi^{'} = \Pi_X \circ \Pi_Y^{-1}$ is bijective.

In the next section, we show that φ parametrizes the wave front set of the FIO's Schwartz kernel which is a conic and Lagrangian sub-manifold of $T^*(X \times Y) \setminus 0$.

1.3.9 Wavefront Set and Analytic Wavefront Set

We now ready to define the wavefront set which is an extension of the notion of sing supp. In fact, the idea is to determine the singularities of $f \in \mathscr{D}'(X)$ by studying the Fourier transform of χf and its decay near a point.

Definition 1.3.16 [Definition 8.1.2-Hörmander (1983a)] We say that $(x_0, \xi^0) \in \mathbf{R}^n \times (\mathbf{R}^n \setminus 0)$ is not in the Wave Front Set of $f \in \mathscr{D}'(\mathbf{R}^n)$, $\mathrm{WF} f$, if there exists $\phi \in C_0^\infty(\mathbf{R}^n)$ with $\phi(x_0) \neq 0$ so that for any N, there exists C_N such that

$$|\widehat{\phi f}(\xi)| \leq C_N(1+|\xi|)^{-N}$$

for ξ in some conic neighborhood of ξ^0.

Remark 1.3.3 The above definition is independent of the choice of ϕ.

Peetre's theorem Peetre (1959) characterizes differential operators the only linear operators which do not increase the support of distributions. In a same, the following lemma states that ΨDOs as the linear operators do not expand the wavefront set. This is the analog of the pseudolocal property.

Lemma 1.3.4 *Let $f \in \mathscr{E}'(X)$. Then for any ΨDO P we have*

$$\mathrm{WF} Pf \subset \mathrm{WF} f.$$

Lemma 1.3.5 *(Elliptic Regularity) Let $f \in \mathscr{E}'(X)$. Then for any elliptic ΨDO P we have*

$$\mathrm{WF} Pf = \mathrm{WF} f.$$

Definition 1.3.17 For the case of a scalar-valued distribution, define the Analytic Wave Front Set, $\mathrm{WF_A}(f)$, as the complement of all $(x, \xi) \in T^*(\mathbf{R}^n \setminus 0)$ such that

$$\int e^{\mathrm{i}\lambda|x-y|\cdot\xi - \frac{\lambda}{2}|x-y|^2} \chi(y) f(y) \mathrm{d}y = \mathscr{O}(e^{-\frac{\lambda}{C}}), \quad \lambda > 0$$

with some $C > 0$ and $\chi \in C_0^\infty$ equal to 1 near x.

Remark 1.3.4 There are three equivalent definitions of Analytic Wave Front Set in the literature due to Bros and Iagolnitzer (1975), Hörmander (1971), and Sato (1969). It has been shown by Bony (1977) and Sjöstrand (1982) that all these definitions are the equivalent.

1.3.10 Stationary Phase Method

The method of stationary phase investigates the behavior of the oscillatory integral I_φ as $\lambda \to \pm\infty$ for a general phase function φ.

Definition 1.3.18 A point x is stationary point of I_φ if $d\varphi(x) = 0$.

One can use a partition of unity argument to split the oscillatory integral in a way that the phase function φ has a unique critical point in the support of amplitude a. Note that by using appropriate coordinates one can assume that this point is at the origin. The following lemma establishes an estimate which is necessary for our results.

Lemma 1.3.6 *Let $a \in C_0^\infty(X)$ and* $\operatorname{supp} a \subset K$. *If $d\varphi(x) \neq 0$ in* $\operatorname{supp} a$, *then the following estimate holds.*

$$|I_\varphi(\lambda)| \leq \frac{C_K}{\lambda} \parallel a(x) \parallel_{C^k} .$$

To get the estimate above, one needs to integrate repeatedly with the operator

$$L = \frac{\nabla\varphi \cdot \nabla}{|\nabla\varphi|^2}.$$

Note that if the phase is non-degenerate then L and reproduces the phase.

VECTORIAL LIGHT-RAY TRANSFORM IN MINKOWSKI SPACES

*** This chapter concludes my original work: "Support Theorem for the Light-Ray Transform of Vector Fields on Minkowski Spaces." Inverse Problems and Imaging, Volume 12, No. 2, 2018: 293-314.**

One of the most fundamental questions in mathematics and physics, which has been profoundly investigated by scientists of different disciplines, is how to determine the shape of the Universe and whether the Universe is finite, infinite, flat, or curved. To address these fundamental questions, scientists have proposed and developed various types of studies, for instance, utilizing the oldest light in the universe, the Cosmic Microwave Background (CMB) radiations. According to NASA, CMB is the leftover radiation from the Big Bang, which provides key information about the formation of the early universe, which goes back to 13.8 billion years ago. In this respect, in 1905 Albert Einstein with his theory of Relativity described how space-time is curved and bent by mass and energy as well as their close relations to the shape of the universe at different stages of life. Due to the tomographic nature of the CMB radiations, we study Light-ray transform of vector fields in Minkowski Space-time. Minkowski space is the most common mathematical structure on which Einstein's special relativity is formulated. In this study, a vector field is a mathematical representation of the shape of the universe, the light-ray transform is the available light-ray measurements (signals) from the early stage of universe, and the goal is to explain the shape of the universe at early stages from the available signals. Therefore, the mathematical representation of our goal would be to reconstruct the vector field from its light-ray measurements. For this purpose, we study a more general problem and found the required geometrical condition under which one can utilize the light-ray measurements to reconstruct the vector field, even in the case where the available signals are limited. We generalize the existing results on scalar-valued functions to vector-valued functions. From the physical point of view, this results work in the Minkowski setting implies that one could expect to extract information from all signals moving slower than light and not the one moving faster than light (physically not possible).

2.1 Existing Results

Let (M,g) be a Lorentzian manifold of dimension $1+n$, $n \geq 2$, with a Lorentzian metric g of signature $(-,+,...,+)$. Given a weight $\kappa \in C^\infty(M \times S^{n-1})$, in general, the weighted Light-Ray transform of a vector field f is defined by:

$$L_\kappa f(\gamma) = \int \kappa(\gamma(s), \gamma'(s)) f_i(\gamma(s)) \gamma'^i(s)\, ds, \tag{2.1}$$

where $\gamma = \gamma_{x,\theta}$ is the family of future pointing light-like geodesics (null-geodesics) on M in the direction of $(1,\theta)$, $\theta \in S^{n-1}$. We choose a certain parametrization for the family of light-like geodesics γ and require the weight function κ to be positively homogeneous of degree zero in its second variable. The homogeneity of κ makes the parameterization of light-like geodesics independent.

Light-ray transform has been attracting a growing interest recently, due to its wide range of applications. One major application of this transform is in the study of hyperbolic equations with time-dependent coefficients to recover the lower order terms from boundary or scattering information, see, e.g., Aicha (2015); Guillemin (1985); Ramm and Rakesh (1991); Ramm and Sjöstrand (1991); Salazar (2013); P. Stefanov (1989); Uhlmann and Vasy (2016a); Waters (2014) and also recovering the lower order terms of time-independent hyperbolic equations Bellassoued and Dos Santos Ferreira (2011); Montalto (2014).

In the case where f is a function and supported in the cylinder $\mathbf{R} \times B(0,R)$ with tempered growth in the Minkowski space, Stefanov in P. Stefanov (2017) has shown that Lf determines f uniquely. The fact that Lf recovers the Fourier transform $\hat{f}$ of f (w.r.t. all variables) in the space-like cone $|\tau| < |\xi|$ in a stable way, is used to show that the potential in the wave equation is uniquely determined by the scattering data. Moreover, since $\hat{f}(\tau,\xi)$ is analytic in the ξ variable (with values distributions in the τ variable), then one can fill in the missing cone by analytic continuation in the ξ variable. In a recent work by P. Stefanov (2017), analytic microlocal methods are applied to show support theorems and injectivity of L_κ for analytic metrics and weights (on an analytic manifolds M) for functions. In particular, the results in P. Stefanov (1989) are generalized to a local data and independent of the tempered growth for large t.

Analytic microlocal method were already used in many works. Boman (1991); Boman and Quinto (1987) proved support theorems for Radon transforms with flat geometry and analytic weights, see also Quinto (1993). For related results using same techniques, we refer to Krishnan (2009); Krishnan and Stefanov (2009) where the support theorem is proved on simple analytic manifolds, see also Frigyik et al. (2008). Uhlmann and Vasy (2016b) used the scattering calculus to prove a support theorem in the Riemannian case near a strictly convex point of a hypersurface in dimensions $n \geq 3$ without the analyticity condition, see also P. Stefanov and Uhlmann (2004, 2005, 2008).

Analytic and non-analytic microlocal analysis have been used to prove the injectivity and stability estimates for tensor fields of order two and higher. For the tensor fields of order two, Pestov and Uhlmann (2005) proved the unique recovery of Riemannian metric on a compact and simple Riemannian surface with boundary, see also Sharafutdinov (1994) for related results. More general results on injectivity up to potential fields of the geodesic ray transform for tensor fields of any order on Riemannian manifold can be found in Paternain, Salo, and Uhlmann (2013). In P. Stefanov and Uhlmann (2005, 2008), a generic s-injectivity up to potential fields and a stability estimate are established on a compact Riemannian manifold M with non-necessarily convex boundary and with possible conjugate points. Microlocal method for tomographic problems is used to detect singularities of the Lorentzian metric of the Universe using measurements of the Cosmic Microwave Background (CMB) radiation in Lassas, Oksanen, Stefanov, and Uhlmann (2018). In Melrose (1994), it is described that which singularities are visible and which cannot be detected. In Krishnan and Stefanov (2009), a Helgason's type of support theorem is proved for the geodesic ray transform of symmetric 2-tensor fields on a Riemannian manifold (with boundary) with a real-analytic metric g. It is shown that the tensor field can be recovered up to a potential field. In Holman and Stefanov (2010), authors studied the problem of recovery of a covector field on simple Riemannian manifold with weight. Under some condition on weight, the recovery up to potential field and uniqueness are shown. See also Denisjuk (2006), for the inversion of three dimensional X-ray transform of symmetric tensor fields of any order with sources on a curve. In a recent work by Lassas, Oksanen, Stefanov, and Uhlmann (2019), authors have studied the weighted light-ray transform L of integrating functions on a Lorentzian manifold over light-like geodesics. They showed that considering the operator L as a FIO, one can reconstruct the space-like singularities via a filtered back-projection if there are no conjugate points.

2.2 Main Results

Our main goal in this paper is to study the local and analytic microlocal invertibility of the operator L acting on vector fields on the Minkowski time-space $\mathbf{R}^{1+n}$ when the weight κ is simply one. We study the following operator L:

$$Lf(x,\theta) = \int f(s, x+s\theta)\cdot(1,\theta)\, ds, \tag{2.2}$$

where $\gamma = \gamma_{x,\theta} = (s, x+s\theta)$ is the family of future pointing light-like lines (light-rays) on the Minkowski time-space $\mathbf{R}^{1+n}$ in the direction of $(1,\theta)$, with $|\theta| = 1$. Note that above operator is a special case of the operator defined (2.1).

The main novelty of our work is that Lf is known only over an open set of light-like lines, Γ, on the Minkowski time-space $\mathbf{R}^{1+n}$ (the Incomplete data case). Our results can be considered as a Helgason's type support theorem. The global invertibility (injectivity) of the operator L (the Complete data case) up to potential fields is already established, see for example Denisjuk (2006); Waters and Salazar (2013).

We generalize the method used in P. Stefanov (2017) to study the stable recovery of the analytic wave front set of vector field f instead of functions, and prove a support theorem in the Minkowski time-space $\mathbf{R}^{1+n}$. To prove our results, we apply the analytic stationary phase approach by Sjöstrand (1982) already used by P. Stefanov (2017) and P. Stefanov and Uhlmann (2008), see also Frigyik et al. (2008); Krishnan (2009); Krishnan and Stefanov (2009).

Theorem 2.2.1 (Main Result) . *Let $n \geq 2$ and $f \in \mathscr{E}'(\mathbf{R}^{1+n})$ be so that* $\operatorname{supp} f$ *expands with a speed less than one. Let G be an open and connected neighborhood of $(x_0,\theta_0) \in \mathbf{R}^n \times S^{n-1}$ and γ_{x_0,θ_0} be a light-like line with direction θ_0 passing through the point x_0.*

i) For $n = 2$, if $Lf(x,\theta) = 0$ in $G_\pm$ and if γ_{x_0,θ_0} does not intersect $\operatorname{supp}\operatorname{curl} f$*, then none of the light-like lines $\gamma_{x,\theta}$, $(x,\theta) \in G_\pm$, does. Here $G_\pm$ is an open and connected neighborhood of $(x_0, \pm\theta_0)$ in $\mathbf{R}^2 \times S^1$.*

ii) For $n \geq 3$, if $Lf(x,\theta) = 0$ in G and if γ_{x_0,θ_0} does not intersect $\operatorname{supp} \mathrm{d}f$*, then none of the light-like lines $\gamma_{x,\theta}$, $(x,\theta) \in G$, does.*

2.3 Preliminaries

We first state some definitions and a proposition which are necessary for our main result.

Definition 2.3.1 We call a vector $u = (u_0, u')$ space-like if $|u_0| < |u'|$. Vectors with $|u_0| > |u'|$ are called time-like. Light-like vectors are those for which we have $|u_0| = |u'|$.

Definition 2.3.2 We say the set K is light-like convex if for any two pints in K, the light-like geodesic connecting them lies in K.

Definition 2.3.3 Let K be a subset of Minkowski time-space $\mathbf{R}^{1+n}$. We say K expands with a speed less than one if

$$K \subset \{(t,x) : |x| \leqslant C|t| + R\}, \quad \text{for some} \quad 0 < C < 1\ , R > 0.$$

Remark 2.3.1 Definition 2.3.3 allows us to integrate over a compact interval. In fact, if the supp f in such a set expands with speed less than one, then the operator defined by (2.2) is integrating over a compact set including $(x_0, \theta_0) \in \mathbf{R}^n \times S^{n-1}$. In other words, the integral of f and χf have the same light-ray transform near (x_0, θ_0), where the function χ is a smooth cut-off with property $\chi = 1$ in a neighborhood of (x_0, θ_0).

From now on, we study the operator defined by (2.2). We know that, any three-dimensional vector field $f = (f_0, f_1, f_2)$, has a three-dimensional curl f. In other words, one may work with the curl f to do the analytic recovery of the analytic wave front set. This, however, is not the case for any vector field f with dimension $n > 3$ as the generalized curl f, $\mathrm{d}f$, does not have the same dimension as the vector field f does. This motivates us to introduce an appropriate operator where it forms an n-dimensional parametrized vector field with all the necessary components of $\mathrm{d}f$ for the analytic recovery process. We now state our first proposition.

Proposition 2.3.1 *Let $f = (f_0, f_1, \ldots, f_n) \in \mathscr{C}^1(\mathbf{R}^{1+n}, \mathbb{C}^{1+n})$ be such that $|f|$ and $|\partial f_i / \partial x^i|$ are bounded by $C(1+|x|)^{-1-\varepsilon}$ with some $\varepsilon > 0$ and constant $C > 0$. Then for any $(x, \theta) \in (\mathbf{R}^n \times S^{n-1})$ and $v \in \mathbf{R}^n$,*

$$(v.\nabla_x) Lf(x, \theta) = \int_{\gamma_{x,\theta}} \tilde{f}_v(x) \cdot (1, \theta)\ ds, \tag{2.3}$$

where $\tilde{f}_v(x) = (\tilde{f}_{0_v}, \tilde{f}_{1_v}, \ldots, \tilde{f}_{n_v})(x) \in \mathscr{S}(\mathbf{R}^{1+n})$ *is a parametrized vector field with*

$$\tilde{f}_{i_v}(x) = \sum_{0\le j\le n} f_{ij}(x)(0,v)^j_{(i)} = \sum_{0\le j\le n} (\partial_j f_i - \partial_i f_j)(x)(0,v)^j_{(i)}, \quad i = 1,2,\ldots,n.$$

Here by $(0,v)_{(i)}$*, we mean the i-th component of* $(0,v)$ *is excluded.*

Proof We show this result for $n = 3$. The proof for higher dimension is analogous. Let $f \in \mathscr{C}^1(\mathbf{R}^{1+3}, \mathbb{C}^{1+3})$ and fix $(1,\theta) \in \mathbf{R} \times S^{n-1}$. For $v \in \mathbf{R}^3$, we take the directional derivative of the operator Lf. Therefore,

$$(v.\nabla_x)Lf(x,\theta) = \int_R (v.\nabla_x) f(s, x+s\theta).(1,\theta) ds.$$

On the other hand, by the Fundamental Theorem of Calculus,

$$\int_R \frac{d}{ds}[f(s,x+s\theta).(0,v)]\, ds = 0.$$

Subtracting above identities, we have

$$(v.\nabla_x)Lf(x,\theta) = \int_R ((0,v).\nabla_z) f(s,x+s\theta).(1,\theta) - \frac{d}{ds}[f(s,x+s\theta).(0,v)]\, ds.$$

Note here that we used $z = (t,x) \in \mathbf{R}^{1+n}$ to balance the dimension of the two terms on the right hand side of above equation. Expanding the right hand side and rearranging all terms with respect to components of $(1,\theta)$, i.e., $1, \theta^1, \theta^2, \theta^3$, we get

$$\int_{\gamma_{x,\theta}} [v^1(\partial_1 f_0 - \partial_0 f_1) + v^2(\partial_2 f_0 - \partial_0 f_2) + v^3(\partial_3 f_0 - \partial_0 f_3)]$$

$$+[v^2(\partial_2 f_1 - \partial_1 f_2) + v^3(\partial_3 f_1 - \partial_1 f_3)]\theta^1 + [v^1(\partial_1 f_2 - \partial_2 f_1) + v^3(\partial_3 f_2 - \partial_2 f_3)]\theta^2$$

$$+[v^1(\partial_1 f_3 - \partial_3 f_1) + v^2(\partial_2 f_3 - \partial_3 f_2)]\theta^3\, ds.$$

Therefore,

$$(v.\nabla_x)Lf(x,\theta) = \int_{\gamma_{x,\theta}} \tilde{f}_v(x) \cdot (1,\theta)\, ds.$$

Here $\gamma_{x,\theta}$ is the light-like lines parameterized by their points of intersection with $t=0$ and direction $(1,\theta)$. ■

Remark 2.3.2 i) For $n=2$, setting v to be $(1,0)$ and $(0,1)$ yields to the following identities.

$$\partial_1 Lf(x,\theta) = \int_{\gamma_{x,\theta}} (\partial_1 f_0 - \partial_t f_1) + \theta^2(\partial_1 f_2 - \partial_2 f_1)\, ds = \int_{\gamma_{x,\theta}} (-c_2 + \theta^2 c_0)\, ds.$$

$$\partial_2 Lf(x,\theta) = \int_{\gamma_{x,\theta}} (\partial_2 f_0 - \partial_t f_2) + \theta^1(\partial_2 f_1 - \partial_1 f_2)\, ds = \int_{\gamma_{x,\theta}} (c_1 - \theta^1 c_0)\, ds.$$

where $(c_0, c_1, c_2) =: \operatorname{curl} f$. Similar results can be seen in [P. Stefanov and Uhlmann (2004), Proposition 2.8].

ii) The vector field $\tilde{f}_v$ has the following property: for any $v \in \mathbf{R}^n$,

$$(0,v)\cdot \tilde{f}_v(x) = v^1 \tilde{f}_{1_v}(x) + v^2 \tilde{f}_{2_v}(x) + \cdots + v^n \tilde{f}_{n_v}(x) = 0.$$

This is analogous to solenoidal condition for vector fields in the Fourier domain.

iii) Each component of $\tilde{f}_v$ is a superposition of components of $\operatorname{curl} f$ (for $n=2$) and of the generalized curl, $\mathrm{d}f$ (for $n \geq 3$.) This is a very important property since it forms an overdetermined system of equations which helps us to recover the curl and generalized curl, $\mathrm{d}f$.

iv) Clearly

$$Lf = 0 \implies (v.\nabla_x) Lf = 0, \quad \forall v \in \mathbf{R}^n.$$

For the case where the vector field f is compactly supported,

$$Lf = 0 \equiv (v.\nabla_x) Lf = 0, \quad \forall v \in \mathbf{R}^n.$$

In fact, the directional derivative of Lf with respect to x is zero for all $v \in \mathbf{R}^n$, which implies that Lf is constant. Now f is compactly supported, therefore $Lf = 0$.

Above properties motivate us to work with $\tilde{f}_v$ and $(v.\nabla_x)L$ instead of f and Lf in the following sections.

2.4 Fourier Analysis

In this section, we consider the case where the light-ray transform is known over all light-like lines (complete data). This allows us to do the Fourier analysis by fixing the initial point and stay in a small neighborhood of the direction $(1,\theta)$. As we mentioned above, this case has been already studied. We do this analysis to have some insight for the microlocal analysis part of our study.

The following proposition is some preliminary results which stats that in the space-like cone $\{(\tau,\xi) : |\tau| < |\xi|\}$, the operator $(v.\nabla_x)L$ recovers the Fourier transform of the curl f and the generalized curl, $\mathrm{d}f$, for $n = 2$ and $n \geq 3$, respectively.

Proposition 2.4.1 *Let $f \in \mathscr{S}(\mathbf{R}^{1+n})$.*

i) For $n = 2$, if $Lf(x,\theta) = 0$ for all x and for θ near $\pm\theta_0$, then $\mathscr{F}(\operatorname{curl} f) = 0$ for ζ close ζ_0, where ζ_0 is the unique space-like vector up to re-scaling with the property $(1,\pm\theta_0)\cdot\zeta_0 = 0$.

ii) For $n \geq 3$, if $Lf(x,\theta) = 0$ for all x and for θ near θ_0, then $\mathscr{F}(\mathrm{d}f) = 0$ for all ζ near the set $\{\zeta \big| (1,\theta)\cdot\zeta = 0\}$.

Proof i) Let $\zeta^0 = (\tau^0,(\xi^1)^0,(\xi^2)^0)$ be a fixed space-like vector, and without loss of generality assume that $\theta_0 = \pm\mathbf{e}_2 \in \mathbf{R}^2$ such that $(1,\pm\theta_0)\cdot\zeta^0 = 0$. One has

$$\tau^0 \pm (\xi^2)^0 = 0 \quad \text{which implies that } \tau^0 = (\xi^2)^0 = 0.$$

Therefore, the vector ζ^0 has to be in the form of $(0,(\xi^1)^0,0)$, which means, up to re-scaling it is a unique ζ^0 with property $(1,\pm\theta_0)\cdot\zeta^0 = 0$. Hence, one may choose $\zeta^0 = \mathbf{e}^1 \in \mathbf{R}^{1+2}$. Note that this choice of ζ^0 can be done since we may apply Lorentzian transformation to any fixed space-like vector and transform it to $\mathbf{e}^1$. We first state the **Vectorial Fourier Slice Theorem** for a general set of lines:

$$\hat{f}(\zeta)\cdot\omega = \int_{\omega^\perp} e^{-\mathrm{i}z\cdot\zeta} Lf(z,\omega)\, \mathrm{d}S_z, \qquad \forall\omega\perp\zeta,\ \forall f \in L^1(\mathbf{R}^n).$$

To prove this, note that the integral on the RHS equals

$$\int_{\omega^\perp}\int_{\mathbf{R}} e^{-\mathrm{i}z\cdot\zeta} f_i(z+s\omega)\omega^i \mathrm{d}s\mathrm{d}S_z = \omega^i \int_{\omega^\perp}\int_{\mathbf{R}} e^{-\mathrm{i}z\cdot\zeta} f_i(z+s\omega)\mathrm{d}s\mathrm{d}S_z.$$

Set $x = z + s\omega$. Then, it is easy to see that when $\omega \perp \zeta$, we have $x \cdot \zeta = z \cdot \zeta$ and therefore above integral equals $\hat{f}_i(\zeta)$. In this paper, we apply the Vectorial Fourier Slice theorem when the set of lines is restricted to a set of light-like lines.

By assumption $(v.\nabla_x)Lf = 0$ for all $v \in \mathbf{R}^2$. Let v be an arbitrary but fixed vector in $\mathbf{R}^2$. For $\zeta = \mathbf{e}^1$, by Vectorial Fourier Slice theorem we have

$$0 = \hat{\hat{f}}_v(\zeta) \cdot (1, \theta) = \hat{\hat{f}}_{0_v}(\zeta) + \hat{\hat{f}}_{1_v}(\zeta)\theta^1 + \hat{\hat{f}}_{2_v}(\zeta)\theta^2, \quad \forall (1,\theta) \perp \zeta. \tag{2.4}$$

Since $(1, \pm\theta_0) \cdot \zeta = 0$, above equation implies

$$\begin{cases} \hat{\hat{f}}_{v_0}(\zeta) = v^1(\xi^1 \hat{f}_0 - \tau \hat{f}_1) + v^2(\xi^2 \hat{f}_0 - \tau \hat{f}_2) = 0, \\ \hat{\hat{f}}_{v_2}(\zeta) = v^1(\xi^1 \hat{f}_2 - \xi^2 \hat{f}_1) = 0. \end{cases}$$

The vector v is arbitrary, therefore one may choose two linearly independent vectors, say $v_1 = \theta^\perp$ and $v_2 = \theta$, to conclude

$$\xi^1 \hat{f}_0 - \tau \hat{f}_1 = \xi^2 \hat{f}_0 - \tau \hat{f}_2 = \xi^1 \hat{f}_2 - \xi^2 \hat{f}_1 = 0 \implies \mathscr{F}(\operatorname{curl} f)(\zeta) = 0.$$

Now let $\zeta = (\tau, \xi) \in \mathbf{R}^{1+2}$ be any non-zero space-like vector. We solve the equation $(1, \theta) \cdot \zeta = 0$, for θ. Set $\theta = a\xi + b\xi^\perp$. Therefore,

$$-\tau = \theta \cdot \xi = (a\xi + b\xi^\perp) \cdot \xi = a|\xi|^2 \quad \implies \quad a = \frac{-\tau}{|\xi|^2}.$$

On the other hand,

$$1 = |\theta|^2 = (a^2 + b^2)|\xi|^2 \quad \implies \quad b = \pm \frac{1}{|\xi|^2} \sqrt{-\tau^2 + |\xi|^2}.$$

For $\xi \in \mathbf{R}^2$, we set

$$\theta = \theta_\pm(\zeta) = \frac{1}{|\xi|^2}(-\tau\xi^1 \mp \sqrt{-\tau^2 + |\xi|^2}\xi^2, -\tau\xi^2 \pm \sqrt{-\tau^2 + |\xi|^2}\xi^1). \tag{2.5}$$

Clearly $(1,\theta_\pm(\zeta))\cdot\zeta = 0$ and $\theta_\pm$ are the only two choices with the property $|\theta_\pm(\zeta)| = 1$. In order to have ζ close to $\zeta_0 = \mathbf{e}^1$, we require $\theta_\pm^1 = 0$, so we have

$$-\tau\xi^1 \mp \sqrt{-\tau^2+|\xi|^2}\xi^2 = 0.$$

Since ζ is a space-like vector, $\sqrt{-\tau^2+|\xi|^2}$ is non-zero which implies that $\tau\xi^1 = \xi^2 = 0$. Note that ξ^1 is not zero, otherwise $\theta_\pm(\zeta)$ would be undefined. This forces τ to be zero, and therefore $\zeta \approx \zeta_0 = \mathbf{e}^1$. In particular, this implies that $\theta = \theta_\pm(\zeta)$ is analytic near $\zeta^0 = \mathbf{e}^1 \in \mathbf{R}^{1+2}$ with $\theta_\pm(\zeta^0) = \theta_0 = \pm\mathbf{e}_2 \in \mathbf{R}^2$. Hence, $\theta_\pm(\zeta)$ is within a neighborhood of $\pm\theta_0$, $\theta \approx \pm\theta_0$, if ζ is within a neighborhood of ζ_0, $\zeta \approx \zeta_0$. Considering our choices of direction $\theta_\pm(\zeta)$, the equation (2.4) can be written as

$$\hat{\tilde{f}}_{0_v}(\zeta) + \frac{1}{|\xi|^2}(-\tau\xi^1 + \sqrt{-\tau^2+|\xi|^2}\xi^2)\hat{\tilde{f}}_{1_v}(\zeta) + \frac{1}{|\xi|^2}(-\tau\xi^2 - \sqrt{-\tau^2+|\xi|^2}\xi^1)\hat{\tilde{f}}_{2_v}(\zeta) = 0, \quad (2.6)$$

and

$$\hat{\tilde{f}}_{0_v}(\zeta) + \frac{1}{|\xi|^2}(-\tau\xi^1 - \sqrt{-\tau^2+|\xi|^2}\xi^2)\hat{\tilde{f}}_{1_v}(\zeta) + \frac{1}{|\xi|^2}(-\tau\xi^2 + \sqrt{-\tau^2+|\xi|^2}\xi^1)\hat{\tilde{f}}_{2_v}(\zeta) = 0. \quad (2.7)$$

Subtract (2.7) from (2.6) to get

$$0 = \xi^2\hat{\tilde{f}}_{1_v}(\zeta) - \xi^1\hat{\tilde{f}}_{2_v}(\zeta) = (\xi\cdot v)[\xi^2\hat{f}_1(\zeta) - \xi^1\hat{f}_2(\zeta)], \quad \text{for the fixed } v \in \mathbf{R}^2. \quad (2.8)$$

Multiplying (2.6) by ξ^1 and using (2.8), we get

$$0 = \tau\hat{\tilde{f}}_{1_v}(\zeta) - \xi^1\hat{\tilde{f}}_{0_v}(\zeta) = (\xi\cdot v)[\tau\hat{f}_1(\zeta) - \xi^1\hat{f}_0(\zeta)], \quad \text{for the fixed } v \in \mathbf{R}^2. \quad (2.9)$$

Note that for $i = 0,1,2$, we expanded $\hat{\tilde{f}}_{i_v}(\zeta, v)$ in (2.8) and (2.9), and rearranged both equations in terms of $\hat{f}_i(\zeta)$, to get the r.h.s of above equations. Now set $v = \xi$, therefore $\xi\cdot v = |\xi|^2 \neq 0$ and

$$\xi^2\hat{f}_1(\zeta) - \xi^1\hat{f}_2(\zeta) = \tau\hat{f}_1(\zeta) - \xi^1\hat{f}_0(\zeta) = 0. \quad (2.10)$$

Clearly $\xi^2\hat{f}_1(\zeta)-\xi^1\hat{f}_2(\zeta)=0$ implies that $\hat{\tilde{f}}_{1_v}(\zeta)=\hat{\tilde{f}}_{2_v}(\zeta)=0$ for $v\in\mathbf{R}^2$. Plugging $\hat{\tilde{f}}_{1_v}(\zeta)=0$ into the LHS of (2.9), we conclude $\xi^1\hat{\tilde{f}}_{0_v}(\zeta)=0$. The vector ζ is space-like with property $\xi^1\neq 0$, therefore

$$\hat{\tilde{f}}_{0_v}(\zeta)=v^1(\xi^1\hat{f}_0-\tau\hat{f}_1)+v^2(\xi^2\hat{f}_0-\tau\hat{f}_2)=0.$$

Since v is arbitrary in $\mathbf{R}^2$, any two linearly independent vectors v_1 and v_2 implies that $\xi^2\hat{f}_0-\tau\hat{f}_2=0$. Notice that one may use the equation on the r.h.s of (2.10) and the fact that v is an arbitrary vector to have the same conclusion. This shows that all three components of $\operatorname{curl} f$ in Fourier domain are zeros, and thus $\mathscr{F}(\operatorname{curl} f)(\zeta)=0$.

ii) Let first $n=3$ and $\zeta=\zeta^0$ be a fixed non-zero space-like vector. Applying the Lorentzian transformation, we may assume that $\zeta^0=\mathbf{e}^2:=(0,0,1,0)\in\mathbf{R}^{1+3}$. Set

$$\theta(a)=\sin(a)\mathbf{e}_1+\cos(a)\mathbf{e}_3=(\sin(a),0,\cos(a)).$$

Clearly $\big|\theta(a)\big|=1$, $\theta_0=\theta(0)=\mathbf{e}_3$, and $(1,\theta(a))\cdot\zeta=0$.

By assumption $(v.\nabla_x)Lf=0$ for all $v\in\mathbf{R}^3$. Let v be an arbitrary fixed vector in $\mathbf{R}^3$. For $\zeta=\mathbf{e}^2$, by Vectorial Fourier Slice theorem

$$0=\hat{\tilde{f}}_v(\zeta)\cdot(1,\theta)=\hat{\tilde{f}}_{0_v}(\zeta)+\hat{\tilde{f}}_{1_v}(\zeta)\theta^1+\hat{\tilde{f}}_{2_v}(\zeta)\theta^2+\hat{\tilde{f}}_{3_v}(\zeta)\theta^3,\quad\forall(1,\theta)\perp\zeta$$

Plugging $\theta=\theta(a)$ into above equation we get

$$0=\hat{\tilde{f}}_v(\zeta)\cdot(1,\theta)=\hat{\tilde{f}}_{0_v}(\zeta)+\hat{\tilde{f}}_{1_v}(\zeta)\sin(a)+\hat{\tilde{f}}_{3_v}(\zeta)\cos(a).\tag{2.11}$$

Differentiating above equation with respect to parameter a once and twice, we get

$$\begin{cases}\hat{\tilde{f}}_{1_v}(\zeta)\cos(a)-\hat{\tilde{f}}_{3_v}(\zeta)\sin(a)=0,\\ -\hat{\tilde{f}}_{1_v}(\zeta)\sin(a)-\hat{\tilde{f}}_{3_v}(\zeta)\cos(a)=0.\end{cases}$$

It is easy to see that the last two equations imply that $\hat{\tilde{f}}_{1_v}(\zeta)=\hat{\tilde{f}}_{3_v}(\zeta)=0$ for $v\in\mathbf{R}^2$. Now by equation (2.11) we conclude that $\hat{\tilde{f}}_{0_v}(\zeta)=0$ for $v\in\mathbf{R}^2$.

Our goal is to show the Fourier transform of the generalized curl of f, $\mathscr{F}(\mathrm{d}f)$, is zero. Let $v=(-\cos(a),1,\sin(a))\in\theta^{\perp}$ and plug it into $\hat{\hat{f}}_{i_v}(\zeta)=0$ for $i=0,1,3$. We have

$$\begin{cases} -(\xi^1\hat{f}_0-\tau\hat{f}_1)\cos(a)+(\xi^2\hat{f}_0-\tau\hat{f}_2)+(\xi^3\hat{f}_0-\tau\hat{f}_3)\sin(a)=0,\\ (\xi^2\hat{f}_1-\xi^1\hat{f}_2)+(\xi^3\hat{f}_1-\xi^1\hat{f}_3)\sin(a)=0,\\ -(\xi^1\hat{f}_3-\xi^3\hat{f}_1)\cos(a)+(\xi^2\hat{f}_3-\xi^3\hat{f}_2)=0. \end{cases}$$

One may repeat above differentiation argument for the first equation to conclude that

$$\xi^1\hat{f}_0-\tau\hat{f}_1=\xi^2\hat{f}_0-\xi^0\hat{f}_3=\xi^3\hat{f}_0-\xi^0\hat{f}_3=0.$$

Using the same argument simultaneously for the second and third equations implies that

$$\xi^2\hat{f}_1-\xi^1\hat{f}_2=\xi^2\hat{f}_3-\xi^3\hat{f}_2=\xi^3\hat{f}_1-\xi^1\hat{f}_3=0.$$

Therefore, $\mathscr{F}(\mathrm{d}f)(\zeta)=0$ for a fixed $\zeta=\mathbf{e}^2$. One may choose three linearly independent vectors $v_1,v_2,v_3\in\mathbf{R}^3$, and conclude the same result.

To have the result for an arbitrary ζ, we use the fact that the Lorentzian transformation is transitive and rotates every space-like vector to a space-like vector. Let $\mathscr{L}_{\zeta^0}$ be a Lorentzian transformation with the property $\mathscr{L}_{\zeta^0}^{-1}\zeta=\zeta^0=\mathbf{e}^2$ and let $\mathscr{L}$ with $\mathscr{L}x=y$ be a Lorentzian transformation whose representation in Fourier domain is given by $\mathscr{L}_{\zeta^0}$. By the definition of Fourier transform, one has

$$\mathscr{F}[(\mathrm{d}f)\mathscr{L}(.)](\zeta)=\int(\mathrm{d}f)(\mathscr{L}x)e^{ix\cdot\zeta}dx=\int(\mathrm{d}f)(y)e^{i\mathscr{L}^{-1}y\cdot\zeta}\left|det\mathscr{L}^{-1}\right|dy$$

$$=\int(\mathrm{d}f)(y)e^{iy\cdot\mathscr{L}_{\zeta^0}^{-T}\zeta}\left|det\mathscr{L}^{-1}\right|dy.$$

Therefore,

$$\mathscr{F}[(\mathrm{d}f)\mathscr{L}(.)](\zeta)=\left|\det\mathscr{L}^{-1}\right|\mathscr{F}(\mathrm{d}f)(\mathscr{L}^{-T}\zeta).$$

But $\mathscr{L}^T=\mathscr{L}$ and $\mathscr{L}^{-1}(\zeta)=\zeta^0$, hence

$$\mathscr{F}[(\mathrm{d}f)\mathscr{L}(.)](\zeta)=\left|\det\mathscr{L}^{-1}\right|\mathscr{F}(\mathrm{d}f)(\zeta^0)=0,$$

since $\mathscr{F}(\mathrm{d}f)(\zeta^0) = 0$. This proves that for any space-like vector ζ near ζ^0, the Fourier transform of generalized curl of f vanishes as desired. For the general case $n > 3$, one needs to choose n linearly independent vectors $v_1, v_2, \ldots, v_n \in \mathbf{R}^n$ to show $\mathscr{F}(\mathrm{d}f)(\zeta) = 0$. ■

Corollary 2.4.1 *Let $f \in \mathscr{C}_0^\infty(\mathbf{R}^{1+n})$.*

i) For $n = 2$, if $Lf(x,\theta) = 0$ for θ near $\pm\theta_0$, then f is a smooth potential field with compact support, that is, $f = d\phi$ with some $\phi(x) \to 0$, as $|x| \to \infty$.

ii) For $n \geqslant 3$, if $Lf(x,\theta) = 0$ for θ near θ_0, then f is a smooth potential field with compact support, that is, $f = d\phi$ with some $\phi(x) \to 0$, as $|x| \to \infty$.

Proof i) The first part of Proposition 2.4.1 implies that $\mathscr{F}(\operatorname{curl} f) = 0$. Since $f \in \mathscr{C}_0^\infty(\mathbf{R}^{1+2})$, we extend f as zero outside of the $\operatorname{supp} f$. Now by analyticity of Fourier transform, $\mathscr{F}(\operatorname{curl} f)$ is zero everywhere. Applying the inverse Fourier transform implies that $\operatorname{curl} f = 0$ everywhere. Since the time-space $\mathbf{R}^{1+2}$ is a simply connected domain, there exists a finite smooth function ϕ such that $f = d\phi$; in fact let $x \in \operatorname{supp} f$ and x_0 be a point outside of $\operatorname{supp} f$. Let $c(t)$ be a path connecting x_0 to x. We define ϕ as follow:

$$\phi(x) = \int_{x_0}^{x} f(c(t)) \cdot c'(t) dt + \phi(x_0),$$

which is smooth and satisfies $f = \mathrm{d}\phi$.

ii) By the second part of Proposition 2.4.1 we know that $\mathscr{F}(\mathrm{d}f) = 0$. Similar argument as part (i) shows $\mathrm{d}f = 0$ and therefore, f is a smooth potential vector field with compact support. ■

Remark 2.4.1 i) For $n = 2$ there are two discrete choices of directions, $\pm\theta_0$, and this is necessary to have the result. Following example shows that one cannot decrease the number of directions from two to one. Let ζ be a space-like vector and $\phi \in \mathscr{S}$ be supported in the interior of open cone $\{|\tau| < |\xi|\}$. Consider $\theta_\pm(\zeta)$ defined by (2.8) and set

$$\eta = \hat{f}(\zeta) = (1, \frac{\xi^2}{\sqrt{-\tau^2 + |\xi|^2}}, \frac{-\xi^1}{\sqrt{-\tau^2 + |\xi|^2}})\hat{\phi}(\zeta).$$

Clearly η is a non-zero vector field in the Schwartz space $\mathscr{S}$ and is in the kernel of light-ray transform as it solves $(1,\theta_+(\zeta))\cdot\hat{f}(\zeta)=0$. Notice that, $(1,\theta_-(\zeta))\cdot\hat{f}(\zeta)\neq 0$. This example does not provide a compactly supported vector field, however, it shows this is an obstruction to consider only one light-ray and stay close to it for the reconstruction. For the Minkowski spaces of signature $1+3$ or higher, however, this is not an obstruction. For instance when $n=3$, one may consider a two-parameter family of directions, $\theta(a,b)$, near a fixed θ_0 and do the reconstruction process by perturbation.

ii) In above proposition for $n\geq 3$, to show the uniqueness results we performed differentiation which is not problematic. However, for the stable inversion results, a differentiation may not preserve the stability. In other words, one may choose several discrete values of non-zero parameters near zero to create an invertible linear system to get stability estimate results. For discussion, we refer the reader to proof of Theorem 2.5.1 for $n\geq 3$.

In the next section, we state a theorem on the recovery of analytic space-like singularities in the Minkowski case which is a tool to prove our main result.

2.5 Microlocal Recovery of Analytic Wavefront Set

In this section, we mainly follow the analytic microlocal analysis argument to show that we can recover all space-like analytic singularities of f conormal to the light-like lines along with integration of operator $(v.\nabla_x)L$. (See also P. Stefanov (2017), Lemma 3.1)

The definition of **Analytic Wave Front Set** (or "analytic singular spectrum) a scalar-valued distribution can be found in Sjöstrand (1982). For a vector-valued distribution $(f_0,f_1,f_2,\ldots,f_n)\in\mathscr{D}'(X,\mathbb{C}^{1+n})$, we define the analytic wave front set of f, $\mathrm{WF_A}(f)$, as the union of $\mathrm{WF_A}(f_i)$. Note that, for the vector-valued distribution f, the analytic wave front set $\mathrm{WF_A}(f)$ does not specify in which component f is singular. In our work, we follow the Sjöstrand's exposition.

Theorem 2.5.1 *Let $f\in\mathscr{E}'(\mathbf{R}^{1+n})$ and let γ_{x_0,θ_0} be a fixed light-like line so that $\gamma_{x,\theta}(s)\notin\operatorname{supp} f$ for $|s|\geq 1/C$ with some C for all (x,θ) near (x_0,θ_0).*

i) For $n=2$, if $Lf(x,\theta)=0$ for all x,θ near $(x_0,\pm\theta_0)$, then $\mathrm{WF_A}(\operatorname{curl} f)$ contains no space-like vectors conormal to $\gamma_{x_0,\pm\theta_0}$.

ii) For $n \geqslant 3$, if $Lf(x,\theta) = 0$ for all x, θ near (x_0, θ_0), then $\mathrm{WF_A}(\mathrm{d}f)$ contains no space-like vectors conormal to γ_{x_0,θ_0}.

Proof i) Let first $f \in \mathscr{C}^1(\mathbf{R}^{1+2})$. By assumption $Lf = 0$ only near γ_{x_0,θ_0}, therefore a localization is needed. We choose a local chart for the lines close to γ_{x_0,θ_0}, and without loss of generality we may assume that $x_0 = 0$ and $\theta_0 = \pm\mathbf{e}_2$. So we have $\gamma_0 = \gamma_{0,\mathbf{e}_2} = (s,0,s)$.

Since $Lf = 0$, we have $(v.\nabla_x)Lf = 0$ for $v \in \mathbf{R}^n$. Let v be an arbitrary fixed vector in $\mathbf{R}^n$ and $\zeta^0 \neq 0$ be a space-like vector conormal to γ_0 at $x_0 = 0$ with property $(1,\theta_0) \perp \zeta^0$. Applying the Lorentz transformation, we may assume that $\zeta^0 = \mathbf{e}^1 := (0,1,0) \in \mathbf{R}^{1+2}$. Our goal is to show that $(0,\zeta^0) \notin \mathrm{WF}_A(\mathrm{curl}\, f)$.

Let $\chi_N \in C_0^\infty(\mathbf{R}^2)$ be supported in $B(0,\varepsilon)$, with $\varepsilon > 0$ and $\chi_N = 1$ near $x_0 = 0$ so that

$$|\partial_x^\alpha \chi_N| \leq (CN)^{|\alpha|}, \quad \text{for } |\alpha| \leq N. \tag{2.12}$$

Then for $0 < \varepsilon \ll 1$, $\lambda > 0$, and θ near θ_0,

$$0 = \int e^{\mathrm{i}\lambda x\cdot\xi}(\chi_N(v.\nabla_x)Lf)(x,\theta)\,\mathrm{d}x = \iint e^{\mathrm{i}\lambda x\cdot\xi}\chi_N(x)\tilde{f}_v(\gamma_{x,\theta}(s))\cdot(1,\theta)\,\mathrm{d}s\,\mathrm{d}x.$$

If $(1,\theta)\cdot\zeta = 0$ with $\zeta = (\tau,\xi)$, then $\gamma_{x,\theta}\cdot\zeta = (s, x+s\theta)\cdot\zeta = x\cdot\xi$. Performing a change of variable $z = \gamma_{x,\theta}$ in above integral yields to

$$0 = \int e^{\mathrm{i}\lambda x\cdot\xi}(\chi_N(v.\nabla_x)Lf)(x,\theta)\mathrm{d}x = \int e^{\mathrm{i}\lambda x(z,\theta)\cdot\xi}a_N(z,\theta)\tilde{f}_{i_v}(z)(1,\theta)^i\mathrm{d}z \tag{2.13}$$

$$= \int e^{\mathrm{i}\lambda z\cdot\zeta}a_N(z,\theta)\tilde{f}_{i_v}(z)(1,\theta)^i\mathrm{d}z,$$

when $(1,\theta)\cdot\zeta = 0$. Notice that $a_N(0,\theta) = 1$.

Now let ζ be a space-like vector near ζ^0 and set $\theta = \theta_\pm(\zeta)$ (see (2.5)). Plugging $\theta_\pm(\zeta)$ into (2.13), we get

$$\int e^{\mathrm{i}\lambda z\cdot\zeta}\tilde{a}_N(z,\zeta)\tilde{f}_{i_v}(z)(1,\theta_\pm(\zeta))^i\,\mathrm{d}z = 0, \quad \text{near } \zeta = \mathbf{e}^1. \tag{2.14}$$

Here $\tilde{a}_N(z,\zeta) = a_N(z,\theta)$ where $\tilde{a}_N(0,\zeta) = 1$. Note also that for $\zeta \approx \zeta_0$, we have $\theta(\zeta) \approx \theta_0$.

In the next step, we apply the complex stationary phase method of Sjöstrand (1982), similar to the case where it is applied to the Calderón problem with partial data in Kenig, Sjöstrand, and Uhlmann (2007) and to the integral geometry problem in Frigyik et al. (2008); P. Stefanov and Uhlmann (2008). We need to analyze the phase function and its critical points.

Fix $0 < \delta \ll 1$ and let χ_δ be the characteristic function of the unit ball $B(0,\delta)$ in $\mathbf{R}^{1+2}$. With some w, $\eta \in \mathbf{R}^{1+2}$ close to $w = 0$, $\eta = \mathbf{e}^1$, multiply the l.h.s of (2.14) by

$$\chi_\delta(\zeta - \eta) e^{\mathrm{i}\lambda(\mathrm{i}(\zeta-\eta)^2/2 - w\cdot\zeta)}$$

and integrate w.r.t. ζ to get

$$\iint e^{\mathrm{i}\lambda\Phi(z,w,\zeta,\eta)} b_N(z,\zeta,\eta) \tilde{f}_{i_v}(z)(1,\theta_\pm(\zeta))^i \,\mathrm{d}z\,\mathrm{d}\zeta = 0, \tag{2.15}$$

where $b_N = \chi_\delta(\zeta-\eta)\tilde{a}_N$ is a new amplitude and

$$\Phi = (z-w)\cdot\zeta + \mathrm{i}(\zeta-\eta)^2/2.$$

Consider the phase function $\zeta \to \Phi$. If $w = z$, there is a unique real critical point $\zeta_c = \eta$, with property $\Im\Phi_{\zeta\zeta} > 0$ at $\zeta = \zeta_c$. For $w \neq z$, the phase Φ, as function of ζ, has a unique critical point $\zeta_c = \eta + \mathrm{i}(z-w)$. We now split the z integral in (2.15) into two parts: over the set $\Sigma = \{z;\ |z-w| \leqslant \delta/C^0\}$, for some $C^0 > 1$, and then over the complement of Σ. Since $|\Phi_\zeta|$ has a (δ-dependent) positive lower bound for $z \in \Sigma$(for ζ real) and there is no real critical point for the function $\zeta \to \Phi$ in this set, we can estimate that part of integral. Using the estimate (2.12), integration by parts N-times w.r.t. ζ, and the fact that on the boundary $|\zeta - \eta| = \delta$, the factor $e^{\mathrm{i}\lambda\Phi}$ is exponentially small with λ, we get

$$\Big| \iint_{\Sigma^c} e^{\mathrm{i}\lambda\Phi(z,w,\zeta,\eta)} b_N(z,\zeta,\eta) \tilde{f}_{i_v}(z)(1,\theta_\pm(\zeta))^i \,\mathrm{d}z\,\mathrm{d}\zeta \Big| \leq C(CN/\lambda)^N + CNe^{-\lambda/C}.$$

Note also that in the estimation above we used the fact that

$$e^{\mathrm{i}\lambda\Phi} = \frac{\bar{\Phi}_\zeta \cdot \partial_\zeta}{i\lambda|\Phi_\zeta|^2} e^{\mathrm{i}\lambda\Phi}.$$

Now on the set $\{z;\ |z-w| \leqslant \delta/\tilde{C}\}, \tilde{C} \gg 1$, we apply the complex stationary phase method for the rest of ζ-integral in (2.15). To estimate (2.15) for $z \in \Sigma$, we set: $\psi(z,w,\eta) = \Phi|_{\zeta=\zeta_c}$. Therefore,

$$\psi = \eta \cdot (z-w) + \mathrm{i}|z-w|^2 - \frac{\mathrm{i}}{2}|z-w|^2 = \eta \cdot (z-w) + \frac{\mathrm{i}}{2}|z-w|^2.$$

Clearly the new phase function $\psi(z,w,\eta)$ satisfies

$$\psi_z(z,z,\zeta) = \zeta, \quad \psi_w(z,z,\zeta) = -\zeta, \quad \psi(z,z,\zeta) = 0.$$

For (z,ζ) close to $(0,\mathbf{e}^1)$, we use this phase function and apply Theorem 2.8 in Sjöstrand (1982)] and the remark after it to the ζ-integral above to get

$$\begin{aligned}
&\iint_\Sigma e^{\mathrm{i}\lambda\Phi_+(z,w,\zeta,\eta)} b_N(z,\zeta,\eta)\tilde{f}_{i_v}(z)(1,\theta_\pm(\zeta))^i \mathrm{d}z\,\mathrm{d}\zeta \\
&= \int_\Sigma e^{\mathrm{i}\lambda\Phi(z,w,\zeta_c,\eta)} b_N(z,\zeta_c,\eta)\tilde{f}_{i_v}(z)(1,\theta_\pm(\zeta_c))^i \mathrm{d}z \\
&= \int_\Sigma e^{\mathrm{i}\lambda\psi(z,w,\eta)} b_\lambda(z,w,\eta)\tilde{f}_{i_v}(z)(1,\theta_\pm(z,w,\eta))^i \mathrm{d}z \\
&= \int_\Sigma e^{\mathrm{i}\lambda\psi(z,\beta)} b_\lambda(z,\beta)\tilde{f}_{i_v}(z)(1,\theta_\pm(z,\beta))^i \mathrm{d}z \\
&= \int_\Sigma e^{\mathrm{i}\lambda\psi(z,\beta)} \tilde{f}_{i_v}(z)\tilde{B}^i_{\lambda_\pm}(z,\beta)\mathrm{d}z = \mathscr{O}(\lambda^{n/2}(CN/\lambda)^N + CNe^{-\lambda/C})
\end{aligned} \tag{2.16}$$

where $\beta = (w,\eta)$, and $\tilde{B}_{\lambda_\pm}$ is a classical elliptic analytic symbol of order 0 with principal part equal

$$\sigma_p(\tilde{B}_{\lambda_\pm}(z,z,\zeta)) \equiv (1,\theta_\pm(\zeta)), \quad \text{up to an elliptic factor near } (z,\beta) = (0,0,\mathbf{e}^1),$$

with $\theta_\pm(\zeta) = (\theta^1_+(\zeta),\theta^2_+(\zeta))$ defined by (2.5). In particular, for $(z,w,\zeta) = (0,0,\mathbf{e}^1)$ we have

$$\sigma_p(\tilde{B}_{\lambda_\pm}(0,0,\mathbf{e}^1)) \equiv (1,\theta_\pm(\mathbf{e}^1)) = (1,0,\pm 1) = (1,\pm\mathbf{e}_2), \quad \text{up to an elliptic factor.}$$

For $z \in \Sigma$ with $\delta \ll 1$ and $|w| \ll 1$, η close to $\mathbf{e}^1$, the variable (z,β) in (2.16) is near $(0,0,\mathbf{e}^1)$ and therefore $\tilde{B}_{\lambda_\pm}$ is independent of N as $\chi_N = 1$ near the origin. Choose now N so that $N \le \lambda/(Ce) \le N+1$ to get the following exponential error on the right,

$$\int_\Sigma e^{\mathrm{i}\lambda\psi(z,\beta)} \tilde{f}_{i_v}(z) \tilde{B}^i_{\lambda_\pm}(z,\beta)\mathrm{d}z = \mathscr{O}(e^{-\lambda/C}). \tag{2.17}$$

Microlocal Ellipticity. Now we show that for $(1,\theta_\pm(\zeta))$, equations in (2.17) form an elliptic system of equations at $(0,0,\zeta^0)$. Let (z,z,ζ) near $(0,0,\zeta^0)$ and v be fixed, and consider the principal symbols $\sigma_p(\tilde{B}_{\lambda_\pm}(z,z,\zeta)) \equiv (1,\theta_\pm(\zeta))$. Microlocal version of ellipticity is equivalent to show that for a constant vector field $\tilde{f}_v = (\tilde{f}_{0_v}, \tilde{f}_{1_v}, \tilde{f}_{2_v})$,

$$(1,\theta_\pm(\zeta))^i \tilde{f}_{i_v} = 0$$

forms an elliptic system. Above equations can be written as

$$\begin{cases} \tilde{f}_{0_v} + \frac{1}{|\xi|^2}(-\tau\xi^1 + \sqrt{-\tau^2+|\xi|^2}\xi^2)\tilde{f}_{1_v} + \frac{1}{|\xi|^2}(-\tau\xi^2 - \sqrt{-\tau^2+|\xi|^2}\xi^1)\tilde{f}_{2_v} = 0, \\ \tilde{f}_{0_v} + \frac{1}{|\xi|^2}(-\tau\xi^1 - \sqrt{-\tau^2+|\xi|^2}\xi^2)\tilde{f}_{1_v} + \frac{1}{|\xi|^2}(-\tau\xi^2 + \sqrt{-\tau^2+|\xi|^2}\xi^1)\tilde{f}_{2_v} = 0. \end{cases}$$

By similar arguments as it is shown in Proposition 2.4.1 for $n=2$, one may conclude that

$$\begin{cases} 0 = \xi^2\tilde{f}_{1_v} - \xi^1\tilde{f}_{2_v} = (\xi\cdot v)(\partial_2 f_1 - \partial_1 f_2) \\ 0 \ = \tau\tilde{f}_{1_v} - \xi^1\tilde{f}_{0_v} = (\xi\cdot v)(\partial_0 f_1 - \partial_1 f_0) \end{cases} \implies \partial_2 f_1 - \partial_1 f_2 = \partial_0 f_1 - \partial_1 f_0 = 0.$$

Clearly $\partial_2 f_1 - \partial_1 f_2 = 0$ implies that $\tilde{f}_{1_v} = \tilde{f}_{2_v} = 0$ (for definition of $\tilde{f}_{i_v}$ see Proposition 2.4.1) and therefore

$$\tilde{f}_{0_v} = v^1(\partial_1 f_0 - \partial_0 f_1) + v^2(\partial_2 f_0 - \partial_0 f_2) = 0.$$

Since v is arbitrary in $\mathbf{R}^2$, any two linearly independent vectors v_1 and v_2 implies that $\partial_2 f_0 - \partial_0 f_2 = 0$. Therefore, the equation (2.17) leads to the following system of equations

$$\begin{cases} \int_\Sigma e^{\mathrm{i}\lambda\psi(z,\beta)}[v^1(\partial_1 f_0 - \partial_0 f_1)(x) + v^2(\partial_2 f_0 - \partial_0 f_2)(x)]B^0_\lambda(z,\beta)\,\mathrm{d}z = \mathscr{O}(e^{-\lambda/C}) \\ \int_\Sigma e^{\mathrm{i}\lambda\psi(z,\beta)}[v^2(\partial_2 f_1 - \partial_1 f_2)]B^1_\lambda(z,\beta)\,\mathrm{d}z = \mathscr{O}(e^{-\lambda/C}) \\ \int_\Sigma e^{\mathrm{i}\lambda\psi(z,\beta)}[v^1(\partial_1 f_2 - \partial_2 f_1)]B^2_\lambda(z,\beta)\,\mathrm{d}z = \mathscr{O}(e^{-\lambda/C}), \end{cases}$$

where up to an elliptic factor, we have

$$\sigma_p(B^i_\lambda(z,z,\zeta)) \equiv \begin{cases} 1 & i=0 \\ \theta^1_+(\zeta) & i=1 \\ \theta^2_+(\zeta) & i=2. \end{cases}$$

The vector v is arbitrary in $\mathbf{R}^2$. Thus, for any choice of two linearly independent vectors, at $(z,z,\zeta)=(0,0,\zeta^0)$ above elliptic system of equations implies that $(0,\zeta^0)\notin \mathrm{WF_A}(\mathrm{curl}\, f)$ as desired. Notice that above system is an overdetermined system of equations since the term $\partial_1 f_2 - \partial_2 f_1$ is repeated in the second and third equations. This is due to the property of $(v.\nabla_x)Lf$ and $\tilde{f}_v$ as we pointed out on Remark 2.3.2.

Now if $f\in\mathscr{E}'(\mathbf{R}^{1+2})$ is a distribution, as stated in the Theorem 2.5.1, the result still holds in the sense of distributions. In fact, one may take a sequence of $\mathscr{C}^1$-smooth functions which converges to the distribution f. The equation (2.14) holds for each smooth function. Now the z-integral in (2.14) can be thought in the sense of distributions as the integrand can be considered as the action of a distribution on a smooth function.

ii) Let first $f\in\mathscr{C}^1(\mathbf{R}^{1+n})$. By assumption, $Lf=0$ only near γ_{x_0,θ_0}, so we choose a local chart for the lines close to γ_{x_0,θ_0}. Since $Lf=0$, we have $(v.\nabla_x)Lf=0$ for $v\in\mathbf{R}^n$. Let v be an arbitrary fixed vector in $\mathbf{R}^n$ and let $x_0=0$ and $\theta_0=\pm\mathbf{e}_n$. Our goal is to show $(0,\zeta^0)\notin \mathrm{WF_A}(\mathrm{d}f)$ for ζ^0 a non-zero space-like vector and conormal to γ_0 at $x_0=0$. Applying the Lorentz transformation, we may assume that $\zeta^0=\mathbf{e}^{n-1}:=(0,\dots,0,1,0)\in\mathbf{R}^{1+n}$. Let $\chi_N\in C^\infty_0(\mathbf{R}^n)$ be supported in $B(0,\varepsilon)$, with $\varepsilon>0$ and $\chi_N=1$ near $x_0=0$ so that

$$|\partial^\alpha_x \chi_N| \le (CN)^{|\alpha|}, \quad \text{for } |\alpha|\le N. \tag{2.18}$$

Then for $0<\varepsilon\ll 1$, $\lambda>0$, and θ near θ_0,

$$0=\int e^{\mathrm{i}\lambda x\cdot\xi}(\chi_N(v.\nabla_x)Lf)(x,\theta)\,\mathrm{d}x = \iint e^{\mathrm{i}\lambda x\cdot\xi}\chi_N(x)\tilde{f}_v(\gamma_{x,\theta}(s))\cdot(1,\theta)\,\mathrm{d}s\,\mathrm{d}x.$$

Similar to the first part of theorem, we make a change of variable $z = \gamma_{x,\theta}$ to get

$$0 = \int e^{\mathrm{i}\lambda x\cdot\xi}(\chi_N(v.\nabla_x)Lf)(x,\theta)\mathrm{d}x = \int e^{\mathrm{i}\lambda x(z,\theta)\cdot\xi}a_N(z,\theta)\tilde{f}_{i_v}(z)(1,\theta)^i\mathrm{d}z \tag{2.19}$$

$$= \int e^{\mathrm{i}\lambda z\cdot\zeta}a_N(z,\theta)\tilde{f}_{i_v}(z)(1,\theta)^i\mathrm{d}z,$$

when $(1,\theta)\perp\zeta$. Notice that $a_N(0,\theta) = 1$.

Let $a_1, a_2, \ldots, a_{n-1}$, be $n-1$ non-zero parameters near zero. We set $\theta(a_1, a_2, \ldots, a_{n-1})$ to be the n-dimensional spherical coordinates where

$$\begin{cases} \theta^1 = \sin(a_{n-1})\sin(a_{n-2})\sin(a_{n-3})\ldots\sin(a_4)\sin(a_3)\sin(a_2)\sin(a_1) \\ \theta^2 = \sin(a_{n-1})\sin(a_{n-2})\sin(a_{n-3})\ldots\sin(a_4)\sin(a_3)\sin(a_2)\cos(a_1) \\ \theta^3 = \sin(a_{n-1})\sin(a_{n-2})\sin(a_{n-3})\ldots\sin(a_4)\sin(a_3)\cos(a_2) \\ \theta^4 = \sin(a_{n-1})\sin(a_{n-2})\sin(a_{n-3})\ldots\sin(a_4)\cos(a_3) \\ \vdots \\ \theta^{n-2} = \sin(a_{n-1})\sin(a_{n-2})\cos(a_{n-3}) \\ \theta^{n-1} = \sin(a_{n-1})\cos(a_{n-2}) \\ \theta^n = \cos(a_{n-1}) \end{cases}$$

Clearly $\left|\theta(a_1, a_2, \ldots, a_{n-1})\right| = 1$, $\theta(a_1, a_2, \ldots, 0) = \mathbf{e}_n$. Considering the n-dimensional spherical coordinate, one may solve the equation $(1,\theta)\cdot\zeta = 0$ for $\zeta = (\tau,\xi)$ to get

$$\zeta((a_1, a_2, \ldots, a_{n-1}),\xi) = (-\theta(a_1, a_2, \ldots, a_{n-1})\cdot\xi, \xi).$$

To simplify our analysis, we show the rest of proof for $n = 3$. For $n > 3$, one may repeat the following arguments to conclude the result. Let

$$\theta(a,b) = \sin(a)\sin(b)\mathbf{e}_1 + \sin(a)\cos(b)\mathbf{e}_2 + \cos(a)\mathbf{e}_3$$

be the 3-dimensional spherical coordinates. Plugging $\theta(a,b)$ into (2.19) we get

$$\int e^{\mathrm{i}\lambda\phi(z,\zeta)}a_N(z,\theta(a,b))\tilde{f}_{i_v}(z)(1,\theta(a,b))^i\,\mathrm{d}z = 0, \quad \text{near } a = 0,$$

where $\phi(z,\zeta) = z\cdot\zeta((a,b),\xi)$ and $a_N(z,\theta(a,b)) = \chi_N(x - s\theta(a,b))$ with $a_N(0,(a,b)) = 1$. Note that

$$\phi_z(0,\zeta) = \zeta, \quad \phi_{z\zeta} = \mathrm{Id}.$$

It is more convenient to work with ζ variable instead of $((a,b),\xi)$. So let b be a non-zero fixed parameter near zero. We show that the map $((a,b),\xi) \to \zeta \in \mathbf{R}^{1+3}$ is a local analytic diffeomorphism near $((0,b),\mathbf{e}^2)$. More precisely, the determinant of Jacobean associated with the map $((a,b),\xi) \to \zeta \in \mathbf{R}^{1+3}$ is

$$-\cos(a)\sin(b)\xi^1 - \cos(a)\cos(b)\xi^2 + \sin(a)\xi^3,$$

which is equal to $-\sin(b)\xi^1 - \cos(b)\xi^2$ near $a = 0$. Now the fixed parameter b (near zero) and our choice of ζ^0 imply that the determinant is $-\cos(b)$ which is non-zero. Hence, one may apply the Implicit Function Theorem near $a = 0$ to locally invert the map to $\zeta \to ((a,b),\xi) \in \mathbf{R}^{1+3}$. One may compute a explicitly to get

$$a = a(\zeta) = -\tan^{-1}\left(\frac{\xi^3}{\sin(b)\xi^1 + \cos(b)\xi^2}\right) + \sin^{-1}\left(-\frac{\tau}{\sqrt{(\sin(b)\xi^1 + \cos(b)\xi^2)^2 + (\xi^3)^2}}\right)$$

which maps $a = 0$ to ζ^0 diffeomorphically. Notice that for the fixed parameter b and $\zeta \approx \zeta^0$, $a(\zeta)$ is the unique solution of the equation

$$-\tau = -\theta(a,b)\cdot\xi = \sin(a)\sin(b)\xi^1 + \sin(a)\cos(b)\xi^2 + \cos(a)\xi^3,$$

near $a = 0$. Therefore, we may work in the ζ variables instead of the $((a,b),\xi)$ to get

$$\int e^{\mathrm{i}\lambda z\cdot\zeta}\tilde{a}_N(z,\zeta)\tilde{f}_{i_\nu}(z)(1,\theta(\zeta))^i\,\mathrm{d}z = 0, \quad \text{near } \zeta = \mathbf{e}^2,$$

where $\tilde{a}_N(z,\zeta) = a_N(z,\theta(a,b))$ and $\tilde{a}_N(0,\zeta) = 1$.

In the next step, we analyze the phase function and its critical points. (A similar argument as in the first part of theorem by applying the complex stationary phase method of Sjöstrand)

Fix $0 < \delta \ll 1$ and let χ_δ be the characteristic function of the unit ball $B(0,\delta)$ in $\mathbf{R}^{1+3}$. With some w, $\eta \in \mathbf{R}^{1+3}$ close to $w = 0$, $\eta = \mathbf{e}^2$, multiply the l.h.s. of above integral equation by

$$\chi_\delta(\zeta - \eta) e^{\mathrm{i}\lambda(\mathrm{i}(\zeta-\eta)^2/2 - w\cdot\zeta)}$$

and integrate w.r.t. ζ to get

$$\iint e^{\mathrm{i}\lambda\Phi(z,w,\zeta,\eta)} b_N(z,\zeta,\eta)\tilde{f}_{i_v}(z)(1,\theta(\zeta))^i \mathrm{d}z\,\mathrm{d}\zeta = 0, \quad \text{near } \zeta = \mathbf{e}^2, \tag{2.20}$$

where $b_N = \chi_\delta(\zeta - \eta)\tilde{a}_N$ is a new amplitude and

$$\Phi = (z-w)\cdot\zeta + \mathrm{i}(\zeta-\eta)^2/2.$$

Now consider the phase function $\zeta \to \Phi$. If $w = z$, there is a unique real critical point $\zeta_c = \eta$, which satisfies $\Im\Phi_{\zeta\zeta} > 0$ at $\zeta = \zeta_c$. For $w \neq z$, the phase Φ, as function of ζ, has a unique critical point $\zeta_c = \eta + \mathrm{i}(z-w)$.

Now we split the z-integral (2.20) into two parts: over $\Sigma = \{z;\ |z-w| \leqslant \delta/C^0\}$, for some $C^0 > 1$, and then over the complement of Σ. Since $|\Phi_\zeta|$ has a (δ-dependent) positive lower bound for $|z-w| > \delta/C^0$(for ζ real) and there is no real critical point for the function $\zeta \to \Phi$ in this set, we can estimate that part of integral. Using the estimate (2.18), integration by parts N-times w.r.t. ζ, and the fact that on the boundary $|\zeta - \eta| = \delta$, the factor $e^{\mathrm{i}\lambda\Phi}$ is exponentially small with λ, we get

$$\Big| \iint_{\Sigma^c} e^{\mathrm{i}\lambda\Phi(z,w,\zeta,\eta)} b_N(z,\zeta,\eta)\tilde{f}_{i_v}(z)(1,\theta(\zeta))^i \mathrm{d}z\,\mathrm{d}\zeta \Big| \leq C(CN/\lambda)^N + CNe^{-\lambda/C}.$$

Similar to part (i), for above inequality we used the fact that

$$e^{\mathrm{i}\lambda\Phi} = \frac{\bar{\Phi}_\zeta \cdot \partial_\zeta}{i\lambda|\Phi_\zeta|^2} e^{\mathrm{i}\lambda\Phi}.$$

Now on the set $\{z;\ |z-w| \leqslant \delta/\tilde{C}\}, \tilde{C} \gg 1$, we apply stationary phase method for the rest of ζ-integral in (2.20). To estimate (2.20) for $z \in \Sigma$, we set: $\psi(z,w,\eta) = \Phi|_{\zeta=\zeta_c}$. Therefore,

$$\psi = \eta\cdot(z-w) + \mathrm{i}|z-w|^2 - \frac{\mathrm{i}}{2}|z-w|^2 = \eta\cdot(z-w) + \frac{\mathrm{i}}{2}|z-w|^2.$$

Notice that $\psi(z,w,\eta)$ satisfies

$$\psi_z(z,z,\eta)=\eta=\phi_z(0,\eta),\quad \psi_w(z,z,\eta)=-\eta=-\phi_z(0,\eta),\quad \psi(z,z,\eta)=0. \tag{2.21}$$

For (z,ζ) close to $(0,\mathbf{e}^2)$, we use this phase function and apply Theorem 2.8 in Sjöstrand (1982) and the remark after it to the ζ-integral above to get

$$\begin{aligned}
&\iint_\Sigma e^{\mathrm{i}\lambda\Phi_\mp(z,w,\zeta,\eta)}b_N(z,\zeta,\eta)\tilde{f}_{i_\nu}(z)(1,\theta(\zeta))^i\,\mathrm{d}z\,\mathrm{d}\zeta\\
&=\int_\Sigma e^{\mathrm{i}\lambda\Phi(z,w,\zeta_c,\eta)}b_N(z,\zeta_c,\eta)\tilde{f}_{i_\nu}(z)(1,\theta(\zeta_c))^i\mathrm{d}z\\
&=\int_\Sigma e^{\mathrm{i}\lambda\psi(z,w,\eta)}b_\lambda(z,w,\eta)\tilde{f}_{i_\nu}(z)(1,\theta(z,w,\eta))^i\mathrm{d}z\\
&=\int_\Sigma e^{\mathrm{i}\lambda\psi(z,\beta)}b_\lambda(z,\beta)\tilde{f}_{i_\nu}(z)(1,\theta(z,\beta))^i\mathrm{d}z\\
&=\int_\Sigma e^{\mathrm{i}\lambda\psi(z,\beta)}\tilde{f}_{i_\nu}(z)\tilde{B}^i_\lambda(z,\beta)\mathrm{d}z=\mathscr{O}(\lambda^{n/2}(CN/\lambda)^N+CNe^{-\lambda/C}).
\end{aligned}\tag{2.22}$$

Here $\beta=(w,\eta)$ and $\tilde{B}_\lambda$ is a classical elliptic analytic symbol of order 0. For $z\in\Sigma$ with $\delta\ll 1$ and $|w|\ll 1$, η near $\mathbf{e}^2$, the variable (z,β) in (2.22) is near $(0,0,\mathbf{e}^2)$ and then $\tilde{B}_\lambda$ is independent of N because $\chi_N=1$ near the origin. We choose N so that $N\le\lambda/(Ce)\le N+1$. Therefore, we get the following exponential error on the right

$$\int_\Sigma e^{\mathrm{i}\lambda\psi(z,\beta)}\tilde{f}_{i_\nu}(z)\tilde{B}^i_\lambda(z,\beta)\mathrm{d}z=\mathscr{O}(e^{-\lambda/C}).$$

Since the phase function satisfies the properties in (2.21), on a small neighborhood of ζ^0, we perform the following change of variable in above integral equation:

$$(z,w,\eta)\longrightarrow(z,w,\zeta)=(z,w,\phi_z(w,\eta)),$$

which yields to

$$\int_\Sigma e^{\mathrm{i}\lambda\psi(z,w,\zeta)}\tilde{f}_{i_\nu}(z)\tilde{B}^i_\lambda(z,w,\zeta)\mathrm{d}z=\mathscr{O}(e^{-\lambda/C}). \tag{2.23}$$

Here $\tilde{B}_\lambda$ is a new classical elliptic symbol of order zero with the principal part of $\sigma_p(\tilde{B}_\lambda(z,z,\zeta)) \equiv (1,\theta(\zeta))$, up to an elliptic factor. In particular, for $(z,w,\zeta) = (0,0,\zeta^0)$ we have

$$\sigma_p(\tilde{B}_\lambda(0,0,\zeta^0)) \equiv (1,\theta(\zeta^0)) = (1,0,0,1) = (1,\mathbf{e}_3).$$

As it is shown above, the map $(a,\xi) \to \zeta$ is a local diffeomorphsim near $a = 0$ (equivalently near $\zeta^0 = \mathbf{e}^2$). Therefore, we work with the principal symbol in terms of (a,ξ) instead, which means up to an elliptic factor

$$\sigma_p(\tilde{B}_\lambda(z,z,(a,\xi)) \equiv (1,\theta(a,b)).$$

To show $(0,\zeta^0) \notin \mathrm{WF_A}(\mathrm{d}f)$, we need to form an elliptic system of equations using (2.23). Let $(z,z,(a,\xi)) \approx (0,0,(0,\xi^0))$ and v be a fixed vector. For our goal, we slightly perturb $\theta(a,b)$ near $a \approx 0$ and b. Let

$$\{\Theta_k\}_{k=0}^3 = \{(1,\theta(a,b)),(1,\theta(-a,b)),(1,\theta(a,-b)),(1,\theta(0,b))\}$$

be the set of perturbations of $\theta(a,b)$, with property $\sigma_p(\tilde{B}_{\lambda_k}(z,z,(a,\xi)) = \Theta_k$, for $k = 0,1,2,3$. Microlocal version of ellipticity is equivalent to show that for a constant vector field $(\tilde{f}_{0_v},\tilde{f}_{1_v},\tilde{f}_{2_v},\tilde{f}_{3_v})$,

$$\Theta\tilde{f}_v = 0$$

forms an elliptic system of equations. Here the matrix $[\Theta]_{4\times4}$ is the associated matrix with above principal symbols, Θ_k. The matrix $[\Theta]$ is invertible since its determinant equals to

$$\det\begin{pmatrix} 1 & \sin(a)\sin(b) & \sin(a)\cos(b) & \cos(a) \\ 1 & -\sin(a)\sin(b) & -\sin(a)\cos(b) & \cos(a) \\ 1 & -\sin(a)\sin(b) & \sin(a)\cos(b) & \cos(a) \\ 1 & 0 & 0 & 1 \end{pmatrix} = 4\sin^2(a)\sin(b)\cos(b)(1-\cos(a))$$

which is non-zero for a and our fixed parameter b near zero. Therefore, $\Theta\tilde{f}_v = 0$ implies that $\tilde{f}_v = 0$. This means the equation (2.23) with $\{\Theta_k\}_{k=0}^3$ leads to the following system of equations related to $\theta_0 = \mathbf{e}_3$:

$$\begin{cases} \int_\Sigma e^{i\lambda\psi(z,\beta)}\tilde{f}_{0_v}B_\lambda^0(z,\beta)\mathrm{d}z = \mathscr{O}(e^{-\lambda/C}) \\ \int_\Sigma e^{i\lambda\psi(z,\beta)}\tilde{f}_{1_v}B_\lambda^1(z,\beta)\mathrm{d}z = \mathscr{O}(e^{-\lambda/C}) \\ \int_\Sigma e^{i\lambda\psi(z,\beta)}\tilde{f}_{2_v}B_\lambda^2(z,\beta)\mathrm{d}z = \mathscr{O}(e^{-\lambda/C}) \\ \int_\Sigma e^{i\lambda\psi(z,\beta)}\tilde{f}_{3_v}B_\lambda^3(z,\beta)\mathrm{d}z = \mathscr{O}(e^{-\lambda/C}), \end{cases}$$

where up to an elliptic factor, we get

$$\sigma_p(B_\lambda^i(z,z,\zeta)) \equiv \begin{cases} 1 & i=0 \\ \sin(a)\sin(b) & i=1 \\ \sin(a)\cos(b) & i=2 \\ \cos(a) & i=3. \end{cases}$$

Here $\tilde{f}_{i_v}$ is defined by Proposition 2.3.1. Also, the phase function ψ satisfies the conditions (2.21) and $\Im\psi > C_0|z-w|^2$ as $\psi_{z\zeta} = \mathrm{Id}$. Note that, some components of $\mathrm{d}f$ are repeated in above equations. This forms an overdetermined system of equations for our fixed vector $v \in \mathbf{R}^3$. Since v is arbitrary, for any choice of three linearly independent vectors $\{v_i\}_{i=1}^3 \subseteq \mathbf{R}^3$, for $(z,z,(z,\xi)) = (0,0,(0,\xi^0))$ one may conclude that $(0,\zeta^0) \notin \mathrm{WF}_A(\mathrm{d}f)$, which proves the second part of the theorem for $n=3$. For the general case $n>3$, one needs to slightly perturb $\theta(a_1,a_2,\ldots,a_{n-1})$ with respect to parameters $a_1,a_2,\ldots,a_{n-1}$. This forms an elliptic system $\Theta\tilde{f}_v = 0$ for the microlocal ellipticity discussion and therefore concludes the result. Now for any vector-valued distribution $f \in \mathscr{E}'(\mathbf{R}^{1+n})$, as we pointed out in the proof of part (i), the result remains true in the sense of distributions. ■

Remark 2.5.1 By Fundamental Theorem of Calculus, the potential field is in the kernel of operator L, so one could only hope to recover $\operatorname{curl} f$ for $n = 2$. For the Riemannian case with dimension $n \geq 3$, foliation (slicing method) can be used to achieve the uniqueness results. One may restrict x to a two-dimensional plane, say $\Pi = \{(t,x) : x^3 = \cdots = x^n = \text{const}\}$, and apply the results in Theorem 2.5.1 when $n = 2$. This only recovers some components of the generalized curl of the vector field f even if different permutations are chosen to fix different components of x. In order to recover all other components, one needs to perturb above two-dimensional planes. Therefore, such a slicing technique can be done as the transform is overdetermined. However, additional assumption which is the information of light-ray for two discrete directions $(1, \pm\theta)$ is required. Even though the foliation method is a simpler approach for the recovery of the vector field f, we do not perform foliation to achieve stronger results.

2.6 Proof of Main Result

For our main result we need the following lemma which is a unique analytic continuation result across a time-like hypersurface in the Minkowski time-space.

Lemma 2.6.1 *Let $f \in \mathscr{C}^\infty(\mathbf{R}^{1+n})$ and let γ_{x_0,θ_0} be a fixed light-like line in the Minkowski time-space so that $\gamma_{x,\theta}$ does not intersect* $\operatorname{supp} f$ *for $|s| \geq 1/C$ with some C for all (x,θ) near (x_0,θ_0). Fix $z_0 = (s_0, x_0 + s_0\theta_0) \in \gamma_{x_0,\theta_0}$, let S be an analytic time-like hypersurface near z_0 and assume that γ_{x_0,θ_0} is tangent to S at z_0.*

i) For $n = 2$, if $Lf(x,\theta) = 0$ near $(x_0, \pm\theta_0)$ and if $\operatorname{curl} f = 0$ *on one side of S near z_0, then* $\operatorname{curl} f = 0$ *near z_0.*

ii) For $n \geq 3$, if $Lf(x,\theta) = 0$ near (x_0,θ_0) and if $\mathrm{d}f = 0$ *on one side of S near z_0, then* $\mathrm{d}f = 0$ *near z_0.*

Proof Let $n \geq 3$ and assume that $z_0 \in \operatorname{supp} \mathrm{d}f$. By assumption $(v.\nabla_x)Lf(x,\theta) = 0$ near (z_0,θ_0). Since $\mathrm{d}f$ is non-zero only in half space S, then there exists ζ_0 such that $(z_0,\zeta_0) \in \mathrm{WF_A}(\mathrm{d}f)$, as $\mathrm{d}f$ cannot be analytic at z_0. By the definition of analytic wave front set for vector-valued distrubitions, there exist a component of $\mathrm{d}f$, say $f_{ij} = \partial_j f_i - \partial_i f_j$, where $(z_0,\zeta_0) \in \mathrm{WF_A}(f_{ij})$. In other words, if the half space S intersects the $\operatorname{supp} \mathrm{d}f$, it must intersect at least one of the components of $\mathrm{d}f$, say f_{ij}, as $\mathrm{d}f$ cannot be analytic at the intersection point. Now by Sato-Kawai-Kashiwara Theorem (see Sato, Kawai, and Kashiwara (1973); Sjöstrand (1982)), $(z_0,\zeta_0 + s\nu(z_0)) \in \mathrm{WF_A}(f_{ij})$, where $\nu(z_0)$ is one of the two unit conormals to S at z_0. This in turn implies that $(z_0, \frac{\zeta_0}{s} + \nu(z_0)) \in \mathrm{WF_A}(f_{ij})$ as the wave front set is a conic set. Now by passing to limit, we have $(z_0,\nu(z_0)) \in \mathrm{WF_A}(f_{ij})$ since the analytic wave front set is closed. By assumption on S, that vector is space-like and is conormal to $\gamma'_{x_0,\theta_0}(s_0)$. This contradicts Theorem 2.5.1 part (ii), which implies that $\mathrm{d}f = 0$ and completes the proof. For $n = 2$, one may repeat above arguments and use the first part of Theorem 2.5.1 to conclude the result. ■

We now are ready to state the proof of the main result.

Proof [*Proof of Theorem 2.2.1.*] Let $n \geq 3$. By assumption $(v.\nabla_x)Lf(x,\theta) = 0$. The proof follows from Theorem 2.1, P. Stefanov (2017) replacing $Lf(x,\theta)$ by $(v.\nabla_x)Lf(x,\theta)$ and applying the second part of Lemma 2.6.1.

To conclude the result for $n = 2$, one may use Lemma 2.6.1 part (i) and repeat the proof of Theorem 2.1, P. Stefanov (2017). ■

In the following examples we illustrate how our result imply the recovery of vector field up to a smooth potential field.

Example1. Let f be a vector field (distribution) supported in cone $\{(t,x) \in \mathbf{R}^{1+n} |\ |x| < c|t|\}$ and let Γ_{ρ_0} be the following surface:

$$\Gamma_{\rho_0} = \{(t,x) \in \mathbf{R}^{1+n} \mid \psi(t,x) = |x-x_0|^2 - c^2|t-t_0|^2 - \rho_0^2 = 0\},$$

for some $\rho_0 \geq 0$ and $0 < c < 1$. Assume now that f integrates to zero over all light-like lines γ in the exterior of Γ_{ρ_0}, $\operatorname{ext}(\Gamma_{\rho_0})$.

We show the vector field f can be recovered up to a potential field in the ext(Γ_{ρ_0}). By definition (z,ζ) is conormal to Γ_{ρ_0} if and only if

$$(z,\zeta) \in N^*\Gamma_{\rho_0} = \{(t,x,\tau,\xi) \in T^*(\mathbf{R}^{1+n} \times \mathbf{R}^{1+n}) | (t,x) \in \Gamma_{\rho_0}, (\tau,\xi) = 0 \text{ on } T_{(t,x)}\Gamma_{\rho_0}\}.$$

Clearly the gradient of ψ, $\nabla\psi$, is normal to surface Γ_{ρ_0} at (t,x). So by definition $\sigma\nabla\psi \cdot (dt,dx)$ is the conormal vector to surface Γ_{ρ_0} at (t,x). In fact, to find the conormal we compute the total differential of ψ, $d\psi$:

$$d\psi(t,x) = -2c^2(t-t_0)dt + 2(x-x_0)dx,$$

and therefore the covector:

$$(z,\zeta) = (t,x,\tau,\xi) = (t,x,-2\sigma c^2(t-t_0), 2\sigma(x-x_0)) \in N^*\Gamma_{\rho_0}, \quad \text{for } \sigma \in \mathbf{R},$$

is conormal to Γ_{ρ_0}. Clearly the $\zeta = (\tau,\xi)$ is space-like in the ext(Γ_{ρ_0}) as it is easy to show $|\tau| = 2\sigma c^2|t-t_0| \leq 2\sigma|x-x_0| = |\xi|$ in the ext(Γ_{ρ_0}). Therefore, for any decreasing family of ρ with the property $\rho \to \rho_0$, the surfaces Γ_ρ will be a family of analytic time-like hypersurfaces in the ext(Γ_{ρ_0}).

Let $\sigma = \frac{1}{2}$, $(t_0,x_0) = (0,0)$, and fixed $\rho > 0$ be the smallest one with the property that supp$f \cap \Gamma_\rho \neq \emptyset$ (supp$f \cap \Gamma_\rho$ is a compact set.) Now assume that γ_0 is tangent to Γ_ρ at z_0 (i.e. (z_0,ζ_0) is conormal to $\dot{\gamma}_0$). By compactness of supp$f$, we have $\gamma \notin$ supp$f$ for any γ approaching γ_0 in the ext(Γ_{ρ_0}). Theorem 2.5.1 implies $\mathrm{WF_A}(\mathrm{d}f)$ contains no space-like vector conormal to $\dot{\gamma}_0$ since by assumption $Lf = 0$ over all light-like lines γ near γ_0 on one side of analytic time-like hypersurface Γ_ρ, see Figure 2.1. Now using the analytic continuation result, Lemma 2.6.1, we can recover the vector field f up to a potential field.

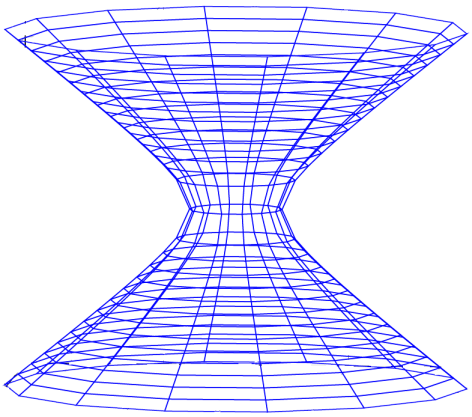

Figure 2.1. Γ_{ρ_0} with $0 < c < 1$.

Example 2. Let $f \in \mathscr{E}'(\mathbf{R}^{1+n})$ be so that supp f expands with a speed less than one and let Γ_0 be the following surface:

$$\Gamma_0 = \{(t,x) \in \mathbf{R}^{1+n} \mid \psi(t,x) = (|x-x_0|-R)^2 - c^2|t-t_0|^2 = 0\}, \quad \text{for some } 0 < c < 1.$$

Assume now that f integrates to zero over all light-like lines γ intersecting supp f outside of the surface Γ_0. We show the vector field f can be recovered up to a potential field in the ext(Γ_ρ), where the surface Γ_ρ with $\rho > 0$ is defined as follow:

$$\Gamma_\rho = \{(t,x) \in \mathbf{R}^{1+n} \mid \psi(t,x) = (|x-x_0|-R)^2 - c^2|t-t_0|^2 - \rho^2 = 0\}.$$

By definition, the covector:

$$(z,\zeta) = (t,x,\tau,\xi) = (t,x,-2\sigma c^2(t-t_0), 2\sigma \frac{x-x_0}{|x-x_0|}(|x-x_0|-R)) \in N^*\Gamma_\rho, \text{for } \sigma \in \mathbf{R},$$

is conormal to Γ_ρ. Note that $|\tau| = 2\sigma c^2|t-t_0|$ and $|\xi| = |2\sigma \frac{x-x_0}{|x-x_0|}(|x-x_0|-R)| = 2\sigma||x-x_0|-R|$. So in the ext$(\Gamma_\rho)$, the covector $\zeta = (\tau,\xi)$ is space-like (i.e. $|\tau| \leq |\xi|$.) Thus, for $\rho > 0$, the surfaces Γ_ρ will be a family of analytic time-like hypersurfaces.

Let $\sigma = \frac{1}{2}$, $z_0 = (t_0, x_0) = (0,0)$, and $\rho > 0$ fixed be the smallest one with the property that $\operatorname{supp} f \cap \Gamma_\rho \neq \emptyset$. Similar argument as in above example shows that the vector field f can be recovered up to a potential field on Γ_ρ. The case where $c = 0$ corresponds to the classical support theorem for balls.

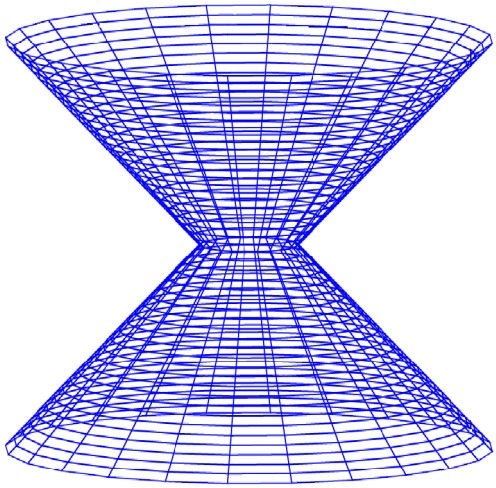

Figure 2.2. Γ_0 with $0 < c < 1$.

Note that on the surface Γ_0, there is no conormal covector at $t = t_0$ as $|x - x_0| = R$. Being outside of Γ_ρ guarantees the existence of conormal covector as $\rho > 0$ on Γ_ρ, see Figure 2.1.

Next example is a partial data case of Example 2 for the inverse recovery of a smooth potential field for the hyperbolic Dirichlet-to-Neumann (DN) maps. It is known that, all the integral lines can be extracted from the DN map for hyperbolic (wave) equations, see, e.g., Aicha (2015); Bellassoued and Dos Santos Ferreira (2011); Ramm and Rakesh (1991); Ramm and Sjöstrand (1991); Salazar (2013); P. D. Stefanov (1989); Waters (2014). Our result provides the optimal way of the inverse recovery process up to a smooth potential. A similar result for recovery of the unknown potential can be found in P. Stefanov and Yang (2018).

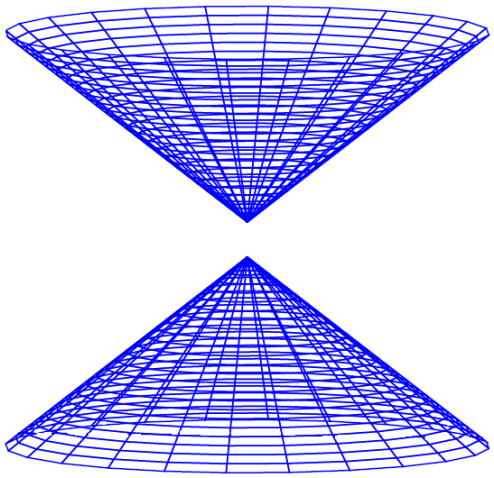

Figure 2.3. Γ_0 with $0 < c < 1$.

Example 3. Let $f \in \mathscr{E}'(\mathbf{R}^{1+n})$ be so that $\operatorname{supp} f$ expands with a speed less than one, and consider the cylinder $[0,T] \times \bar{\Omega}$ for some $T > 0$ and $\Omega \subset \mathbf{R}^n$. In Example 2 we showed that the vector field f can be recovered up to a smooth potential field in the exterior of Γ_ρ. Now consider the surface Γ as union of all those exteriors of time-like hypersurfaces for $t \in [0,T]$. This surface includes all light-like lines $\gamma_{x,\theta} = (s, x + s\theta)$, $(z,\theta) \in \mathbf{R}^n \times S^{n-1}$, not intersecting the top and the bottom of the cylinder $[0,T] \times \bar{\Omega}$, see Figure 2.3.

By Theorem 2.2.1, we can recover f up to $d\phi$, $\phi = 0$ on $[0,T] \times \bar{\Omega}$ in the set covered by those lines for $n \geq 3$. As we pointed out on Remark 2.4.1, for $n = 2$ there are two discrete choices of directions which means that for recovery of f up to a potential $d\phi$ one needs to know Lf along light-like $\gamma_{x,\theta}$ as well as knowing Lf along $\gamma_{x,-\theta}$. Note that our uniqueness results do not require the vector field to be compactly supported in time. Moreover, we are not considering any Cauchy data on circles on top and bottom of the cylinder, which means there is no internal measurement. This is the optimal way one can wish to recover the vector field f in this set. Uniqueness result in this paper and result in P. Stefanov and Yang (2018) (recovery of the unknown potential q in Γ) generalize the uniqueness results in Aicha (2015); Bellassoued and Dos Santos Ferreira (2011); Ramm and Rakesh (1991); Ramm and Sjöstrand (1991); Salazar (2013); P. D. Stefanov (1989); Waters (2014).

DYNAMIC X-RAY TOMOGRAPHY

*** This chapter concludes my original work: "Invertibility and stability for a generic class of radon transforms with application to dynamic operators." J. Inverse Ill-Posed Probl. 2018; https://doi.org/10.1515/jiip-2018-0014.**

Mathematical Tomography (or slice imaging) is in the forefront of scientific investigation due to its wide range of applications in medical imaging, biology, material sciences, and non-destructive testing. For instance, one may cite Cormack's Nobel Prize in medical imaging in 1979 where the Nobel Prize Committee realized his work, a Mathematical One.

The goal of tomography is to find the internal structure of an object by sending waves (acoustic waves or electromagnetic waves like radio/microwaves, visual light, X-rays, γ-rays) through the object and creating film (tomographic) images of objects using Radon transform.

The intricate mathematical process of image reconstruction (using inverse Radon transform) from X-ray projection of measured data at many different angles around the patient is called Computed Tomography (CT). In medical imaging, image reconstruction has fundamental impacts on image quality and therefore on radiation dose. Therefore, balancing a need for spatial clarity for diagnostic usefulness while constraining patient radiation exposure is a substantial question in this respect, as it plays an extremely crucial role in a patient's health and safety. To reduce the level of the risk in patient's treatment, one needs to lower the level of radiation exposure, which in turns leads to lack of data and therefore fundamental impacts on image quality in terms of high-resolution reconstructions.

This chapter, motivated by Cormack's contributions, is among the main objectives of modern integral geometry and inverse problems in particular in the area of Dynamic X-ray Tomography. We investigate the current challenges in data collection and image reconstruction of objects that move and change their shapes by time. Among the applications of this work, one can consider its major role in the X-ray CT scanning or MRI (Magnetic Resonance Imaging) of the heart or the lunges in medical imaging. Ignoring the dynamic behavior of the heart or the lunges, results in low spatial or temporal resolution of the reconstructed images, which leads to unreliable diagnosis and therefore irreversible consequences in patients' health and life. This is not only a pragmatic question, but an ethical and mathematical one which has been a subject of profound scientific studies. How much further risk should a patient be exposed in order to treat a current ailment? Mathematically, what methods can be used to reduce the radiation dose exposure to achieve the same levels of diagnostic accuracy? We found that one could utilize the proposed Global Bolker Condition to quantify how errors in the available measurements (X-ray signals) translate into errors in the image reconstructions of an object for instance the heart. Leveraging the insights provided by this result, scientists and doctors can answer the crucial question "For a given radiation dose, what is a desirable image reconstruction with the lowest possible noise without sacrificing image accuracy, spatial resolution, and most importantly, a patients' safety and health?"

The chapter concludes my original work which is published in the journal of Inverse and Ill-posed Problems. RabieniaHaratbar (2019)

3.1 Existing Results

The Tomography of moving objects has been attracting a growing interest recently, due to its wide range of applications in medical imaging, for example, X-ray of the heart or the lungs. Data acquisition and reconstruction of the object which changes its shape during the measurement is one of the challenges in computed tomography and dynamic inverse problems. The major difficulty in the reconstruction of images from the measurement sets is the fact that object changes between measurements but does not move fast enough compared to the speed of X-rays. This means that some singularities of the object might not be detectable even if the source fully rotates around the object. The application of known reconstruction methods (based on the inversion of the Radon transform) usually results in many motion artifacts within the reconstructed images if the motion is not taken into account. One extreme example will be the case when the object (or some small part of it) rotates with the same rate as the scanner. This leads to integration over the same family of rays (see also Natterer (1986)), and therefore, one cannot locally recover all the singularities.

Analytic techniques for reconstruction of dynamic objects, known as motion compensation, have been used widely for different types of motion. For affine deformation, see Crawford, King, Ritchie, and Godwin (1996),Desbat, Roux, and Grangeat (2007), B. Hahn (2014), B. N. Hahn (2014), A. I. Katsevich (1997), A. Katsevich (2008), A. Katsevich (2010), Roux, Desbat, Koenig, and Grangeat (2004).

For non-affine deformations, there is no inversion formula. Iterative reconstructions, however, do exist in order to detect singularities by approximation of inversion formulas for the parallel and fan beam geometries A. Katsevich (2006), as well as cone beam geometry A. Katsevich, Silver, and Zamyatin (2011). In a recent work, B. N. Hahn and Quinto (2016) studied the dynamic operator

$$\mathscr{A}f(s,t) = \int_{z\cdot\omega(t)=s} \mu(t,z) f(\psi_t(z)) \mathrm{d}S_z, \qquad \omega(t) = (\cos t, \sin t), \tag{3.1}$$

with a smooth motion where the limited data case has been analyzed, and characterization of visible and added singularities have been investigated.

Our work in this paper is motivated by these dynamic measurements. We first show this dynamic problem can be reduced to an integral geometry problem integrating over level curves. By an appropriate change of variable (see next section), $\mathscr{A}$ can be written as

$$\mathscr{A}f(s,t) = \int_{\psi_t^{-1}(x)\cdot\omega(t)=s} \hat{\mu}(t,x)f(x)\mathrm{d}S.$$

Therefore, we study the following general operator:

$$\mathscr{A}f(s,t) = \int_{\phi(t,x)=s} \mu(t,x)f(x)\mathrm{d}S_{s,t},$$

which allows us to study the original dynamic problem with a more general set of curves (see also Frigyik et al. (2008),) and then transfer the result to a dynamic operator $\mathscr{A}$ given by (3.1).

The dynamic operator $\mathscr{A}$ formulated as above falls into the general microlocal framework studied by Beylkin Beylkin (1984) (see also B. N. Hahn (2014)) which goes back to Guillemin and Sternberg Guillemin (1985); Guillemin and Sternberg (1977) who studied the integral geometry problems with a more general platform from the microlocal point of view. See also Frigyik et al. (2008), where a weighted integral transform has been studied on a compact manifold with a boundary over a general set of curves (a smooth family of curves passing through every point in every direction).

3.2 Main Results

The main novelty of our work, compared to previous works which are concentrated on the microlocal invertibility, is that for the dynamic problem, under some natural microlocal conditions, the actual uniqueness and stability results have been established. In fact, our imposed natural microlocal conditions guarantee that one can recover each singularity, and a functional analysis argument leads to stability results. We show that under these conditions, the dynamic operator is stably invertible in a neighborhood of pairs (ϕ,μ) in a generic set, and in particular, it is injective and stable for slow enough motion (which is not required to be periodic). This is similar to stability result studied in Homan and Zhou (2017) for the generalized Radon transform and in Frigyik et al. (2008) which coincide when the dimension is two.

The data is cut (restricted) in a way to have the normal operator related to the localized dynamic operator $\mathscr{A}$ as a pseudodifferential operator (ΨDO) near each singularity. We do not analyze the case where these conditions are not satisfied globally, but our analysis (see B. N. Hahn and Quinto (2016)) shows that one can still recover the visible singularities in a stable way, and periodicity or non-periodicity plays no role in the reconstruction process.

We also show that, due to the generality of our approach, our results can be implemented to other geometries, for instance, fan beam geometry. In a recent work by B. Hahn and Garrido (2019), a generalized Radon transform has been used to model the dynamic imaging operators. Using microlocal analysis results, they a reconstruction process which approximates the solution via a filtered back-projection type algorithm.

In this section, we first introduce the dynamic operator and then reduce it to an integral geometry problem integrating over level curves. After some necessary propositions, we state our main results.

Definition 3.2.1 Let X be a fixed open set in $\mathbf{R}^2$ and Y be the open sets of lines determined by (s,t) in $\mathbf{R}^2$. For $\mathscr{A} : C_0^\infty(X) \to C^\infty(Y)$, the operator of the dynamic inverse problem is defined by

$$\mathscr{A}f(s,t) = \int_{x\cdot\omega(t)=s} \mu(t,x) f(\psi_t(x)) \mathrm{d}S_x,$$

where $\omega(t) = (\cos t, \sin t)$ and the function μ is a non-vanishing smooth weight changing with respect to the variable t and the position x.

Here ψ_t is a diffeomorphism in $\mathbf{R}^2$, which is identity outside X, smoothly depending on the variable t, and $\mathrm{d}S_x$ is the euclidean measure restricted to the lines parametrized by $\{s = x\cdot\omega(t)\}$. Notice that each point (position) $x \in X$, lies on the lines in Y parametrized by (s,t).

The operator $\mathscr{A}$ can be written in the following format:

$$\mathscr{A}f(s,t) = \iint_{\mathbf{R}^2} \mu(t,x) f(\psi_t(x)) \delta(s - x\cdot\omega(t)) \mathrm{d}x.$$

Since ψ_t is a diffeomorphism, by performing a change of variable $z = \psi_t(x)$, we get $x = \psi_t^{-1}(z)$ and therefore, we have

$$\mathscr{A}f(s,t) = \iint_{\mathbf{R}^2} J(t,z)\mu(t,\psi_t^{-1}(z))f(z)\ \delta(s-\psi_t^{-1}(z)\cdot\omega(t))\ dz.$$

From now on, we do most of our analysis on the following general operator:

$$\mathscr{A}f(s,t) = \int_{\phi(t,x)=s} \mu(t,x)f(x)\mathrm{d}S_{s,t}, \tag{3.2}$$

where μ is a new positive and real analytic weight and the map

$$x = (x^1,x^2) \longrightarrow \phi(t,x),$$

with analytic function ϕ, is real-valued. Here $\mathrm{d}S_{s,t}$ is the Euclidean measure of the level curves of function ϕ, defined as

$$H(s,t) = \{x \in X : s = \phi(t,x)\}, \quad s \in \mathbf{R},\ t \in \mathbf{R}.$$

We, first, need to show for any time t and point x, there exists a curve passing through the point x with direction $\omega(t)$.

Proposition 3.2.1 *Let $H(s,t)$ be the level curves of ϕ. Then, locally near (s_0,t_0) and near a fixed $x_0 \in H(s,t)$ the followings are equivalent.*
i) The map from the variable t to the unit normal vector ν of the level curves $H(s,t)$:

$$t \longrightarrow \nu(t,x) = \frac{\partial_x\phi(t,x)}{|\partial_x\phi(t,x)|}, \quad \partial_x\phi(t,x) \neq 0, \tag{3.3}$$

is a local diffeomorphism, where $\partial_x = (\partial_{x^1},\partial_{x^2})$.
*ii) The **Local Bolker Condition**:*

$$h(t,x) = \det\Big(\ \tfrac{\partial\phi}{\partial x^j}, \tfrac{\partial^2\phi}{\partial t\partial x^j}\ \Big)\Big|_{(t,x)=(t_0,x_0)} \neq 0, \tag{3.4}$$

holds locally near (s_0,t_0) and near x_0.

Remark 3.2.1 i) The proof of Proposition 3.2.1 is postponed to the next section. In our setting, the equation (3.4) is the generalization of what it is known as a Bolker condition in [Theorem 14 (2), B. N. Hahn and Quinto (2016)].

ii) One can always rotate the unit normal vector ν by $\frac{\pi}{2}$ (at a fixed point x on the curve) to get the tangent vector at that fixed point. Now the first part in Proposition 3.2.1 implies that the map from the variable t to the tangent vector at point x on the level curve $H(s,t)$, is also a local diffeomorphism.

iii) We work locally near (s_0,t_0) and a fixed x_0 on the level curve. Let l_0 denote the unit tangent (normal) vector at x_0. By the first part, for any unit tangent vector l in some small neighborhood of l_0 (l is some perturbation of l_0), the map from the variable t to the unit tangent vector at a fixed point x is a local diffeomorphism. Now the Implicit Function Theorem implies that for any given t, there exists a curve passing through the fixed point x with a tangent vector l. This indeed is what to expect if we want the level curves to behave like the geodesic curves.

iv) The local Bolker condition requires that when the object moves in time, the curve changes its direction. A counterexample when the local Bolker condition does not hold is the case where an object and the scanner move with the same rate. In this situation, the object can be considered stationary where it is being scanned with stationary parallel rays. The above proposition guarantees that locally and microlocally this situation will not happen and the parameter t changes the angle if we keep the object stationary. (i.e the movement is not going to be synchronized with the scanner)

v) Proposition 3.3.1 in the next section, shows that one can connect the local Bolker condition to Fourier Integral Operator (FIO) theory by extending the function ϕ to a homogeneous function of order one (see Beylkin (1984)), and therefore one can use the condition (3.4) for the analysis.

For main results, we first state the following definitions.

Definition 3.2.2 The function ϕ satisfies the **Visibility condition** at $(x,\xi) \in T^*X \setminus 0$ if there exists a pair (s,t) with property $\phi(t,x) = s$, such that $\partial_x \phi(t,x) \parallel \xi$. Here T^*X is the cotangent bundle of X.

The visibility condition requires that at a point x and co-direction ξ, locally, there exists a curve passing through x which is conormal to ξ. As we pointed out in Remark 3.2.1, this property is a natural property of level curves as are expected to behave like geodesic curves. It also means that each singularity can be probed locally.

Definition 3.2.3 Let $(x_0,(s_0,t_0)) \in X \times Y$ be a fixed point with property $s_0 = \phi(t_0,x_0)$. The function ϕ satisfies the **Semi-Global Bolker Condition** at $(x_0,(s_0,t_0))$ if there exists a neighborhood of $(x_0,(s_0,t_0))$, V and U, such that for any $(x,(s,t)) \in V \times U$ and $y \in X$

$$\begin{cases} \phi(t,x) = \phi(t,y) = s \\ \partial_t \phi(t,x) = \partial_t \phi(t,y) \end{cases} \implies x = y. \tag{3.5}$$

The first equation in (3.5) implies that at instance t, both points x and y belong to the same level curve ϕ. The second equation implies that a perturbation in the variable t, cannot distinguish between these two points as they both belong to the same perturbed level curve. Note that, if the level curves ϕ are geodesics, it is required that the point x (close to a fixed point x_0) has no conjugate points along the curve passing through it with conormal ξ. This is indeed a semi-global condition, as x only varies in the open set V, but y can be anywhere along the level curve ϕ, not necessary close to x.

We now are ready to state our main result for the operator $\mathscr{A}$ given by (3.2).

Theorem 3.2.1 *Consider the operator $\mathscr{A}$ with a nowhere vanishing smooth weight μ. Let Σ be a set of all possible pairs (ϕ,μ) which are smooth in some C^k-topology with k an arbitrary large natural number. Assume that for any $(x,\xi) \in T^*X \setminus 0$, (i) the visibility condition holds and (ii) the local and semi-global Bolker conditions are satisfied for some (s,t) given by the visibility condition.*

Then within Σ, there exists a dense and open (generic) set Λ of pairs of (ϕ,μ) such that locally near any pair in Λ, the uniqueness results and therefore stability (injectivity) estimates given by Proposition 3.6.2 hold.

To formulate above result for the dynamic operator $\mathscr{A}$ given by (3.1), we first state the visibility, and the local and semi-global Bolker conditions for $\mathscr{A}$.

Visibility. This condition implies that for $(x,\xi) \in T^*X \setminus 0$, the map

$$t \to \frac{\xi}{|\xi|} \in S^1 \tag{3.6}$$

is locally surjective. Here the point (s,t) lies on the level curve $s = \psi_t^{-1}(x) \cdot \omega(t)$.

Local Bolker Condition. This condition (see Proposition 3.4.1) implies that

$$h(t,x) = \det\Big(\frac{\partial \psi_t^{-1}(x)\cdot\omega(t)}{\partial x^j}, \frac{\partial^2 \psi_t^{-1}(x)\cdot\omega(t)}{\partial t \partial x^j} \Big) \neq 0. \tag{3.7}$$

Semi-global Bolker condition (No conjugate points condition). By condition (3.5), semi-global Bolker condition holds if the map

$$x \to \big(\psi_t^{-1}(x)\cdot\omega(t), \partial_t(\psi_t^{-1}(x)\cdot\omega(t))\big) \tag{3.8}$$

is one-to-one.

Now for the dynamic forward operator $\mathscr{A}$ given by (3.1), we have the following result:

Theorem 3.2.2 *Consider the dynamic operator $\mathscr{A}$ with a nowhere vanishing smooth weight μ. Let Σ be a set of all possible pairs (ψ,μ) which are smooth in some C^k-topology with k an arbitrary large natural number. Assume that for any $(x,\xi) \in T^*X \setminus 0$, (i) the visibility condition (3.6) holds and (ii) the local and semi-global Bolker conditions given by (3.7) and (3.8) are satisfied for some (s,t) given by the visibility condition.*

Then within Σ, there exists a dense and open (generic) set Λ of pairs of (ψ,μ) such that locally near any pair in Λ, the uniqueness results and therefore stability (injectivity) estimates hold.

Corollary 3.2.1 *In particular, for a small perturbation of $\phi(t,x) = x\cdot\omega(t)$ where there is no motion or the motion is small enough $(\mu \approx 1)$, we have the actual injectivity and invertibility as the set of pairs of (ϕ,μ) is included in Λ.*

Remark 3.2.2 The Corollary 3.2.1 follows from the fact that the stationary Radon transform is analytic and for a small perturbation of phase function, the invertibility and injectivity still hold.

3.3 Preliminaries

In this section, we first prove Proposition 3.2.1 and then connect the local Bolker condition (3.4) to Fourier Integral Operator theory. At the end, we state some definitions which will be used in the following sections.

Definition 3.3.1 *A set Σ is conic, if $\xi \in \Sigma$ then $r\xi \in \Sigma$ for all $r > 0$.*

Proof [**Proof of Proposition 3.2.1**] i) $\rightarrow$ ii) Fix (t_0, x_0) and let $\phi(t_0, x_0) = s_0$. We work on some neighborhood of (s_0, t_0) and x_0. Since $\partial_x \phi(t,x) \neq 0$, the map (3.3) is well-defined and there exists a tangent at a fixed time t when x varies. The map (3.3) is a local diffeomorphism, therefore $\partial_t \nu(t,x) \neq 0$ and its inverse exists with non-zero derivative in a conic neighborhood.

Assume now that $h(t,x) = 0$. Then there exists a non-zero constant c such that

$$\partial_t \partial_x \phi(t,x) = c \partial_x \phi(t,x). \tag{3.9}$$

Plugging (3.9) into $\partial_t \nu(t,x)$:

$$\partial_t \nu(t,x) = \frac{\partial_t \partial_x \phi(t,x)}{|\partial_x \phi(t,x)|} - \partial_x \phi(t,x) \frac{\partial_x \phi(t,x) \cdot \partial_t \partial_x \phi(t,x)}{|\partial_x \phi(t,x)|^3}$$

we get $\partial_t \nu(t,x) = 0$, which is a contradiction. Therefore

$$h(t,x) \neq 0.$$

ii)$\rightarrow$ i) Assume that (3.4) is true. This in particular implies that $\partial_x \phi(t,x)$ and $\partial_t \partial_x \phi(t,x)$ are non-zero and linearly independent. For any t, let $\nu(t,x) = \frac{\partial_x \phi(t,x)}{|\partial_x \phi(t,x)|}$ denotes the unit normal at a fixed point x on the curve. To show the map in (3.3) is a local diffeomorphism, we need to show $\partial_t \nu(t,x) \neq 0$ in a conic neighborhood. Note that this map is well-defined as $\partial_x \phi(t,x) \neq 0$. Assume that $\partial_t \nu(t,x) = 0$. Then

$$\frac{\partial_t \partial_x \phi(t,x)}{|\partial_x \phi(t,x)|} = \partial_x \phi(t,x) \frac{\partial_x \phi(t,x) \cdot \partial_t \partial_x \phi(t,x)}{|\partial_x \phi(t,x)|^3}$$

which implies that

$$\partial_t\partial_x\phi(t,x) = c\partial_x\phi(t,x), \quad c = \frac{\partial_x\phi(t,x)\cdot\partial_t\partial_x\phi(t,x)}{|\partial_x\phi(t,x)|^2}.$$

This contradicts with the fact that $\partial_x\phi(t,x)$ and $\partial_t\partial_x\phi(t,x)$ are linearly independent. Now by Inverse Function Theorem, the map (3.3) is a local diffeomorphism as it is smooth and its Jacobian is nowhere vanishing. ■

One can extend the function ϕ to a homogeneous function of order one as follow:

$$\varphi(x,\theta) = \psi^{-1}_{\arg\theta}(x)\cdot\theta = |\theta|\phi(\arg\theta, x), \quad \text{where } \theta = (\theta^1,\theta^2) = |\theta|(\cos t, \sin t) \in \mathbf{R}^2\setminus 0. \quad (3.10)$$

As we pointed out above, we work locally in a conic neighborhood of t_0 and s_0. This guarantees that function $\arg\theta$ is single-valued. To connect the local Bolker condition to Fourier Integral Operator theory, we have the following proposition.

Proposition 3.3.1 *For the function φ defined by ϕ in (3.10), the local Bolker condition (3.4) holds if and only if*

$$\det\left(\ \frac{\partial^2\varphi}{\partial\theta^i\partial x^j}\ \right) \neq 0.$$

Proof Since $\partial_x\varphi = |\theta|\partial_x\phi \neq 0$, we have

$$\frac{\partial^2\varphi}{\partial\theta^1\partial x^j} = \frac{\partial}{\partial\theta^1}(|\theta|\frac{\partial\phi}{\partial x^j}) = \frac{\theta^1}{|\theta|}\frac{\partial\phi}{\partial x^j} - \frac{\theta^2}{|\theta|}\frac{\partial^2\phi}{\partial t\partial x^j},$$

and

$$\frac{\partial^2\varphi}{\partial\theta^2\partial x^j} = \frac{\partial}{\partial\theta^2}(|\theta|\frac{\partial\phi}{\partial x^j}) = \frac{\theta^2}{|\theta|}\frac{\partial\phi}{\partial x^j} + \frac{\theta^1}{|\theta|}\frac{\partial^2\phi}{\partial t\partial x^j},$$

where $t = \arg\theta$. Assume first that $\partial_x\phi(t,x)$ and $\partial_t\partial_x\phi(t,x)$ are linearly independent. We show that columns in the matrix $\frac{\partial^2\varphi}{\partial\theta^i\partial x^j}$ are linearly independent for $i = 1,2$. So let

$$c_1\frac{\partial^2\varphi}{\partial\theta^1\partial x^j} + c_2\frac{\partial^2\varphi}{\partial\theta^2\partial x^j} = 0.$$

Then we have

$$(c_1\frac{\theta^1}{|\theta|} + c_2\frac{\theta^2}{|\theta|})\frac{\partial\phi}{\partial x^j} + (-c_1\frac{\theta^2}{|\theta|} + c_2\frac{\theta^1}{|\theta|})\frac{\partial^2\phi}{\partial t\partial x^j} = 0.$$

Since $\partial_x\phi(t,x)$ and $\partial_t\partial_x\phi(t,x)$ are linearly independent, we have

$$c_1\theta^1 + c_2\theta^2 = 0, \quad -c_1\theta^2 + c_2\theta^1 = 0,$$

which simply implies that $c_1 = c_2 = 0$, and therefore $\frac{\partial^2\varphi}{\partial\theta^i\partial x^j}$ are linearly independent for $i = 1,2$.

Assume now that $\frac{\partial^2\varphi}{\partial\theta^i\partial x^j}$ are linearly independent for $i = 1,2$. We show that $\partial_x\phi(t,x)$ and $\partial_t\partial_x\phi(t,x)$ are linearly independent. We first rewrite $\partial_x\phi(t,x)$ and $\partial_t\partial_x\phi(t,x)$ as follow:

$$\theta^1\frac{\partial^2\varphi}{\partial\theta^1\partial x^j} = \frac{(\theta^1)^2}{|\theta|}\frac{\partial\phi}{\partial x^j} - \frac{\theta^1\theta^2}{|\theta|}\frac{\partial^2\phi}{\partial t\partial x^j},$$

and

$$\theta^2\frac{\partial^2\varphi}{\partial\theta^2\partial x^j} = \frac{(\theta^2)^2}{|\theta|}\frac{\partial\phi}{\partial x^j} + \frac{\theta^1\theta^2}{|\theta|}\frac{\partial^2\phi}{\partial t\partial x^j}.$$

Adding the last two equations we get

$$\frac{\theta^1}{|\theta|}\frac{\partial^2\varphi}{\partial\theta^1\partial x^j} + \frac{\theta^2}{|\theta|}\frac{\partial^2\varphi}{\partial\theta^2\partial x^j} = \frac{\partial\phi}{\partial x^j}.$$

Consider

$$-\theta^2\frac{\partial^2\varphi}{\partial\theta^1\partial x^j} = -\frac{\theta^1\theta^2}{|\theta|}\frac{\partial\phi}{\partial x^j} + \frac{(\theta^2)^2}{|\theta|}\frac{\partial^2\phi}{\partial t\partial x^j},$$

and

$$\theta^1\frac{\partial^2\varphi}{\partial\theta^2\partial x^j} = \frac{\theta^1\theta^2}{|\theta|}\frac{\partial\phi}{\partial x^j} + \frac{(\theta^1)^2}{|\theta|}\frac{\partial^2\phi}{\partial t\partial x^j}.$$

Adding the last two equations, we have

$$-\frac{\theta^2}{|\theta|}\frac{\partial^2\varphi}{\partial\theta^1\partial x^j} + \frac{\theta^1}{|\theta|}\frac{\partial^2\varphi}{\partial\theta^2\partial x^j} = \frac{\partial^2\phi}{\partial t\partial x^j}.$$

Now assume that

$$\tilde{c}_1\frac{\partial\phi}{\partial x^j} + \tilde{c}_2\frac{\partial^2\phi}{\partial t\partial x^j} = 0.$$

In a similar way as we showed above and using the fact that $\frac{\partial^2\varphi}{\partial\theta^i\partial x^j}$ are linearly independent for $i = 1,2$, we conclude that $\tilde{c}_1 = \tilde{c}_2 = 0$. This proves the proposition. ■

In principle, Proposition 3.2.1 implies that we can use our analysis with (3.4), see Beylkin (1984).

3.4 Microlocal Analyticity

In this section, we study the microlocal analyticity of operator $\mathscr{A}$ for a given f. We first compute the adjoint operator.

Adjoint Operator $\mathscr{A}^*$. Let $\phi \in C^\infty(\mathbf{R} \times \tilde{X})$ be given, where X is embedded in an open set $\tilde{X}$. We extend our function f to be zero on $\tilde{X} \setminus X$. Consider now the one-dimensional level curves

$$H(s,t) = \{x \in \tilde{X} : s = \phi(t,x)\}, \quad s \in \mathbf{R},\ t \in \mathbf{R}$$

with Euclidean measure $\mathrm{d}S_x$ induced by the volume form $\mathrm{d}x$ in the domain X. There exists a non-vanishing and smooth function $J(t,x)$ such that

$$\mathrm{d}S_{s,t}(x) \wedge \mathrm{d}s = J(t,x)\mathrm{d}x.$$

Therefore,

$$\begin{aligned}\int_{T_1}^{T_2} \int_{\mathbf{R}} (\mathscr{A}f)\bar{g}\mathrm{d}s\mathrm{d}t &= \int_{T_1}^{T_2} \int_{\mathbf{R}} \int_{H(s,t)} \mu(t,x) f(x) \bar{g}(s,t) \mathrm{d}S_{s,t}\mathrm{d}s\mathrm{d}t \\ &= \int_{T_1}^{T_2} \int_{\tilde{X}} \mu(t,x) f(x) \bar{g}(\phi(t,x),t) J(t,x)\mathrm{d}x\mathrm{d}t,\end{aligned}$$

where $T_1 < t < T_2$ and $0 < T_2 - T_1 \ll 2\pi$. In the second equality above, we used the fact that the double integral $\int_{\mathbf{R}} \int_{H(s,t)}$ equals to an integral over $\tilde{X}$, by Fubini's Theorem. Thus, the adjoint of $\mathscr{A}$ in $L^2(X, \mathrm{d}x)$ is

$$\mathscr{A}^* g(x) = \int_{\mathbf{R}} \bar{\mu}(t,x) \bar{J}(t,x) g(\phi(t,x),t)\mathrm{d}t,$$

where μ is supported in $\{t \in \mathbf{R} : T_1 < t < T_2\}$. In fact, the adjoint $\mathscr{A}^* g(x)$ is localized in t and is an average over all lines or curves $H(s,t)$ that go through x.

Schwartz Kernel. Now we compute the Schwartz kernel of the operator $\mathscr{A}$.

Lemma 3.4.1 *The Schwartz kernel $K_{\mathscr{A}}$ of $\mathscr{A}$ is*

$$K_{\mathscr{A}}(s,t,y) = \delta(s - \phi(t,y))\mu(t,y)J(t,y),$$

where $J(t,y) = |\mathrm{d}_y\phi| = (\sum |\partial_{y^j}\phi|^2)^{\frac{1}{2}}$.

Proof Let $\Phi(s,t,y) = s - \phi(t,y)$. By (3.2) we have

$$\mathscr{A}f(s,t) = \int_{\phi(t,y)=s} \mu(t,y)f(y)\mathrm{d}S_{s,t} = \int_{\phi(t,y)=s} \mu(t,y)f(y)|\mathrm{d}_y\Phi||\mathrm{d}_y\Phi|^{-1}\mathrm{d}S_{s,t}.$$

Since $\partial_{y^j}\Phi = -\partial_{y^j}\phi$ and $\partial_{y^j}\phi \neq 0$ when $\Phi = 0$, by Theorem (6.1.5) Hörmander (1985), we have

$$|\mathrm{d}_y\Phi|^{-1}\mathrm{d}S_{s,t} = \Phi^*\delta_0.$$

Here * is pullback with $\Phi^*\delta_0 = \delta_0 \circ \Phi$. The second integral above can be written as

$$\int \Phi^*\delta_0\mu(t,y)f(y)|\mathrm{d}_y\Phi|\mathrm{d}y = \langle \Phi^*\delta_0\mu|\mathrm{d}_y\Phi|, f\rangle.$$

Therefore, the Schwartz kernel of $\mathscr{A}$ is

$$K_{\mathscr{A}}(s,t,y) = \delta(s-\phi(t,y))\mu(t,y)|\mathrm{d}_y\Phi|.$$

■

Remark 3.4.1 One can compute the Schwartz kernel of $\mathscr{A}^*$ and $\mathscr{N} = \mathscr{A}^*\mathscr{A}$:

$$K_{\mathscr{A}^*}(s,t,x) = \delta(\phi(t,x)-s)\bar{\mu}(t,x)J(t,x),$$

$$K_{\mathscr{N}}(s,t,x,y) = \int_{\mathbf{R}} \delta(\phi(t,x)-\phi(t,y))\bar{\mu}(t,x)J(t,x)\mu(t,y)J(t,y)\mathrm{d}t.$$

The following lemma shows that the operator $\mathscr{A}$ is an elliptic Fourier Integral Operator (FIO).

Lemma 3.4.2 *Let* $M = \{(s,t,x) : \Phi(s,t,x) = s - \phi(t,x) = 0\} \subset Y \times X$. *Then the operator* $\mathscr{A}$ *is an elliptic FIO of order* $-\frac{1}{2}$ *associated with the conormal bundle of* M*:*

$$N^*M = \{(s,t,x,\sigma,\tau,\xi) \in T^*(Y\times X)\big| \quad (\sigma,\tau,\xi) = 0 \quad \text{on} \quad T_{(s,t,x)}M\},$$

where (s,t,σ,τ) *and* (x,ξ) *are the coordinates on* T^*Y *and* T^*X*, respectively.*

Proof By Lemma 3.4.1 the Schwartz kernel $K_{\mathscr{A}}$ has singularities conormal to the manifold M. Since $\dim X = \dim Y = 2$, the Schwartz kernel $K_{\mathscr{A}}$ is conormal type in the class $I^{-\frac{1}{2}}(Y \times X; M)$, see (Section 18.2, Hörmander (1985)). This shows that the operator $\mathscr{A}$ is an elliptic FIO of order $-\frac{1}{2}$ associated with the conormal bundle N^*M. Note that σ is a one-dimensional non-zero variable. ■

We now compute the canonical relation $\mathscr{C}$ and show it is a four-dimensional non-degenerated conic submanifold of N^*M parametrized by (t,x,σ). Note that N^*M is a Lagrangian submanifold of $T^*(Y \times X)$.

Proposition 3.4.1 *Let $\mathscr{C}$ be the canonical relation associated with M. Then*

$$\mathscr{C} = \{(\phi(t,x),t,\sigma,-\sigma\partial_t\phi(t,x);x,\sigma\partial_x\phi(t,x)\big|(\phi(t,x),t,x) \in M, \quad 0 \neq \sigma \in \mathbf{R}\}.$$

Furthermore, the canonical relation $\mathscr{C}$ is a local canonical graph if and only if for any t, the map

$$x \to (\phi(t,x), \partial_t\phi(t,x)) \tag{3.11}$$

is locally injective and local Bolker condition (3.4) holds.

Proof The twisted conormal bundle of M:

$$\mathscr{C} = (N^*M \setminus 0)' = \{(s,t,\sigma,\tau;x,\xi)\big| \quad (s,t,\sigma,\tau;x,-\xi) \in N^*M\},$$

gives the canonical relation associated with M. We first calculate the differential of the function $\Phi(s,t,x) = s - \phi(t,x)$. We have

$$\mathrm{d}\Phi(s,t,x) = \mathrm{d}s - \partial_t\phi(t,x)\mathrm{d}t - \partial_x\phi(t,x)\mathrm{d}x.$$

Therefore, the canonical relation is given by

$$\mathscr{C} = \{(\phi(t,x),t,\sigma,-\sigma\partial_t\phi(t,x);x,\sigma\partial_x\phi(t,x)\big|(\phi(t,x),t,x) \in M, \quad 0 \neq \sigma \in \mathbf{R}\}.$$

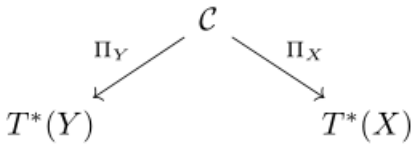

Now consider the microlocal version of double fibration:
where

$$\Pi_X(\phi(t,x),t,\sigma,-\sigma\partial_t\phi;x,\sigma\partial_x\phi) = (x,\sigma\partial_x\phi),$$

$$\Pi_Y(\phi(t,x),t,\sigma,-\sigma\partial_t\phi;x,\sigma\partial_x\phi) = (\phi(t,x),t,\sigma,-\sigma\partial_t\phi).$$

Our goal is to find out when the Bolker condition (locally) holds for $\mathscr{C}$, that is, $\Pi_Y : \mathscr{C} \to T^*(Y)$ is an injective immersion. We first compute its differential:

$$\mathrm{d}_{t,x,\sigma}\Pi_Y = \begin{pmatrix} \partial_t\phi & \partial_{x^1}\phi & \partial_{x^2}\phi & 0 \\ 1 & 0 & 0 & 0 \\ 0 & 0 & 0 & 1 \\ -\sigma\partial_t^2\phi & -\sigma\partial^2_{t,x^1}\phi & -\sigma\partial^2_{t,x^2}\phi & \partial_t\phi \end{pmatrix}.$$

If $\mathrm{d}_{t,x,\sigma}\Pi_Y$ has rank equal to four, then the Bolker condition is locally satisfied. Indeed, this is true, as $\mathrm{d}_{t,x,\sigma}\Pi_Y$ has rank equal to four if and only if the condition (3.4) holds. This implies that $\dim\mathscr{C} = 4$. Since the map in (3.11) is one-to-one, the projection $\Pi_Y : \mathscr{C} \to T^*(Y)$ is an injective immersion. Hence, Π_Y is a local diffeomorphism. ■

The following lemma states whether position singularities and measurement singularities can affect each other.

Lemma 3.4.3 *Let X be a fixed open set in $\mathbf{R}^2$ and Y be the open sets of lines determined by (s,t) in $\mathbf{R}^2$. Then, the map*

$$\Pi_X \circ \Pi_Y^{-1} : T^*(Y) \longrightarrow T^*(X)$$

is a local diffeomorphism.

Proof Consider the map $\Pi_Y : \mathscr{C} \to T^*(Y)$. We show that for a given $(s,t,\sigma,-\sigma\partial_t\phi) \in T^*(Y)$, one can determine $(x,\xi) \in T^*(X)$. Since $\partial_t\phi$ is non-zero (σ and $\sigma\partial_t\phi$ are both non-zero,) for a given (s,t) there exists a tangent vector to each level curve $H(s,t)$. By Remark 3.2.1, one can find a non-zero normal vector $\partial_x\phi$ on each level curve, and therefore $\xi = \sigma\partial_x\phi$. On each level curve $H(s,t)$, we have $s = \phi(t,x)$. Since $\partial_x\phi \neq 0$, the Implicit Function Theorem implies that the variable t determines x. Hence, the map Π_Y is a local diffeomorphism.

Now consider the map $\Pi_X : \mathscr{C} \to T^*(X)$. Our goal is to determine $(s,t,\sigma,-\sigma\partial_t\phi) \in T^*(Y)$, for a given $(x,\xi) = (x,\sigma\partial_x\phi) \in T^*(X)$. By Proposition 3.2.1, the map

$$\frac{\xi}{|\xi|} = \frac{\partial_x\phi}{|\partial_x\phi|} \longrightarrow t,$$

is a local diffeomorphism for a fixed point x provided that the condition (3.4) holds. Thus, $(x, \frac{\xi}{|\xi|})$ determines the variable t. In particular, for a given (x,ξ) this implies that one can identify the level curve $H(s,t)$, as (t,x) determines ϕ, and therefore s (on each level curve we have $s = \phi(t,x)$.) Since $\xi = \sigma\partial_x\phi$ with $\xi \neq 0$, one can determine $\sigma = \frac{|\xi|}{|\partial_x\phi|}$. To determine the last variable $\sigma\partial_t\phi$, it is enough to take the partial derivative of ϕ with respect to the variable t. Thus, the map Π_X is a local diffeomorphism. We remind that the above argument is valid when the condition (3.4) is satisfied.

Now since dim(Y)=dim(X) and

$$\Pi_X : \mathscr{C} \to T^*(X), \quad \Pi_Y : \mathscr{C} \to T^*(Y)$$

are local diffeomorphisms, the map

$$\Pi_X \circ \Pi_Y^{-1} : T^*(Y) \longrightarrow T^*(X)$$

$$(s,t,\sigma,\tau) \longmapsto (x,\xi)$$

will be a local diffeomorphism. ■

Remark 3.4.2 i) Note that, by [Proposition 4.1.4, Duistermaat and Hörmander (1972)], if we show one of the maps Π_Y or Π_X is a local diffeomorphism, then the other map is also a local diffeomorphism as dim(Y)=dim(X). We, however, in above lemma have shown that both maps are local diffeomorphisms, as the proof reveals whether each map will be a global diffeomorphism or not. In fact, for a fixed $(x,\xi) \in T^*(X)$ there might be more than one curve which resolves the same singularity.

ii) The map $\Pi_Y : \mathscr{C} \to T^*(Y)$ being a local diffeomorphism implies that one can always track the position singularities $(x, \sigma\partial_x\phi) \in \text{WF}(f)$ by having the measurement singularities

$$(\phi(t,x), t, \sigma, -\sigma\partial_t\phi(x,\xi)) \in \text{WF}(\mathscr{A}f)$$

. iii) The map $\Pi_X : \mathscr{C} \to T^*(X)$ being a local diffeomorphism means that for any fixed position x and covector ξ, there exists a curve not necessarily unique passing through x perpendicular to ξ.

This means singularities in data, i.e. $(x, \sigma\partial_x\phi) \in \text{WF}(f)$, can affect the measurement singularities, i.e. $(\phi(t,x), t, \sigma, -\sigma\partial_t\phi\ (x,\xi)) \in \text{WF}(\mathscr{A}f)$.

iv) Proposition 3.4.1 and Lemma 3.4.3 show the local surjectivity of the map

$$[T_1, T_2] \ni t \to \frac{\partial_x\phi(t,x)}{|\partial_x\phi(t,x)|} \in S^1, \quad \text{for a fixed } x.$$

Note that if the visibility condition holds, then we have the global surjectivity on S^1.

3.5 Global Bolker Condition

In this section, we study the microlocalized version of the normal operator $\mathscr{N} = \mathscr{A}^*\mathscr{A}$ to prove a stability estimate. It is known that the normal operator $\mathscr{N}$ is a ΨDO if the projection $\Pi_Y : \mathscr{C} \to T^*(Y)$ is an injective immersion (see Proposition 8.2, Guillemin and Sternberg (1979)). For our analysis, in addition to the visibility and local Bolker conditions, we assume that the semi-global Bolker condition is satisfied which is similar to the *No Conjugate Points* assumption for the geodesics ray transform studied in (Frigyik et al. (2008); Krishnan (2009)).

To construct the operator $\mathscr{N}$, we perform the microlocalization in a conic neighborhood of a fixed covector $(x_0,\xi^0)\in T^*X\setminus 0$. By the visibility condition, there exists some (s_0,t_0) such that $\phi(t_0,x_0)=s_0$ and $\partial_x\phi(t_0,x_0)\parallel\xi^0$; which means for each point x_0 and co-direction ξ^0, there exists a curve passing through x_0 where ξ^0 is normal to it. By semi-global Bolker condition, there exists a pair of neighborhoods of $(x_0,(s_0,t_0))$, V and U, such that for any $(x,(s,t))\in V\times U$, the visibility condition is preserved under small perturbations in t variable. We now shrink V and U sufficient enough such that the local Bolker condition is also satisfied.

Define $\mathscr{N}=\chi_X\mathscr{A}^*\chi_Y\mathscr{A}$, where $\chi_X(x)$ and $\chi_Y(s,t)$ are non-negative cut-off functions in a neighborhood of x_0 and (s_0,t_0), respectively, with property that the projections $\Pi_X:\mathscr{C}\to T^*(X)$ and $\Pi_Y:\mathscr{C}\to T^*(Y)$ are embeddings above $\mathrm{supp}(\chi_X)$ and $\mathrm{supp}(\chi_Y)$. In fact, the smooth cut-off functions χ_X and χ_Y are localizations on the base variables x and (s,t) and they are not ΨDOs. The following theorem shows that the (microlocalized) normal operator $\mathscr{N}=\chi_X\mathscr{A}^*\chi_Y\mathscr{A}$ is a ΨDO of order -1.

Theorem 3.5.1 *Let $(x_0,\xi^0)\in T^*X\setminus 0$ be a fixed covector. Assume that the visibility, the local and semi-global Bolker conditions are satisfied near (x_0,ξ^0). Let χ_X and χ_Y be non-negative cut-off functions defined above. Then the operator $\mathscr{N}=\chi_X\mathscr{A}^*\chi_Y\mathscr{A}$ is a classical ΨDO of order -1 with principal symbol*

$$p(x,\xi)=(2\pi)^{-1}\chi_X\frac{W(x,x,\xi)+W(x,x,-\xi)}{\tilde{h}(x,\xi)}$$

near (x_0,ξ^0). The functions W and $\tilde{h}$ are defined as

$$W(x,x,\xi)=\chi_Y(\phi(t,x),t)|\mu(t,x)|^2J^2(t,x),\quad\text{and}\quad\tilde{h}(x,\xi)=\frac{|\xi|}{|\partial_x\phi(t,x)|}h(t,x),$$

where $t=t(x,\xi)$ is well-defined locally by Lemma 3.4.3.

Proof For the proof we mainly follow (Lemma 2, Homan and Zhou (2017)). By the equation (3.2), we have

$$\chi_Y(s,t)\mathscr{A}f(s,t)=\int_{\phi(t,x)=s}\chi_Y(\phi(t,x),t)\mu(t,x)f(x)\mathrm{d}S_{s,t}.$$

Considering the Schwartz kernel of the microlocalized normal operator $\mathscr{N} = \chi_X(x)\mathscr{A}^*\chi_Y(s,t)\mathscr{A}$, we split the integration over $\mathbf{R}$ into $\{\sigma > 0\}$ and $\{\sigma < 0\}$. We have

$$K_{\mathscr{N}} = \int_{\mathbf{R}}\int_0^{+\infty} e^{\mathrm{i}(\phi(t,x)-\phi(t,y))\sigma}\chi_X(x)W(t,x,y)\mathrm{d}\sigma\mathrm{d}t$$

$$+\int_{\mathbf{R}}\int_0^{+\infty} e^{-\mathrm{i}(\phi(t,x)-\phi(t,y))\sigma}\chi_X(x)W(t,x,y)\mathrm{d}\sigma\mathrm{d}t = K_{\mathscr{N}^+} + K_{\mathscr{N}^-},$$

where $K_{\mathscr{N}^+}$ and $K_{\mathscr{N}^-}$ are the Schwartz kernels of the operators $\mathscr{N}^+$ and $\mathscr{N}^-$ with $\mathscr{N} = \mathscr{N}^+ + \mathscr{N}^-$. We first consider $K_{\mathscr{N}^+}$. Note that $K_{\mathscr{N}^+}$, localized as the function ϕ, priori satisfies the local Bolker condition (3.4). By semi-global Bolker condition (3.5), we have

$$\begin{cases} \phi(t,x) = \phi(t,y) = s \\ \partial_t\phi(t,x) = \partial_t\phi(t,y) \end{cases} \Longrightarrow x = y.$$

Now a stationary phase method implies that $K_{\mathscr{N}^+}$ is smooth away from the diagonal $\{x = y\}$. Since $\partial_x\phi(t,x) \neq 0$, for a fixed x there exists a neighborhood $\mathscr{U}$ on which we have normal vectors. We work on normal coordinates (x^i, y^i) as coordinates on $\mathscr{U}\times\mathscr{U}$, with $x^i = y^i$. In these local coordinates, one can expand the phase function near the diagonal $\{x = y\}$. Let

$$(\phi(t,x)-\phi(t,y))\sigma = (x-y)\cdot\xi(t,\sigma,x,y), \tag{3.12}$$

where $\xi(t,\sigma,x,y)$ is defined by the map

$$(t,\sigma) \to \xi(t,\sigma,x,y) = \int_0^1 \sigma\partial_x\phi(t,x+\tau(y-x))\mathrm{d}\tau.$$

On the diagonal, we have $\xi(t,\sigma,x,x) = \sigma\partial_x\phi(t,x) = \xi$ and the map is a smooth diffeomorphism as

$$\det\left(\frac{\partial\xi}{\partial(t,\sigma)}\right)\Big|_{x=y} = \det\left(\ \frac{\partial\phi}{\partial x^j}, \sigma\frac{\partial^2\phi}{\partial t\partial x^j}\ \right) = \sigma h(t,x) \neq 0.$$

Notice that $\sigma = \frac{|\xi|}{|\partial_x\phi(t,x)|}$ and $t = t(x,\xi)$ is locally well-defined by Lemma 3.4.3. Therefore,

$$\tilde{h}(x,\xi) = \frac{|\xi|}{|\partial_x\phi|}h(t,x) \neq 0.$$

Using the above change of variable (3.12) on the diagonal yields

$$K_{\mathscr{N}^+}(s,t,x,y) = (2\pi)^{-1} \iint_{\mathbf{R}^2} e^{\mathrm{i}(x-y)\cdot\xi}\ \chi_X(x) W(x,y,\xi) |\tilde{h}(x,\xi)|^{-1} \mathrm{d}\xi,$$

where the function W is defined above. By restricting the amplitude to diagonal $\{x = y\}$, one can find the principal symbol of $K_{\mathscr{N}^+}$. Now the principal symbol of $K_{\mathscr{N}}$ is given by the sum of those for $K_{\mathscr{N}^+}$ and $K_{\mathscr{N}^-}$. Since the weight μ is a positive real analytic function, the normal operator $\mathscr{N}$ is a classical ΨDO with principal symbol $p(x,\xi)$ provided the function ϕ satisfies the local and semi-global Bolker condition. Now since μ is nowhere vanishing and by local Bolker condition (3.4) $h(t,x) \neq 0$, the operator $\mathscr{N}$ is an elliptic ΨDO if the visibility condition is satisfied. ■

3.6 Analysis of Global Problem and Stability

In previous sections, we studied the operators $\mathscr{A}$ and $\mathscr{N}$. We showed that under the visibility, local and semi-global Bolker conditions, the microlocalized normal operator $\mathscr{N}$ is a ΨDO of order -1 in a small conic neighborhood of a fixed covector $(x,\xi) \in T^*X \setminus 0$.

To reconstruct $f \in L^2(X)$ from its measurements $\mathscr{A}f$ using the operator $\mathscr{N}$, we need to expand our results globally. As we pointed out in the begining of section five, the visibility, local and semi-global Bolker conditions (which are open conditions in a small conic neighborhood of (x_0,ξ^0)) are required for the analysis. We also employ non-negative cut-off functions χ_X and χ_Y in neighborhoods of x_0 and (s_0,t_0), where the projections Π_X and Π_Y are embeddings above $\mathrm{supp}(\chi_X)$ and $\mathrm{supp}(\chi_Y)$.

Let $K \subset X$ be a compact subset and $(x_0, \xi^0) \in T^*K \setminus 0$ be a fixed covector. There exists a pair of conic neighborhoods $(\mathcal{V}, \tilde{\mathcal{V}})$ with property $(x_0, \xi^0) \in \mathcal{V}$ and $\mathcal{V} \Subset \tilde{\mathcal{V}}$ such that the visibility, local and semi-global Bolker conditions are satisfied for $\tilde{\mathcal{V}}$. Let $\{\mathcal{V}_\alpha\}$ be an open covering for $T^*K \setminus 0$. Since $T^*K \setminus 0$ is conically compact subset of $T^*X \setminus 0$, by a compactness argument, there exists a finite subcover of $\{\mathcal{V}_i\}$. By Theorem 5.1, the microlocally restricted normal operators $\mathcal{N}_i = \chi_{i_X} \mathcal{A}^* \chi_{i_Y} \mathcal{A}$ are ΨDOs of order -1 supported in a conic neighborhood $\mathcal{V}_i$ (where the visibility, local and semi-global Bolker conditions are satisfied), with the principal symbols

$$p_i(x,\xi) = (2\pi)^{-1} \chi_{i_X}(x) \frac{W_i(x,x,\xi) + W_i(x,x,-\xi)}{\tilde{h}(x,\xi)},$$

where

$$W_i(x,x,\xi) = \chi_{i_Y}(\phi(t,x),t) |\mu(t,x)|^2 J^2(t,x), \qquad \tilde{h}(x,\xi) = \frac{|\xi|}{|\partial_x \phi(t,x)|} h(t,x),$$

and $t = t(x,\xi)$ is well-defined locally by Lemma 3.4.3. Here $\{\chi_{i_X}\}$ and $\{\chi_{i_Y}\}$ are families of smooth cut-off functions which are non-negative in neighborhoods of $V_i \ni x_0$ and $U_i \ni (s_0, t_0)$, with property that $\operatorname{supp} \chi_{i_X} \subset V_i$ and $\operatorname{supp} \chi_{i_Y} \subset U_i$. We remind that, the smooth cut-off functions χ_{i_X} and χ_{i_Y} are localizations on the base variables x and (s,t) and they are not ΨDOs.

Set $\mathcal{N} = \sum \mathcal{N}_i$. Now for any (x,ξ), there exists k such that $\chi_{k_X}(x) \neq 0$ and all other terms are non-negative. Hence $\sum \mathcal{N}_i$ is elliptic, and therefore the operator $\mathcal{N}$ is a classical ΨDO of order -1 with principal symbol $P(x,\xi) = \sum p_i(x,\xi)$.

Remark 3.6.1 It should be noted that in our analysis, the cut-off functions are used for the C^∞ results. For the case of analytic arguments, one cannot use cut-off functions.

In the following proposition, we show that for any neighborhood of a fixed covector $(x_0, \xi^0) \in T^*X \setminus 0$, ellipticity holds along normals in a conic neighborhood of this covector. We point out that, one can use the "eating away at supp f" argument, first stated by Boman and Quinto Boman, Quinto, et al. (1987), to conclude the similar results.

Proposition 3.6.1 *Assume that the dynamic operator $\mathscr{A}$ satisfies the visibility, the local Bolker, and the semi-global Bolker conditions for all $(s,t) \in Y$ and $(x_0,\xi^0) \in T^*(X) \setminus 0$. Let ϕ be a real analytic function and μ be a positive real analytic weight. Let $f \in L^2(X)$ with $\operatorname{supp} f \subset X$. If $\mathscr{A} f = 0$ in a neighborhood of some level curves, l_0, determined by (s_0,t_0), then*

$$\mathrm{WF_A}(f) \cap N^*(l_0) = \emptyset.$$

Proof Let $(x_0,\xi^0) \in T^*X \setminus 0$ be fixed. By the visibility condition, there exists (s_0,t_0) such that $\phi(t_0,x_0) = s_0$ and $\partial_x \phi(t_0,x_0) \parallel \xi^0$. Now the proof follows directly from [Proposition 1, Homan and Zhou (2017)] and applying it to all conormals of the fixed curve l_0, determined by (s_0,t_0). ■

Remark 3.6.2 For the results in Proposition 3.6.1, we only need the visibility, the local and semi-global Bolker conditions to be satisfied near $N^*(l_0)$. However, to conclude the following corollary, we need to have the above three conditions satisfied globally, i.e. for all $(s,t) \in Y$ and $(x_0,\xi^0) \in T^*(X) \setminus 0$.

Corollary 3.6.1 *Under the assumption of Proposition 3.6.1, $\mathscr{A} f = 0$ implies that $f = 0$.*

Proof Let $\tilde{X} \supset \operatorname{supp} f$ be an open set where the function f is extended to be zero on $\tilde{X} \setminus X$ (X is embedded in the set $\tilde{X}$.) Consider all level curves intersecting $\tilde{X}$. By visibility condition, there exists a level curve l_0 determined by (s_0,t_0) such that $\phi(t_0,x_0) = s_0$ and $\partial_x \phi(t_0,x_0) \parallel \xi^0$ (i.e. each singularity is visible). On the other hand, the local and semi-global Bolker conditions guarantee that there exist some lines in the exterior of $\operatorname{supp} f$. By assumption, $\mathscr{A} f = 0$ for all these level curves. Now, Proposition 3.6.1 implies that f is analytic in the interior of $\tilde{X}$. Since f is identically zero on $\tilde{X} \setminus X$, f must be identically zero on all of X. Hence $\mathscr{A}$ is injective. ■

The following proposition is a standard stability estimate which follows from elliptic regularity see (Theorem 2, P. Stefanov and Uhlmann (2004)) and (Proposition V.3.1, Taylor (1981)).

Proposition 3.6.2 *Let the real analytic function ϕ satisfies the visibility, the local and semi-global Bolker conditions and μ be a positive real analytic weight. Let K be a compact subset of X. Then for all $f \in L^2(K)$ and $s > 0$ there exists $C > 0$ and $C_s > 0$ depending on s such that*

$$\| f \|_{L^2(K)} \leq C \| \mathscr{N} f \|_{H^1(\tilde{X})} + C_s f \|_{H^{-s}}, \quad \forall s.$$

Moreover, if $\mathscr{N} : L^2(K) \to H^1(\tilde{X})$ is injective, then there exists a stability estimate,

$$\| f \|_{L^2(K)} \leq C' \| \mathscr{N} f \|_{H^1(\tilde{X})}$$

where $C' > 0$ is a constant.

Proof The proof directly follows from Theorem 3.5.1 and above arguments. ■

Remark 3.6.3 Note that the way the parametrix is constructed in above proposition, one has control on how the constant C to be chosen. This, however, is not the case for C' in the second inequality.

In what follows, we perturb ϕ and μ, and prove that the perturbation yields a small constant times an L^2-norm of the function f which can be absorbed by the left-hand side of above estimate. The following lemma is in the spirit of [Lemma 4, Homan and Zhou (2017)].

Lemma 3.6.1 *Let $\mathscr{A}$ be a dynamic operator satisfying the visibility, the local and semi-global Bolker conditions with a real analytic function ϕ and positive real analytic weight μ. There exists a $k \gg 2$ and $(\tilde{\phi}, \tilde{\mu}) \in C^k$ such that if*

$$\| \phi - \tilde{\phi} \|_{C^k(\mathbf{R}\times\tilde{X})}, \quad \| \mu - \tilde{\mu} \|_{C^k(\mathbf{R}\times\tilde{X})} < \delta \ll 1,$$

then there exists $C \geq 0$ depending on the $C^k(\mathbf{R} \times \tilde{X})$ norm of ϕ and μ such that

$$\| (\mathscr{N} - \tilde{\mathscr{N}}) f \|_{H^1(\tilde{X})} \leq C\delta \| f \|_{L^2(\tilde{X})} .$$

Here

$$\mathscr{N} = \sum_i \mathscr{N}_i = \sum_i \chi_{i_X} \mathscr{A}^* \chi_{i_Y} \mathscr{A}, \qquad \tilde{\mathscr{N}} = \sum_i \tilde{\mathscr{N}_i} = \sum_i \chi_{i_X} \tilde{\mathscr{A}}^* \chi_{i_Y} \tilde{\mathscr{A}}$$

are two microlocally restricted normal operators corresponding μ and $\tilde{\mu}$, respectively, and the cut-off functions χ_{i_X} and χ_{i_Y} are defined as above.

Proof Let $(x_0, \xi^0) \in T^*(X) \setminus 0$ be a fixed covector. By the visibility condition, there exists a line l_0, determined by (s_0, t_0), such that $\phi(t_0, x_0) = s_0$ and $\partial_x \phi(t_0, x_0) \parallel \xi^0$. Let χ_X and χ_Y be smooth cut-off functions defined above in neighborhoods of x_0 and l_0 corresponding to $\phi \in C^k$ with k large enough. By Lemma 3.4.2 and Remark 3.4.3, for any level curve l close to l_0, a perturbation of $\phi \in C^k$ results in the perturbation of the family of the level curves near $\phi(t_0, x) = s_0$. Since the local and semi-global Bolker conditions are open conditions, the visibility condition is preserved under the small perturbation in a neighborhood of l_0. On the other hand, a priori, we assumed that ϕ and $\tilde{\phi}$ are δ-close with C^k-topology. Therefore, one can choose the same cut-off function χ_X and χ_Y such that both projections Π_Y and $\tilde{\Pi}_Y$ are embeddings on their support and the visibility, the local and semi-global Bolker conditions are satisfied in each neighborhood. Therefore for each i, Theorem 3.5.1 implies that the microlocally restricted normal operators $\mathscr{N}_i = \chi_{i_X} \mathscr{A}^* \chi_{i_Y} \mathscr{A}$ and $\tilde{\mathscr{N}_i} = \chi_{i_X} \tilde{\mathscr{A}}^* \chi_{i_Y} \tilde{\mathscr{A}}$ are elliptic ΨDOs with symbols depending on ϕ, μ and $\tilde{\phi}$, $\tilde{\mu}$, respectively.

We now directly apply the argument on [Lemma 4, Homan and Zhou (2017)] to $\mathscr{N}_i^{\pm} - \tilde{\mathscr{N}_i}^{\pm}$, to conclude that for each i

$$\| \mathscr{N}_i^{\pm} - \tilde{\mathscr{N}_i}^{\pm} \|_{L_c^2(\tilde{X}) \to H^1(\tilde{X})} = \mathscr{O}(\delta),$$

and hence,

$$\| (\mathscr{N}_i - \tilde{\mathscr{N}_i}) f \|_{H^1(\tilde{X})} \leq C\delta \| f \|_{L^2(\tilde{X})} .$$

Now the fact that the operator $\mathscr{N}$ is a finite sum of operators of the form $\mathscr{N}_i$, as well as using the triangle inequality

$$\| (\mathscr{N} - \tilde{\mathscr{N}}) f \|_{H^1(\tilde{X})} \leq \sum_i \| (\mathscr{N}_i - \tilde{\mathscr{N}_i}) f \|_{H^1(\tilde{X})},$$

conclude the results. ■

Next result is a stability estimate for a generic class of dynamic operators satisfying the visibility, the local and semi-global Bolker conditions.

Theorem 3.6.1 *Let X be an open set of points (positions) x lying on lines in Y, where Y is the open sets of lines determined by (s,t) in $\mathbf{R}^2$. Let $\mathscr{A} : L^2(X) \to H^1(\tilde{X})$, satisfying the visibility, the local and semi-global Bolker conditions, be an injective dynamic operator defined by the real analytic function ϕ and positive real analytic weight μ. Then*

i) For any $\tilde{\phi} \in \text{neigh}(\phi)$ *and* $\tilde{\mu} \in \text{neigh}(\mu)$ *with* C^k*-topology* (k *an arbitrary large natural number*) *and for all* $f \in L^2(K)$ *with* K *a compact subset of* X*, there exists* $C \geq 0$ *such that*

$$\| f \|_{L^2(K)} \leq C \| \tilde{\mathscr{N}} f \|_{H^1(\tilde{X})} .$$

In particular, the operator $\tilde{\mathscr{A}}$ *is injective.*

ii) The following stability estimate remains true for any perturbation of ϕ *and* μ*:*

$$\| f \|_{L^2(K)} / C \leq \| \mathscr{N} f \|_{H^1(\tilde{X})} \leq C \| f \|_{L^2(K)} .$$

Proof i) $\mathscr{A}$ is injective, thus by Proposition 3.6.2, we have the following stability estimate:

$$\| f \|_{L^2(\tilde{X})} \leq C_1 \| \mathscr{N} f \|_{H^1(\tilde{X})} = C_1 \| \tilde{\mathscr{N}} f + (\mathscr{N} - \tilde{\mathscr{N}}) f \|_{H^1(\tilde{X})}$$

$$\leq C_1 \| \tilde{\mathscr{N}} f \|_{H^1(\tilde{X})} + C_1 \| (\mathscr{N} - \tilde{\mathscr{N}}) f \|_{H^1(\tilde{X})} .$$

By Lemma 3.6.1, there exists a constant $C_2 \geq 0$ such that

$$\| (\mathscr{N} - \tilde{\mathscr{N}}) f \|_{H^1(\tilde{X})} \leq C_2 \delta \| f \|_{L^2(\tilde{X})},$$

and therefore,

$$\| f \|_{L^2(\tilde{X})} \leq C_1 \| \tilde{\mathscr{N}} f \|_{H^1(\tilde{X})} + C_1 C_2 \delta \| f \|_{L^2(\tilde{X})} .$$

Letting $\delta < \min\{(2C_1C_2)^{-1}, 1/2\}$ yields

$$\| f \|_{L^2(K)} \leq C \| \tilde{\mathscr{N}} f \|_{H^1(\tilde{X})} .$$

Assume now that $\tilde{\mathscr{A}} f = 0$. Then

$$\tilde{\mathscr{N}} f = \sum_i \tilde{\mathscr{A}}^* \chi_i \tilde{\mathscr{A}} f = 0, \quad \text{as } \tilde{\mathscr{A}} f = 0.$$

The last inequality above implies that $f = 0$. Hence, the operator $\tilde{\mathscr{A}}$ is injective.

ii) This part follows directly from the first part and the continuity of pseudodifferential operator $\tilde{\mathscr{N}}$. ■

Proof [**Proof of Theorem 3.2.1**] The proof directly follows from Theorem 3.6.1. ■

3.7 Analysis of Dynamic Operator

In this section, we state the implications of our analysis for the partial case, where the dynamic operator is given by (3.1). This corresponds to the initial example of scanning the moving object with changing its shape. Some part of above results, the local and semi-global Bolker assumptions, are also given in [Theorem 14, B. N. Hahn and Quinto (2016)] and the problem of recovery of singularities has been analyzed. The periodic and non-periodic motions with $\phi(t,x) = \psi_t^{-1}(x)\cdot\omega(t)$ have been studied in B. N. Hahn and Quinto (2016) to explain which singularities are visible (see Theorems 24, 26).

Using a change of variable $x = \psi_t(z)$, the dynamic operator $\mathscr{A}$ can be written as:

$$\mathscr{A}f(s,t) = \iint_{\mathbf{R}^2} J(t,x)\mu(t,\psi_t^{-1}(x))f(x)\ \delta(s-\psi_t^{-1}(x)\cdot\omega(t))\ dx,$$

where $\psi_t^{-1}(x)\cdot\omega(t)$ is the level curve corresponding to $\mathscr{A}$.

Canonical relation. Setting $\Phi(s,t,x) = s-\psi_t^{-1}(x)\cdot\omega(t)$ in Proposition 3.4.1, the canonical relation $\mathscr{C}$ associated with $\mathscr{A}$ will be

$$\mathscr{C} = \{(\psi_t^{-1}(x)\cdot\omega(t),t,\sigma,-\sigma(\partial_t\psi_t^{-1}(x)\cdot\omega(t)+\psi_t^{-1}(x)\cdot\omega^{\perp}(t));x,\sigma\partial_x\psi_t^{-1}(x)\cdot\omega(t))\big|(s,t,x)\in M\}.$$

The microlocal version of double fibration is given by: where

$$\Pi_X(\psi_t^{-1}(x)\cdot\omega(t),t,\sigma,-\sigma\partial_t(\psi_t^{-1}(x)\cdot\omega(t));x,\sigma\partial_x\psi_t^{-1}(x)\cdot\omega(t)) = (x,\sigma\partial_x\psi_t^{-1}(x)\cdot\omega(t)),$$

$$\Pi_Y(\psi_t^{-1}(x)\cdot\omega(t),t,\sigma,-\sigma\partial_t(\psi_t^{-1}(x)\cdot\omega(t));x,\sigma\partial_x\psi_t^{-1}(x)\cdot\omega(t))$$

$$= (\psi_t^{-1}(x)\cdot\omega(t),t,\sigma,-\sigma\partial_t(\psi_t^{-1}(x)\cdot\omega(t))).$$

Visibility. The operator $\mathscr{A}$ satisfies in the visibility condition if for any $(x,\xi) \in T^*X \setminus 0$, the map given by (3.6) is locally surjective.

Local Bolker Condition. As it is shown in Proposition 3.4.1, the projection Π_Y is an immersion if the matrix $\mathrm{d}_{t,x,\sigma}\Pi_Y$ has rank equal to four or equivalently $\det(\mathrm{d}_{t,x,\sigma}\Pi_Y) \neq 0$. Since

$$\det(\mathrm{d}_{t,x,\sigma}\Pi_Y) = \det\left(\frac{\partial \psi_t^{-1}(x)\cdot\omega(t)}{\partial x^j}, \frac{\partial^2 \psi_t^{-1}(x)\cdot\omega(t)}{\partial t \partial x^j} \right) = h(t,x),$$

the projection Π_Y being an immersion is equivalent to the condition (3.4) being non-zero, i.e. $h(t,x) \neq 0$.

Semi-global Bolker condition (No conjugate points condition). By condition (3.4), Π_Y is injective if the map

$$x \to \left(\psi_t^{-1}(x)\cdot\omega(t), \partial_t(\psi_t^{-1}(x)\cdot\omega(t))\right)$$

is one-to-one.

The normal operator $\mathscr{N}$ is a ΨDO of order -1. Under the local and the semi-global Bolker conditions, Theorem 3.5.1 implies that the normal operator $\mathscr{N}$ associated with the dynamic operator $\mathscr{A}$ is a ΨDO of order -1 with principal symbol $p(x,\xi)$ near each (x_0,ξ^0). The principal symbol is given by

$$p(x,\xi) = (2\pi)^{-1}|\partial_x \psi_t^{-1}(x)\cdot\omega(t)| \frac{|\mu(x,\xi)|^2 J^2(x,\xi) + |\mu(x,-\xi)|^2 J^2(x,-\xi)}{|\xi| h(x,\xi)},$$

where $t = t(x,\xi)$ is locally well-defined by Lemma 3.4.3.

Remark 3.7.1 *Note that we do not require the function $\phi(t,x)$ to be smoothly periodic.*

Fan Beam Geometry. In previous sections, we showed that the dynamic operator $\mathscr{A}$ with $\phi(t,x) = \psi_t^{-1}(x)\cdot\omega(t)$ in parallel beam geometry, belongs to a more general integral geometry problem. We formulated the visibility, local and semi-global Bolker conditions, and derived our results for the case when $\phi(t,x) = \psi_t^{-1}(x)\cdot\omega(t)$.

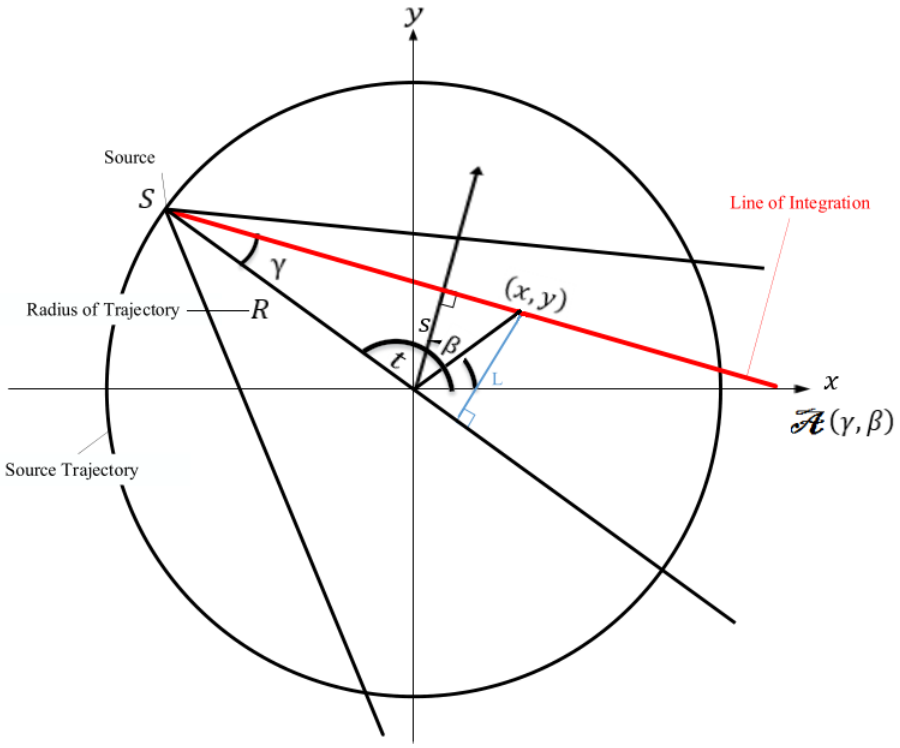

Figure 3.1. Parallel-Fan beam geometry relation.

Another common geometry which is often used in numerical simulations is Fan beam geometry. In this geometry, the assumption is that each scan is taken from a boundary point S (Source) and all directions instantly but the object moves when we change S (see Figure 3.1).

Using the Parallel-Fan beam relation

$$s = R\sin\gamma \qquad \beta = t + \gamma - \frac{\pi}{2},$$

and finding an appropriate level curve ϕ, one can show the dynamic operator $\mathscr{A}$ (in fan beam geometry) is also a special case of the general integral geometry problem discussed in this paper. Although the dynamic operator $\mathscr{A}$ has different time-parameterizations in parallel and fan beam geometries, they both can be categorized by the same general integral geometry problem.

For simplicity, our analysis in this section is restricted to a static case, i.e. $\phi(t,x) = x \cdot \omega(t)$, as the visibility, the local and semi global Bolker conditions are clearly satisfied when there is no motion. One can achieve the same results for the general case where the motion is not necessarily small. We, however, do not provide details on how to formulate the visibility, the local and semi-global Bolker conditions and rather state that our results are valid if these conditions are satisfied.

Let lines along which the dynamic operator of f is known, are specified by γ (the angle between the incident ray direction and the line from the source to the rotation center) and t (the angular position of the source). Then the fan beam data at time t is given by

$$\mathscr{A}_F f(t,\gamma) = \int_0^\infty f(S(t) + p\theta(\gamma))\, dp, \quad \theta(\gamma) \in S^1,$$

where $S(t)$ is the source at time t which moves along the trajectory with radius R. Here t is both a parameter along the source trajectory and the time variable. Note also that using the Parallel-Fan beam geometry relation one can derive the fan beam dynamic operator $\mathscr{A}_F$, given by

$$\mathscr{A}_F f(t,\gamma) = \mathscr{A}_P f(R\sin\gamma, t+\gamma-\frac{\pi}{2}).$$

Since the Jacobian

$$\left|\frac{\partial(s,\beta)}{\partial(t,\gamma)}\right| = R\cos\gamma$$

is non-zero, the transformation between these two geometries is smooth.

To implement our results in fan beam geometry, we need to find appropriate level curves ϕ. Let $S(t)$ be the source and x be the point on the incident ray, see Figure 3.1. We first set

$$\vec{\alpha} = x - S(t) = (x^1 - R\cos t, x^2 - R\sin t),$$

and then compute the perpendicular vector $\vec{\alpha}^\perp$ as follow:

$$\vec{\alpha}^\perp = \frac{\text{sign}(x^1 - R\cos t)}{|\vec{\alpha}|}(R\sin t - x^2, x^1 - R\cos t) = (\cos\alpha^\perp, \sin\alpha^\perp).$$

We only work with one direction from two possible orientations for $\vec{\alpha}^{\perp}$; say the one with $\text{sign}(x^1 - R\cos t) > 0$. For a fixed point x on the incident ray and a specific time t, the polar angle $\alpha^{\perp}$ is determined by

$$\alpha^{\perp} = \arg(\vec{\alpha}^{\perp}) = \tan^{-1}\big(\frac{x^1 - R\cos t}{R\sin t - x^2}\big).$$

We set

$$\phi(t,x) = \arg(\vec{\alpha}^{\perp}).$$

Now our results are valid if the visibility, the local and semi-global Bolker conditions are satisfied for this choice of function ϕ. Note that, here the function arg is not globally defined but this does not affect the analysis, as our results are local and we have chosen the branch where $\text{sign}(x^1 - R\cos t) > 0$. One can choose another branch of $\tan^{-1}$, however, this plays no role in differentiation which is involved in all above main three conditions.

BIHARMONIC OPERATORS AND INVERSE SCATTERING THEORY

*** This chapter concludes my original work: "Inverse Scattering and Stability Estimates for The Biharmonic Operator." Under the review in the journal of Inverse Problems.**

One of the fundamental theories in mathematics and physics, are *Wave Propagations* and *Scattering Theory* where the main objective is to investigate how radiation or particles are scattered based on the interaction of incident waves with medium of interest with a certain properties. The *Inverse Scattering Theory* is an inverse problem where the goal is to reconstruct geometric/physical properties of the medium, utilizing the scattered data from the incident wave.

4.1 Existing Results

Consider the following biharmonic equation:

$$(P-\lambda^4)u = (\Delta^2 + \mathbf{A}\cdot\nabla + V - \lambda^4)u = 0. \tag{4.1}$$

where Δ is Laplacian and $\cdot$ is the dot product $a\cdot b$ in $\mathbf{R}^n$. Here $\mathbf{A}$ is a vector-valued function representing the magnetic field and V is a scalar-valued function representing the potential function, with both $\mathbf{A}$ and V regular enough and compactly supported.

The scattering and the inverse scattering problems for the Schrödinger operators have a long history. One major application of the operator (4.1) is in the study of the theory of vibrations of beams and the elasticity theory, see Gazzola, Grunau, and Sweers (2010) for the case of the linear beam equation and Pausader (2010) for the nonlinear scattering problems. In a work by Tyni and Serov Tyni and Serov (2017), a Saito's type formula has been proved and it is shown that one can uniquely recover $V - \frac{1}{2}\nabla\cdot\mathbf{A}$, where $\mathbf{A} \in W^1_{p,2\delta}(\mathbf{R}^n)$ and $V \in L^p_{2\delta}(\mathbf{R}^n)$.

For the well-studied scattering problem of the Schrödinger equations, it has been shown that one can fully recover **curl A** and V and there is a gauge invariance, that is, for any two compactly supported magnetic fields with the same **curl** the measurement cannot distinguish between them.

4.2 Main Results

Our goal is to show what information about $\mathbf{A}$ and V can be recovered from the high-frequency asymptotic of scattering amplitude. We do not consider the whole amplitude at zero or near-zero frequencies (Calderon's problem). In the case of inverse boundary value problem at zero frequency, one can fully reconstruct the potential V and magnetic field $\mathbf{A}$, and in particular, there is no gauge invariance (see Katchalov, Kurylev, and Lassas (2001); Krupchyk, Lassas, and Uhlmann (2012); Nakamura, Sun, and Uhlmann (1995); Sun (1993)). The main result of this work is the following.

Theorem 4.2.1 *Let V and $\boldsymbol{A} \in C^k(\mathbf{R}^3)$ for k large enough. Then the high-frequency asymptotic expansion of scattering amplitude $a(\omega,\theta,\lambda)$ up to $\mathscr{O}(\lambda^{-4})$ recovers **curl** $\boldsymbol{A}$ and $V-\frac{1}{2}\nabla\cdot\boldsymbol{A}$ uniquely.*

In other words, for another pair $(\tilde{\mathbf{A}},\tilde{V})$ with scattering amplitude $\tilde{a}$ so that $a=\tilde{a}+\mathscr{O}(\lambda^{-4})$, then $\mathbf{curl}\ \mathbf{A}=\mathbf{curl}\ \tilde{\mathbf{A}}$ and $V-\frac{1}{2}\nabla\cdot\mathbf{A}=\tilde{V}-\frac{1}{2}\nabla\cdot\tilde{\mathbf{A}}$. We prove the following high-frequency approximation of the scattering amplitude

$$a(\omega,\theta,\lambda)=\mathrm{i}\lambda\,\theta\cdot\hat{\mathbf{A}}(\lambda(\omega-\theta))+\hat{V}(\lambda(\omega-\theta))+\mathscr{O}(\lambda^{-1})\quad\text{as}\quad\lambda\to\infty.$$

We study the near-field scattering problem and show that knowing the high-frequency asymptotic expansion up to an error of order $\mathscr{O}(\lambda^{-4})$ recovers the same two above quantities but contains no additional information about $\mathbf{A}$ and V. Our recovery process is constructive and explicit, and in principal stable, but we do not formally study stability.

4.3 Preliminaries

Our goal is to find a special solution of equation (4.1) and corresponding amplitude which are called scattering solution and scattering amplitude. We first define the outgoing resolvent and solution which are fundamental notations.

Definition 4.3.1 We define the outgoing free resolvent operator $R_0(\lambda):=(\Delta^2-\lambda^4)^{-1}$ from C_0^∞ to C^∞ as the analytic continuation of the operator

$$\mathscr{F}(R_0(\lambda)f)(\xi)=\frac{\hat{f}(\xi)}{|\xi|^4-\lambda^4},\quad\text{from}\quad\mathscr{I}m\,\lambda>0\quad\text{to}\quad\mathbf{C}.$$

Definition 4.3.2 Let $V$and $\mathbf{A} \in C^k(\mathbf{R}^3)$ for k large enough. We denote the outgoing resolvent operator by $R(\lambda) : C_0^\infty(\mathbf{R}^n) \to C^\infty(\mathbf{R}^n)$ and define as

$$R(\lambda) = \lim_{\varepsilon \to 0^+} (\Delta^2 + \mathbf{A}\cdot\nabla + V - \lambda^4 - \mathrm{i}\varepsilon)^{-1}.$$

Definition 4.3.3 Given $\lambda \in \mathbf{C}$, we say that the function u is λ-outgoing, if there exists $c > 0$ and $f \in \mathscr{E}'$ such that $u_{|_{|x|>c}} = R_0(\lambda) f_{|_{|x|>c}}$. In applications, the constant c is larger than the radius of the support of the perturbations.

For $f \in C_0^\infty(\mathbf{R}^3)$, we have the following integral operator representation

$$[R_0(\lambda)f](x) = \int G_0(x,y,\lambda) f(y)\mathrm{d}y, \qquad G_0(x,y,\lambda) = \frac{e^{\mathrm{i}\lambda|x-y|} - e^{-\lambda|x-y|}}{8\pi\lambda^2|x-y|}. \tag{4.2}$$

where G_0 is a 3-dimensional fundamental solution of $\Delta^2 - \lambda^4$, i.e. the kernel of $(\Delta^2 - \lambda^4 - \mathrm{i}0)^{-1}$. Note that the operator $\Delta^2 - \lambda^4$ can be written as $(-\Delta - \lambda^2)(-\Delta + \lambda^2)$. Since the operator $-\Delta + \lambda^2$ is elliptic, i.e. the principle symbol is $|\xi|^2 + \lambda^2$, there is no geometric optics. The operator $-\Delta - \lambda^2$ is the Helmholtz operator.

We now formulate the scattering amplitude where the derivation mainly follows Tyni and Serov (2017). Let $u = e^{\mathrm{i}\lambda x\cdot\theta} + u_{sc}$ be a solution for equation (4.1), with $e^{\mathrm{i}\lambda x\cdot\theta}$ the harmonic plane wave with incoming direction $\theta \in S^2$ (i.e. incident wave which is neither outgoing nor incoming), and u_{sc} the scattered solution which is assumed to be outgoing. To formulate the scattering amplitude a, we first formulate the Lippmann-Schwinger integral equation. One has

$$(\Delta^2 + \mathbf{A}\cdot\nabla + V - \lambda^4)(e^{\mathrm{i}\lambda x\cdot\theta} + u_{sc}) = 0 \quad \Longrightarrow \quad (\Delta^2 - \lambda^4)(e^{\mathrm{i}\lambda x\cdot\theta} + u_{sc}) = -(\mathbf{A}\cdot\nabla + V)u$$

$$\Longrightarrow \quad (\Delta^2 - \lambda^4)u_{sc} = -(\mathbf{A}\cdot\nabla + V)u \quad \Longrightarrow \quad u_{sc} = -[R_0(\lambda)(\mathbf{A}\cdot\nabla + V)]u.$$

Since u_{sc} is an outgoing scattered solution, one may invert the operator $(\Delta^2 - \lambda^4)$ to have an explicit formula for the scattering solution u_{sc} using equation (4.2):

$$u_{sc} = -\int G_0(x,y,\lambda)\big(\mathbf{A}(y)\cdot\nabla + V(y)\big)u_{(y,\theta,\lambda)}\mathrm{d}y.$$

Note that since $\mathbf{A}$ and V are compactly supported, by definition $R_0(\lambda)(\mathbf{A}\cdot\nabla+V)$ is outgoing and therefore u_{sc} is unique. On the other hand,

$$(\Delta^2+\mathbf{A}\cdot\nabla+V-\lambda^4)(e^{\mathrm{i}\lambda x\cdot\theta}+u_{sc})=0 \quad \Longrightarrow \quad u_{sc}=-[R(\lambda)(\mathbf{A}\cdot\nabla+V)]e^{\mathrm{i}\lambda x\cdot\theta},$$

where $R(\lambda)$ is defined by Definition 4.3.2 We need to justify that the r.h.s of the last equation is also outgoing. Assume that the resolvent exists for some λ. Similar to [Corollary 4.4, Tyni and Serov (2017)], by the resolvent identity,

$$R(\lambda)-R_0(\lambda)=-R_0(\lambda)(\mathbf{A}\cdot\nabla+V)R(\lambda) \quad \Longrightarrow \quad R(\lambda)=R_0(\lambda)+\sum_{k=1}^{\infty}\big(-R_0(\lambda)(\mathbf{A}\cdot\nabla+V)\big)^k R_0(\lambda).$$

Using Agmon's estimates, one can show the above series converges in $H^1_{-\delta}$ and hence a unique solution exists. Therefore, for a compactly supported function, $R(\lambda)$ is a well-defined outgoing operator and the following important identity holds

$$u_{sc}=-[R_0(\lambda)(\mathbf{A}\cdot\nabla+V)]u=-[R(\lambda)(\mathbf{A}\cdot\nabla+V)]e^{\mathrm{i}\lambda x\cdot\theta}.$$

We are particularly interested in an outgoing solution of (4.1). Since every outgoing solution has a far-field pattern (see **?**), for any $(\omega,\theta,\lambda)\in S^2\times S^2\times\mathbf{R}^+$, there exists a function $a=a(\omega,\theta,\lambda)$ such that

$$u(x,\theta,\lambda)=e^{\mathrm{i}\lambda x\cdot\theta}-C_3\frac{e^{\mathrm{i}\lambda|x|}}{\lambda^2|x|}a(\omega,\theta,\lambda)+\mathscr{O}(\frac{1}{|x|^2}),\ \text{as } |x|\to\infty,$$

where $\omega=\frac{x}{|x|}$ is an outgoing direction. The scattering amplitude $a(\omega,\theta,\lambda)$ is given by

$$2.2a(\omega,\theta,\lambda)=\int e^{-\mathrm{i}\lambda\omega\cdot y}(\mathbf{A}_{(y)}\cdot\nabla+V_{(y)})u_{(y,\theta,\lambda)}\mathrm{d}y. \tag{4.3}$$

The scattering amplitude a measures scattering in direction θ, for a plane wave at frequency λ propagating in direction ω. Next section provides necessary tools to proof the main result. We use the above representation of scattering solution to find appropriate estimates for our results.

4.4 High Frequency Asymptotic Expansion

Consider the following ansatz expansion for the solution of biharmonic equation (4.1):

$$u(x,\theta,\lambda) = e^{\mathrm{i}\lambda x\cdot\theta}(a_0 + \frac{\mathrm{i}}{\lambda}a_1 + \frac{1}{\lambda^2}a_2 + \frac{1}{\lambda^3}a_3 + \frac{1}{\lambda^4}a_4 + \frac{1}{\lambda^5}a_5 + \mathscr{O}(\frac{1}{\lambda^6})) = e^{\mathrm{i}\lambda x\cdot\theta}\mathbf{a}.$$

Since the wave before entering the support is just a plane wave $e^{\mathrm{i}\lambda x\cdot\theta}$ propagating in direction $\theta \in S^2$, we assume the following initial condition where $a_0(x,\theta)_{|_{x\cdot\theta\ll 0}} = 1$ and $a_i(x,\theta)_{|_{x\cdot\theta\ll 0}} = 0$ for $i = 1,2,3,\ldots$. The proposition below gives explicit expression for the coefficient a_i for the measurement up to $\mathscr{O}(\lambda^{-3})$.

Proposition 4.4.1 *If u is the solution of biharmonic equation (4.1), then for $i = 0,1,\ldots,5$, the coefficient a_i solves the following zero-initial condition system of equations:*

$$\begin{cases} a_0 = 1, \quad a_1 = 0, \quad 4(\theta\cdot\nabla)a_2 = \theta\cdot\boldsymbol{A}, \quad 4\mathrm{i}(\theta\cdot\nabla)a_3 = -2(\Delta + 2(\theta\cdot\nabla)^2)a_2 + V, \\ 4\mathrm{i}(\theta\cdot\nabla)a_4 = -2(\Delta + 2(\theta\cdot\nabla)^2)a_3 + \mathrm{i}(4(\theta\cdot\nabla)\Delta + \theta\cdot\boldsymbol{A})a_2, \\ 4\mathrm{i}(\theta\cdot\nabla)a_5 = -2(\Delta + 2(\theta\cdot\nabla)^2)a_4 + \mathrm{i}(4(\theta\cdot\nabla)\Delta + \theta\cdot\boldsymbol{A})a_3 + \mathrm{i}(\Delta^2 + \boldsymbol{A}\cdot\nabla + V)a_2. \end{cases} \tag{4.4}$$

Moreover, for

$$E(x,\theta,\lambda) := u(x,\theta,\lambda) - e^{\mathrm{i}\lambda x\cdot\theta}(1 + \frac{1}{\lambda^2}a_2 + \frac{1}{\lambda^3}a_3) = u(x,\theta,\lambda) - e^{\mathrm{i}\lambda x\cdot\theta}(1+\tilde{\mathbf{a}}), \tag{4.5}$$

the following estimates hold;

$$\| E(x,\theta,\lambda) \|_{L^2(\mathbf{R}^3)} = \mathscr{O}(\lambda^{-4}), \qquad \| E(x,\theta,\lambda) \|_{H^1(\mathbf{R}^3)} = \mathscr{O}(\lambda^{-3}).$$

Proof Let $u(x,\theta,\lambda) = e^{\mathrm{i}\lambda x\cdot\theta}\mathbf{a}$ be solution of biharmonic equation (4.1). Since

$$\begin{cases} \mathbf{A}\cdot\nabla(e^{\mathrm{i}\lambda x\cdot\theta}\mathbf{a}) = e^{\mathrm{i}\lambda x\cdot\theta}[\mathrm{i}\lambda\mathbf{A}\cdot\theta + \mathbf{A}\cdot\nabla]\mathbf{a} \\ \Delta^2(e^{\mathrm{i}\lambda x\cdot\theta}\mathbf{a}) = e^{\mathrm{i}\lambda x\cdot\theta}[\Delta^2 + 4\mathrm{i}\lambda(\theta\cdot\nabla)\Delta - 2\lambda^2\Delta - 4\lambda^2(\theta\cdot\nabla)^2 - 4\mathrm{i}\lambda^3(\theta\cdot\nabla) + \lambda^4]\mathbf{a}, \end{cases}$$

we have

$$(P-\lambda^4)u = e^{\mathrm{i}\lambda x\cdot\theta}[-4\mathrm{i}\lambda^3(\theta\cdot\nabla) - 2\lambda^2(\Delta + 2(\theta\cdot\nabla)^2) + \mathrm{i}\lambda(4(\theta\cdot\nabla)\Delta + \mathbf{A}\cdot\theta) + \Delta^2 + \mathbf{A}\cdot\nabla + V]\mathbf{a} = 0.$$

Rearranging all terms with respect to the power of λ and equating singular coefficients, we get the following transport equations for a_i:

$$\begin{cases} \mathscr{O}(\lambda^3): & -4\mathrm{i}(\theta\cdot\nabla)a_0 = 0, \\ \mathscr{O}(\lambda^2): & 4(\theta\cdot\nabla)a_1 - 2(\Delta + 2(\theta\cdot\nabla)^2)a_0 = 0, \\ \mathscr{O}(\lambda): & -4\mathrm{i}(\theta\cdot\nabla)a_2 - 2\mathrm{i}(\Delta+2(\theta\cdot\nabla)^2)a_1 + \mathrm{i}(4(\theta\cdot\nabla)\Delta + \theta\cdot\mathbf{A})a_0 = 0, \\ \mathscr{O}(1): & -4\mathrm{i}(\theta\cdot\nabla)a_3 - 2(\Delta+2(\theta\cdot\nabla)^2)a_2 - (4(\theta\cdot\nabla)\Delta + \theta\cdot\mathbf{A})a_1 + (\Delta^2 + \mathbf{A}\cdot\nabla + V)a_0 = 0, \\ \mathscr{O}(\lambda^{-1}): & -4\mathrm{i}(\theta\cdot\nabla)a_4 - 2(\Delta+2(\theta\cdot\nabla)^2)a_3 + \mathrm{i}(4(\theta\cdot\nabla)\Delta + \theta\cdot\mathbf{A})a_2 + \mathrm{i}(\Delta^2 + \mathbf{A}\cdot\nabla + V)a_1 = 0, \\ \mathscr{O}(\lambda^{-2}): & -4\mathrm{i}(\theta\cdot\nabla)a_5 - 2(\Delta+2(\theta\cdot\nabla)^2)a_4 + \mathrm{i}(4(\theta\cdot\nabla)\Delta + \theta\cdot\mathbf{A})a_3 + \mathrm{i}(\Delta^2 + \mathbf{A}\cdot\nabla + V)a_2 = 0. \end{cases}$$

The first transport equation above and the initial condition $a_{0|_{x\cdot\theta\ll 0}} = 1$ implies that $a_0 \equiv 1$. To compute a_1, by the second equation above we have

$$4(\theta\cdot\nabla)a_1(x) - 2(\Delta+2(\theta\cdot\nabla)^2)a_0(x) = 0 \quad \Longrightarrow \quad (\theta\cdot\nabla)a_1(x) = 0.$$

Since $a_{1|_{x\cdot\theta\ll 0}} = 0$, therefore $a_1 \equiv 0$. Considering the transport equation corresponding $\mathscr{O}(\lambda)$, we have

$$-4\mathrm{i}(\theta\cdot\nabla)a_2(x) - 2\mathrm{i}(\Delta+2(\theta\cdot\nabla)^2)a_1(x) + \mathrm{i}(4(\theta\cdot\nabla)\Delta + \theta\cdot\mathbf{A}(x))a_0(x) = 0 \Longrightarrow (\theta\cdot\nabla)a_2(x) = \frac{1}{4}\theta\cdot\mathbf{A}(x).$$

Integrating the last equation along the flow $x + t\theta$ yields

$$\int_{-\infty}^{0} (\theta\cdot\nabla)a_2(x+s\theta)\, ds = \frac{1}{4}\int_{-\infty}^{0} \theta\cdot\mathbf{A}(x+s\theta)\, ds.$$

Since $\theta\cdot\nabla = \partial_t$ along the null bi-characteristics (i.e. $x\cdot\theta = t$), one has

$$\int_{-\infty}^{0} \partial_s a_2(x+s\theta)\, ds = \frac{1}{4}\int_{-\infty}^{0} \theta\cdot\mathbf{A}(x+s\theta)\, ds \quad \Longrightarrow \quad a_2(x) = \frac{1}{4}\int_{-\infty}^{0} \theta\cdot\mathbf{A}(x+s\theta)\, ds,$$

which is the X-ray transform of the magnetic field $\mathbf{A}$ along the lines $x\cdot\theta = t$. Notice that for $i = 3,4,5$ all the coefficients a_i depend on the potential and magnetic fields V and $\mathbf{A}$ can be computed recursively, by considering the transport equation corresponding to $\mathscr{O}(\lambda^{-i})$ and integrating along the flow as above.

Our next goal is to establish an estimate for the error term $E(x,\theta,\lambda)$ in (4.5). Since u solves the biharmonic equation, we have

$$-(P-\lambda^4)E(x,\theta,\lambda) = (P-\lambda^4)\big(e^{\mathrm{i}\lambda x\cdot\theta}(1+\tilde{\mathbf{a}})\big)$$

$$= e^{\mathrm{i}\lambda x\cdot\theta}[-4\mathrm{i}\lambda^3(\theta\cdot\nabla) - 2\lambda^2(\Delta+2(\theta\cdot\nabla)^2) + \mathrm{i}\lambda(4(\theta\cdot\nabla)\Delta+\mathbf{A}\cdot\theta)+\Delta^2+\mathbf{A}\cdot\nabla+V]\big(1+\tilde{\mathbf{a}}\big).$$

Expanding the r.h.s of above equation and using transport equations (4.4) implies that

$$-(P-\lambda^4)E = \frac{e^{\mathrm{i}\lambda x\cdot\theta}}{\lambda}\big(-2(\Delta+2(\theta\cdot\nabla)^2)a_3 + \mathrm{i}\lambda^2(4(\theta\cdot\nabla)\Delta+\mathbf{A}\cdot\theta)(\tilde{\mathbf{a}}) + \lambda(\Delta^2+\mathbf{A}\cdot\nabla+V)(\tilde{\mathbf{a}})\big).$$

Notice that although the scattering solution $u_{sc} = u - e^{\mathrm{i}\lambda\cdot\theta}$ is outgoing (see Definition 4.3.2), the above error term E is not outgoing as it has infinite support. To apply the resolvent $R(\lambda)$, we first need to localize the r.h.s of above error in $L^2(\mathbf{R}^3)$: Let the compact set K denotes the support of perturbation $\nabla\cdot\mathbf{A}+V$, and $\chi\in C_0^\infty(\mathbf{R}^3)$ be a smooth cut-off function such that $\chi(x)=1$ near the support K. We define

$$E_\chi(x,\theta,\lambda) := u(x,\theta,\lambda) - e^{\mathrm{i}\lambda x\cdot\theta}(1+\chi\tilde{\mathbf{a}}),$$

where $u = e^{\mathrm{i}\lambda x\cdot\theta}+u_{sc}$ solves the biharmonic equation (4.1). For all x away from K, $\chi(x)=0$, and therefore $E=u_{sc}$ is outgoing. On the other hand, for $\lambda\gg 1$, E is outgoing as $\chi(x)=1$ for $x\in K$. We have

$$\begin{aligned}-(P-\lambda^4)E_\chi = e^{\mathrm{i}\lambda x\cdot\theta}\Big(&\lambda\big(-4\mathrm{i}(\theta\cdot\nabla)(\chi a_2)+\mathrm{i}\theta\cdot\mathbf{A})\big) - \big(4\mathrm{i}(\theta\cdot\nabla)(\chi a_3)+2(\Delta+2(\theta\cdot\nabla)^2)(\chi a_2)+V\big)\\ &+\frac{1}{\lambda}\big(-2(\Delta+2(\theta\cdot\nabla)^2)(\chi a_3)+\mathrm{i}(4(\theta\cdot\nabla)\Delta+\mathbf{A}\cdot\theta)(\chi a_2)\big)\\ &+\frac{1}{\lambda^2}\big(\mathrm{i}(4(\theta\cdot\nabla)\Delta+\mathbf{A}\cdot\theta)(\chi a_3)+(\Delta^2+\mathbf{A}\cdot\nabla+V)(\chi a_2)\big)\\ &+\frac{1}{\lambda^3}(\Delta^2+\mathbf{A}\cdot\nabla+V)(\chi a_3)\Big)\end{aligned}$$

Using the Lie bracket notation and the fact that $\chi\mathbf{A}=\mathbf{A}$ and $\chi V = V$

$$-(P-\lambda^4)E_\chi = e^{\mathrm{i}\lambda x\cdot\theta}\Big(-4\mathrm{i}\lambda^3[\theta\cdot\nabla,\chi]\tilde{\mathbf{a}} - 2\lambda^2\big([\Delta+2(\theta\cdot\nabla)^2,\chi]\tilde{\mathbf{a}}\big) + \mathrm{i}\lambda[4\theta\cdot\nabla\Delta+\mathbf{A}\cdot\theta,\chi]\tilde{\mathbf{a}}$$

$$+[\Delta^2+\mathbf{A}\cdot\nabla+V,\chi]\tilde{\mathbf{a}}+\frac{\chi}{\lambda}\big(-2(\Delta+2(\theta\cdot\nabla)^2)a_3+\lambda(\Delta^2+\mathbf{A}\cdot\nabla+V)\tilde{\mathbf{a}}+\mathrm{i}\lambda^2(4\theta\cdot\nabla\Delta+\mathbf{A}\cdot\theta)\tilde{\mathbf{a}}\big)\Big)$$

$$=e^{\mathrm{i}\lambda x\cdot\theta}(E_1+\frac{\chi}{\lambda}E_2).$$

Now we may apply the resolvent $R(\lambda)$ to both sides of the above equation as the r.h.s is compactly supported. Our goal is to show that $\| E_\chi \|_{L^2}=\mathscr{O}(\lambda^{-4})$, for $\lambda>0$ large enough. Note that since $\tilde{\mathbf{a}}=\mathscr{O}(\lambda^{-2})$, the problematic terms in establishing the estimate for E_χ in the r.h.s of above equation will be

$$\lambda^2[\Delta+2(\theta\cdot\nabla)^2,\chi]\tilde{\mathbf{a}}=\mathscr{O}(1)\quad\text{and}\quad\lambda^3[\theta\cdot\nabla,\chi]\tilde{\mathbf{a}}=\mathscr{O}(\lambda),\tag{4.6}$$

as the rest of above terms are of $\mathscr{O}(\lambda^{-1})$ which combined with the resolvent estimates given by Agmon's estimate gives the desired estimates for E_χ. Consider the first term in (4.6). By the resolvent identity

$$R_0(\lambda)-R(\lambda)=R_0(\lambda)(\mathbf{A}\cdot\nabla+V)R(\lambda)\quad\Longrightarrow\quad R(\lambda)=R_0(\lambda)(I-(\mathbf{A}\cdot\nabla+V)R(\lambda)).$$

Therefore,

$$R(\lambda)\big[\lambda^2e^{\mathrm{i}\lambda x\cdot\theta}[\Delta+2(\theta\cdot\nabla)^2,\chi]\tilde{\mathbf{a}}\big]=R_0(\lambda)(I-(\mathbf{A}\cdot\nabla+V)R(\lambda))\big[\lambda^2e^{\mathrm{i}\lambda x\cdot\theta}[\Delta+2(\theta\cdot\nabla)^2,\chi]\tilde{\mathbf{a}}\big]$$

$$=R_0(\lambda)\big[\lambda^2e^{\mathrm{i}\lambda x\cdot\theta}[\Delta+2(\theta\cdot\nabla)^2,\chi]\tilde{\mathbf{a}}\big]-R_0(\lambda)(\mathbf{A}\cdot\nabla+V)R(\lambda)\big[\lambda^2e^{\mathrm{i}\lambda x\cdot\theta}[\Delta+2(\theta\cdot\nabla)^2,\chi]\tilde{\mathbf{a}}\big]$$

$$=\mathscr{I}_1+\mathscr{I}_2.$$

Similarly, for the second term in (4.6), one has

$$R(\lambda)\big[\lambda^3e^{\mathrm{i}\lambda x\cdot\theta}[\theta\cdot\nabla,\chi]\tilde{\mathbf{a}}\big]=R_0(\lambda)(I-(\mathbf{A}\cdot\nabla+V)R(\lambda))\big[\lambda^3e^{\mathrm{i}\lambda x\cdot\theta}[\theta\cdot\nabla,\chi]\tilde{\mathbf{a}}\big]$$

$$=R_0(\lambda)\big[\lambda^3e^{\mathrm{i}\lambda x\cdot\theta}[\theta\cdot\nabla,\chi]\tilde{\mathbf{a}}\big]-R_0(\lambda)(\mathbf{A}\cdot\nabla+V)R(\lambda)\big[\lambda^3e^{\mathrm{i}\lambda x\cdot\theta}[\theta\cdot\nabla,\chi]\tilde{\mathbf{a}}\big]=\mathscr{J}_1+\mathscr{J}_2.$$

Now we are ready establish estimates for $\mathscr{I}_1$, $\mathscr{I}_2$, $\mathscr{J}_1$, and $\mathscr{J}_2$. Note that the integrands in above free-resolvent operators are compactly supported and therefore, all integrals above are well-defined (see equation (4.2)).

Estimating $\mathscr{I}_2$, $\mathscr{J}_2$. By Agmon's estimate

$$\| \mathscr{I}_2 \|_{L^2_{-\delta}} = \| R_0(\lambda)(\mathbf{A}\cdot\nabla + V)R(\lambda)\big[\lambda^2 e^{\mathrm{i}\lambda x\cdot\theta}[\Delta + 2(\theta\cdot\nabla)^2, \chi]\tilde{\mathbf{a}}\big] \|_{L^2_{-\delta}}$$

$$\leq \frac{C_0}{\lambda} \| (\mathbf{A}\cdot\nabla + V)R(\lambda)\big[e^{\mathrm{i}\lambda x\cdot\theta}[\Delta + 2(\theta\cdot\nabla)^2, \chi]\tilde{\mathbf{a}}\big] \|_{L^2_{\delta}}$$

$$\leq \frac{C_0}{\lambda}\Big(\| \mathbf{A}\cdot\nabla R(\lambda)\big[e^{\mathrm{i}\lambda x\cdot\theta}[\Delta + 2(\theta\cdot\nabla)^2, \chi]\tilde{\mathbf{a}}\big] \|_{L^2_{\delta}}$$

$$+ \| VR(\lambda)\big[e^{\mathrm{i}\lambda x\cdot\theta}[\Delta + 2(\theta\cdot\nabla)^2, \chi]\tilde{\mathbf{a}}\big] \|_{L^2_{\delta}} \Big) \leq \frac{C_0}{\lambda}\Big(\frac{C_1}{\lambda^4} + \frac{C_2}{\lambda^5}\Big) = \mathscr{O}(\lambda^{-5}),$$

where we used the fact that $\mathbf{A}$, V are compactly supported. Similarly,

$$\| \mathscr{J}_2 \|_{L^2_{-\delta}} = \| R_0(\lambda)(\mathbf{A}\cdot\nabla + V)R(\lambda)\big[\lambda^3 e^{\mathrm{i}\lambda x\cdot\theta}[\theta\cdot\nabla, \chi]\tilde{\mathbf{a}}\big] \|_{L^2_{-\delta}}$$

$$\leq C_0 \| (\mathbf{A}\cdot\nabla + V)R(\lambda)\big[e^{\mathrm{i}\lambda x\cdot\theta}[\theta\cdot\nabla, \chi]\tilde{\mathbf{a}}\big] \|_{L^2_{\delta}}$$

$$\leq C_0\Big(\| \mathbf{A}\cdot\nabla R(\lambda)\big[e^{\mathrm{i}\lambda x\cdot\theta}[\theta\cdot\nabla, \chi]\tilde{\mathbf{a}}\big] \|_{L^2_{\delta}} + \| VR(\lambda)\big[e^{\mathrm{i}\lambda x\cdot\theta}[\theta\cdot\nabla, \chi]\tilde{\mathbf{a}}\big] \|_{L^2_{\delta}} \Big)$$

$$\leq C_0\Big(\frac{C_1}{\lambda^4} + \frac{C_2}{\lambda^5}\Big) = \mathscr{O}(\lambda^{-4}),$$

Estimating $\mathscr{I}_1$, $\mathscr{J}_1$. We mainly follow the idea in P. D. Stefanov (1989) to estimate $\mathscr{I}_1$, $\mathscr{J}_1$. Let Γ be the set where the derivatives of χ is supported, and

$$S = \{y = x + t\theta \mid x \in B(0,R),\ t \geq 0\}.$$

Then for any $x \in B(0,R)$ and $y \in \Gamma \cap S$ the kernel $G_0(x,y,\lambda)$, given by (4.2), is smooth as $x \neq y$. We have

$$\mathscr{I}_1 = R_0(\lambda)(\lambda^2 e^{\mathrm{i}\lambda x\cdot\theta}[\Delta + 2(\theta\cdot\nabla)^2, \chi]\tilde{\mathbf{a}})(x)$$

$$= \int \frac{e^{\mathrm{i}\lambda(|x-y| + y\cdot\theta)} - e^{-\lambda|x-y|}e^{\mathrm{i}\lambda y\cdot\theta}}{8\pi|x-y|}[\Delta_y + 2(\theta\cdot\nabla_y)^2, \chi_y]\tilde{\mathbf{a}}(y)\mathrm{d}y$$

$$= \int K(x,y,\lambda,\theta)[\Delta_y + 2(\theta\cdot\nabla_y)^2, \chi_y]\tilde{\mathbf{a}}(y)\mathrm{d}y$$

Splitting the above integral, we have oscillating integrals with a real phase function $\phi_1(x,y) = |x-y| + y\cdot\theta$ and a complex phase function $\phi_2(x,y) = y\cdot\theta + \mathrm{i}|x-y|$. The contribution of the phase ϕ_2 is exponentially small as there is a lower bound of $|x-y|$. In fact, for λ large enough, away from the diagonal $\{x=y\}$, the term $e^{-\lambda|x-y|}$ exponentially approaches to zero. Therefore, we can concentrate on the phase ϕ_1, by employing the stationary phase method. By a simple calculation, one has

$$\nabla_y\phi_1 = \frac{y-x}{|y-x|} + \theta \quad \Longrightarrow \quad \theta\cdot\nabla_y\phi_1 = \frac{(y-x)\cdot\theta}{|y-x|} + 1 > 1,$$

for any $x \in B(0,\mathbf{R})$ and $y \in \Gamma \cap S$. Since

$$e^{\mathrm{i}\lambda\phi_1} = \frac{\nabla_y\phi_1\cdot\nabla_y}{\mathrm{i}\lambda|\nabla_y\phi_1|^2}e^{\mathrm{i}\lambda\phi_1},$$

multiple integration by parts yields $\| \mathscr{I}_1 \|_{L^2_{-\delta}(\mathbf{R}^n)} = \mathscr{O}(\lambda^{-4})$. Similarly, several integration by parts on

$$\mathscr{J}_1 = R_0(\lambda)(\lambda^3 e^{\mathrm{i}\lambda x\cdot\theta}[\theta\cdot\nabla,\chi]\mathbf{a})(x) = \int \lambda K(x,y,\lambda,\theta)[\theta\cdot\nabla_y,\chi_y]\tilde{\mathbf{a}}(y)\mathrm{d}y.$$

yields $\| \mathscr{J}_1 \|_{L^2_{-\delta}(\mathbf{R}^n)} = \mathscr{O}(\lambda^{-4})$.

It remains to establish $\| E \|_{H^1_{-\delta}(\mathbf{R}^n)} = \mathscr{O}(\lambda^{-3})$. Consider the operator $\nabla R(\lambda) : L^2_\delta(\mathbf{R}^n) \to L^2_\delta(\mathbf{R}^n)$, with

$$3.4\nabla R(\lambda)[e^{\mathrm{i}\lambda x\cdot\theta}(E_1 + \frac{\chi}{\lambda}E_2)]. \tag{4.7}$$

Since $R(\lambda)$ is the resolvent with constant coefficient, the gradient, and the resolvent commute. Therefore, the problematic terms in (4.7) will be the same as the ones discussed in (4.6) and all terms of the form $R_0(\lambda)f$ and $R(\lambda)f$ in (4.7) will have the desired H^1_δ estimates by Agmon's estimate. Now we need to revisit the argument for those terms in (4.7) with stationary phase similar to $\mathscr{I}_1$ and $\mathscr{J}_1$, where an integration by part argument has been used to establish estimates. We recall that we do not use Agmon's estimates to find H^1_δ estimates. Applying the gradient directly to $K(x,y,\lambda,\theta)$, one has

$$K(x,y,\lambda,\theta) = \lambda\tilde{K}(x,y,\lambda,\theta)$$

where $\tilde{K}$ is smooth bounded away from the diagonal $\{x=y\}$. Now integration by parts argument establishes the desired H^1_δ estimates of $\mathscr{O}(\lambda^{-N})$, where N depends on the regularity of magnetic field $\mathbf{A}$ and potential function V. This proves the proposition. ■

4.5 Near-field Scattering

In this section we study the near-field scattering problem. Let u be the biharmonic solution of equation (4.1) and B_R be a ball with radius $R > 0$ large enough containing the perturbation $\mathbf{A}$ and V ($\operatorname{supp}\mathbf{A} \cup \operatorname{supp} V \subset B_R$). To study the near-field scattering, we only consider $u_{|_{x\cdot\theta=R}}$ as our scattering data and do not study the scattering amplitude to reconstruct the high-frequency asymptotic expansion of the solution. In the following proposition, we demonstrate that all terms up to order $\mathscr{O}(\lambda^{-4})$ contains no additional information.

Proposition 4.5.1 *Assume that the scattering data $u_{|_{x\cdot\theta=R}}$ is known up to error of order $\mathscr{O}(\lambda^{-4})$. Then*

*i) The scattering data recovers **curl** $\boldsymbol{A}$ and $V - \frac{1}{2}\nabla\cdot\boldsymbol{A}$.*

ii) The scattering data known up to error of order $\mathscr{O}(\lambda^{-4})$ contains no additional information on $\boldsymbol{A}$ and V.

Proof i) Let u and $\tilde{u}$ be a pair of biharmonic solutions corresponding to pairs $(\mathbf{A}, V)$ and $(\tilde{\mathbf{A}}, \tilde{V})$ such that

$$(u - \tilde{u})_{|_{x\cdot\theta=R}} = \mathscr{O}(\lambda^{-4}).$$

By Proposition 4.4.1, we have

$$a_2(x) = \frac{1}{4}\int_{-\infty}^{0} \theta\cdot\mathbf{A}(x+s\theta)\, ds,$$

which is the X-ray transform of the magnetic field $\mathbf{A}$ along the lines $x + t\theta$, (see Sharafutdinov (n.d.)). The function $\delta u = u - \tilde{u}$ has near-field data up to the error of order $\mathscr{O}(\lambda^{-4})$. Hence $\delta a_2 \equiv 0$ implies that there exists a compactly supported function ϕ such that $\delta\mathbf{A} = d\phi$. This shows that the scattering data recovers **curl A**. To show the scattering data recovers $V - \frac{1}{2}\nabla\cdot\mathbf{A}$, we recall that

$$4\mathrm{i}(\theta\cdot\nabla)a_3(x) = -2\Delta a_2(x) - 4(\theta\cdot\nabla)^2 a_2(x) + V(x).$$

To have an explicit formula for a_3 we need to invert the Radon transform as follows: by integrating above equation along the flow and using the fact that $\theta\cdot\nabla = \partial_t$ and $(\theta\cdot\nabla)a_2(x) = \frac{1}{4}\theta\cdot\mathbf{A}(x)$ we have

$$a_3(x) = \frac{1}{4\mathrm{i}}[-2\int_{-\infty}^{0} \Delta a_{2(x+s\theta)}\, ds - 4\int_{-\infty}^{0} (\theta\cdot\nabla)^2 a_{2(x+s\theta)}\, ds + \int_{-\infty}^{0} V_{(x+s\theta)}\, ds$$

$$\Longrightarrow \qquad a_3(x) = \frac{1}{4\mathrm{i}} \int_{-\infty}^{0} V_{(x+s\theta)} - 2\Delta a_{2(x+s\theta)}\, ds + \frac{\mathrm{i}}{4}\theta \cdot \mathbf{A}(x).$$

Since $\delta u = u - \tilde{u}$ has near-field data up to the error of order $\mathscr{O}(\lambda^{-4})$ and $\delta\mathbf{A}$ vanishes outside of the support, $\delta a_3 \equiv 0$ implies that

$$\int_{-\infty}^{0} 2\delta V_{(x+s\theta)} - \Delta\phi_{(x+s\theta)}\, ds = 0,$$

as $\delta a_2(x) = \frac{1}{4}\phi(x)$. For $x \cdot \theta = R$, the standard arguments for inverting the X-ray transform implies that

$$2\delta V = 2(V - \tilde{V}) = \Delta\phi = \nabla \cdot d\phi = \nabla \cdot \delta\mathbf{A}.$$

This shows that the scattering data up to error of order $\mathscr{O}(\lambda^{-4})$ recovers $V - \frac{1}{2}\nabla \cdot \mathbf{A}$.

ii) By part i) we know that $\delta\mathbf{A} = d\phi$ and $\delta V = \frac{1}{2}\Delta\phi$. Therefore, point-wise we have

$$\begin{cases} \delta a_2(x) = \frac{1}{4}\int_{-\infty}^{0} \theta \cdot \nabla\phi_{(x+s\theta)}\, ds = \frac{1}{4}\int_{-\infty}^{0} \partial_s\phi_{(x+s\theta)}\, ds \quad \Longrightarrow \quad \delta a_2(x) = \frac{1}{4}\phi(x) \\ \delta a_3(x) = \frac{\mathrm{i}}{4}\theta \cdot \nabla\phi(x), \end{cases}$$

which shows that the scattering data contains no additional information on $\mathbf{A}$ and V up to error of $\mathscr{O}(\lambda^{-4})$. To calculate δa_4, we have

$$\delta a_4(x) = \frac{1}{4\mathrm{i}}[\int_{-\infty}^{0} -2\Delta\delta a_{3(x+s\theta)} - 4(\theta\cdot\nabla)^2\delta a_{3(x+s\theta)} + 4\mathrm{i}(\theta\cdot\nabla)\Delta\delta a_{2(x+s\theta)} + \mathrm{i}\theta\cdot\delta(\mathbf{A}a_2)_{(x+s\theta)}\, ds].$$

The nonlinear term δa_4 can be rewritten as

$$\theta\cdot\delta(\mathbf{A}a_2) = (\theta\cdot\mathbf{A})\delta a_2 + (\theta\cdot\delta\mathbf{A})\tilde{a}_2 = \frac{1}{4}(\theta\cdot\mathbf{A})\phi + (\theta\cdot\nabla\phi)a_2 - \frac{1}{4}(\theta\cdot\nabla\phi)\phi$$

$$= \frac{1}{4}(\theta\cdot\mathbf{A})\phi + (\theta\cdot\nabla)(\phi a_2) - (\theta\cdot\nabla a_2)\phi - \frac{1}{4}(\theta\cdot\nabla\phi)\phi = (\theta\cdot\nabla)(\phi a_2) - \frac{1}{4}(\theta\cdot\nabla\phi)\phi,$$

where we used the equations for $\delta a_2, \delta a_3$, $\delta\mathbf{A}$, and the fact that $\frac{1}{4}(\theta\cdot\mathbf{A}) = (\theta\cdot\nabla a_2)$. By a simple calculation

$$\delta a_4(x) = \frac{1}{8}[\Delta\phi(x) - 2(\theta\cdot\nabla)^2\phi(x) - \frac{1}{4}\phi^2(x) + 2\phi(x)a_2(x)],$$

which shows that due to non-linearity, the Radon and inverse Fourier transform techniques do not provide any insight in how to show that $\phi = 0$. ■

4.6 Proof of Main Result

We first derive the asymptotic expansion of scattering amplitude, known as Born approximation, see Tyni and Harju (2017).

Theorem 4.6.1 *Let $V, \boldsymbol{A} \in C^k(\mathbf{R}^3)$ for k large enough. Then*

$$a(\omega,\theta,\lambda) = \mathrm{i}\lambda\,\theta\cdot\hat{A}(\lambda(\omega-\theta)) + \hat{V}(\lambda(\omega-\theta)) + \mathscr{O}(\lambda^{-1}) \quad \text{as} \quad \lambda\to\infty,$$

with the remainder uniform in θ, ω.

Proof Let $u = e^{\mathrm{i}\lambda x\cdot\theta} + e^{\mathrm{i}\lambda x\cdot\theta}(\mathbf{a}-1)$ be the biharmonic solution given by Proposition 4.4.1. Plugging u into (4.3), we have

$$\begin{aligned} a(\omega,\theta,\lambda) &= \int e^{-\mathrm{i}\lambda(\omega-\theta)\cdot y}\big(\mathrm{i}\lambda\,\theta\cdot\mathbf{A}(y) + V(y)\big)\mathrm{d}y \\ &+ \int e^{-\mathrm{i}\lambda(\omega-\theta)\cdot y}\big(\mathrm{i}\lambda\,\theta\cdot\mathbf{A}(y) + \mathbf{A}(y)\cdot\nabla + V(y)\big)(\mathbf{a}-1)(y)\mathrm{d}y \\ &= \mathrm{i}\lambda\,\theta\cdot\hat{A}(\lambda(\omega-\theta)) + \hat{V}(\lambda(\omega-\theta)) + R(\omega,\theta,\lambda). \end{aligned} \tag{4.8}$$

Now by Proposition 3.1 we have $\| \mathbf{a}-1 \|_{L^2(\mathbf{R}^2)}$, $\| \nabla(\mathbf{a}-1) \|_{L^2(\mathbf{R}^2)} \leq C\lambda^{-2}$ for some constant C. Therefore, $R = \mathscr{O}(\lambda^{-1})$ which completes the proof. ■

Remark 4.6.1 Given $\mathbf{A}, V \in C_0^\infty$, for λ large enough, the first two terms on the r.h.s of above amplitude decay faster that the remainder, if $\omega \neq \theta$ are fixed. In other words, $\frac{a(\omega,\theta,\lambda)}{\lambda}$ is bounded for regular enough $\mathbf{A}$ and V. Therefore, $\sup\limits_{\substack{\omega,\theta,\lambda \\ 0<\lambda_0\leq\lambda}} \left|\frac{1}{\lambda}a(\omega,\theta,\lambda)\right|$ is a well-defined norm for a fixed $\lambda_0 > 0$.

Theorem 4.6.2 *Let $\boldsymbol{A}, V \in C^k(\mathbf{R}^3)$ for k large enough and $\theta \in S^2$ be fixed. Then for any $\xi \neq 0$ with $\xi\cdot\theta = 0$, the scattering amplitude $a(\omega,\theta,\lambda)$ uniquely determines $\theta\cdot\hat{\boldsymbol{A}}(\xi)$ and $-\mathrm{i}\xi\cdot\hat{\boldsymbol{A}}(\xi) + 2\hat{V}(\xi)$.*

Proof Let $\theta \in S^2$ be a fixed unit vector. For a fixed $\xi \neq 0$ with $\xi \perp \theta$, we show that one can construct a sequence $\{(\omega_\mu, \tilde{\omega}_\mu, \lambda_\mu)\}_\mu$ such that

$$\xi = \lambda_\mu(\omega_\mu - \tilde{\omega}_\mu).$$

Let $\omega, \tilde{\omega}$ be two vectors that are symmetric w.r.t the fixed unit vector θ. Choose the parameter $\mu \in \mathbf{R}$ small enough (see **?**) such that

$$\omega^+ = \omega_\mu^+ = \theta\cos\mu + \frac{\xi}{|\xi|}\sin\mu, \quad \omega^- = \omega_\mu^- = \theta\cos\mu - \frac{\xi}{|\xi|}\sin\mu.$$

Clearly for $\xi \neq 0$,

$$|\omega^+| = |\omega^-| = 1, \quad \omega^+ - \omega^- = 2\frac{\xi}{|\xi|}\sin\mu, \quad \mu = \sin^{-1}(2\frac{\xi}{|\xi|}(\omega^+ - \omega^-)).$$

Setting $\lambda_{(\mu)} = \frac{|\xi|}{2\sin\mu}$ yields $\xi = \lambda(\omega^+ - \omega^-)$. Note that $\omega^+, \omega^- \to \theta$ and $\lambda \to \infty$ as $\mu \to 0$. By Theorem 4.6.1,

$$\begin{cases} a^+ = a(\omega^+,\omega^-,\lambda) = \mathrm{i}\lambda\,\omega^- \cdot \hat{\mathbf{A}}(\xi) + \hat{V}(\xi) + \mathscr{O}(\lambda^{-1}) \\ a^- = a(-\omega^-,-\omega^+,\lambda) = -\mathrm{i}\lambda\,\omega^+ \cdot \hat{\mathbf{A}}(\xi) + \hat{V}(\xi) + \mathscr{O}(\lambda^{-1}). \end{cases}$$

with remainders uniform in ω^+, ω^-. Therefore,

$$\begin{cases} a^+ - a^- = 2\mathrm{i}\lambda\cos\mu\ \theta \cdot \hat{\mathbf{A}}(\xi) + \mathscr{O}(\lambda^{-1}) \\ a^+ + a^- = -\mathrm{i}\xi \cdot \hat{\mathbf{A}}(\xi) + 2\hat{V}(\xi) + \mathscr{O}(\lambda^{-1}). \end{cases} \tag{4.9}$$

The analogous formulae for the Schrödinger operator are presented in Serov (2017); P. D. Stefanov (1989). The first equation above implies that $\theta \cdot \hat{\mathbf{A}}(\xi)$ can be recovered and the second equation implies that one can reconstruct $-\mathrm{i}\xi \cdot \hat{\mathbf{A}}(\xi) + 2\hat{V}(\xi)$ for $\theta \perp \xi$. This completes the proof. ■

Proof of Theorem 4.2.1 By Theorem 4.6.2. we know that $\theta \cdot \hat{\mathbf{A}}(\xi)$ can be recovered for any $0 \neq \xi \perp \theta$. For a non-zero vector $\alpha \in \mathbf{R}^3$, set $\theta = \frac{\alpha\times\xi}{|\alpha\times\xi|}$. By Theorem 4.6.2,

$$(\alpha \times \xi) \cdot \hat{\mathbf{A}}(\xi) = \alpha \cdot (\xi \times \hat{\mathbf{A}}(\xi)),$$

is known as $(\alpha \times \xi) \perp \xi$. The r.h.s of above equation is the Fourier transform of the **curl A** projected on an arbitrary non-zero vector $\alpha \neq 0$. Therefore, one can recover

$$\xi \times \hat{\mathbf{A}}(\xi) = \frac{1}{\mathrm{i}}\mathscr{F}(\mathbf{curl\ A})$$

for $\xi \perp \theta$. Since θ is arbitrary, $\mathscr{F}(\mathbf{curl}\ \mathbf{A})$ can be recovered everywhere. Taking the inverse Fourier transform yields **curl A** can be recovered. On the other hand, by Theorem 4.6.2, $-\mathrm{i}\xi \cdot \hat{\mathbf{A}}(\xi) + 2\hat{V}(\xi)$ can be recovered for $\theta \perp \xi$. Since

$$-\mathrm{i}\xi \cdot \hat{\mathbf{A}} + 2\hat{V} = \mathscr{F}(-\nabla \cdot \mathbf{A} + 2V)$$

one can recover $V - \frac{1}{2}\nabla \cdot \mathbf{A}$ which completes the proof of the main theorem. ■

Next, we present stability estimate results.

Proposition 4.6.1 *For $j = 1,2$, let a_j be the scattering amplitude corresponding to pair of magnetic and potentials fields $(\mathbf{A}_j, V_j)$ with $\| A_j \|_{C^k} < C_0$ and $\| V_j \|_{C^k} < C_0$ for some constant $C_0 > 0$ and $k \gg 0$. Then there exists $C > 0$ and λ_0 depending a priori on C_0 such that for $\varepsilon = \sup_{\substack{\omega,\theta,\lambda \\ 0<\lambda_0\leq\lambda}} \left| \frac{1}{\lambda}(a_1 - a_2)(\omega,\theta,\lambda) \right|$ small enough, the following stability estimates hold*

$$\sup_{\xi} \left| \frac{(\widehat{\boldsymbol{curl}\, \boldsymbol{A}}_1 - \widehat{\boldsymbol{curl}\, \boldsymbol{A}}_2)(\xi)}{\langle \xi \rangle} \right| < \varepsilon, \qquad \sup_{\xi} |(\hat{V}_1 - \hat{V}_2) - \frac{1}{2}\mathrm{i}\xi \cdot (\hat{\boldsymbol{A}}_1 - \hat{\boldsymbol{A}}_2)|_{L^\infty} < C\varepsilon^{\frac{1}{2}}.$$

Proof Let $u_j = e^{\mathrm{i}\lambda x \cdot \theta}\mathbf{a}_j$, $j = 1,2$, be the biharmonic solution given by the Proposition 4.4.1 with corresponding amplitude a_j and the pair $(\mathbf{A}_j, V_j)$. Similarly, by Theorem 4.6.2, for a fixed $\xi \neq 0$ with $\xi \perp \theta$ and $\mu \ll \delta$ (i.e small enough), one can choose $\lambda_\mu = \frac{|\xi|}{2\sin\mu}$, ω_μ^+, and ω_μ^-, so that $\xi = \lambda_\mu(\omega_\mu^+ - \omega_\mu^-)$. Note that for small enough μ, one has $\frac{|\xi|}{2\lambda_\mu} = \sin\mu \leq \mu \ll \delta$ and therefore $\frac{|\xi|}{2\delta} \leq \lambda_\mu$. Set $C_0 = \frac{1}{2\delta}$ and $\lambda_0 = \frac{|\xi|}{2\delta}$. Assume now that the pair $(\mathbf{A}_j, V_j)$ satisfies the priori assumption in the theorem. For a fixed and large k, by equation (4.9) we have

$$\begin{cases} a_j^+ - a_j^- = 2\mathrm{i}\lambda\cos\mu\ \theta \cdot \hat{\mathbf{A}}_j(\xi) + (R_j^+ - R_j^-) \\ a_j^+ + a_j^- = -\mathrm{i}\xi \cdot \hat{\mathbf{A}}_j(\xi) + 2\hat{V}_j(\xi) + (R_j^+ + R_j^-), \end{cases} \quad \text{with} \quad |R_j^\pm| \leq \frac{C}{\lambda}, \quad j = 1,2, \qquad (4.10)$$

where C depends on the a priori upper bound C_0. Indeed, this estimate comes from Agmon's lemma and Proposition 4.4.1 where all estimates are uniform, provided that one has control over differentiations (finitely many times). Using the first equation in (4.10) and setting $R^\pm = (R_1 - R_2)^\pm$, one has

$$\theta \cdot \delta\hat{A}(\xi) = \frac{1}{2\mathrm{i}\lambda_\mu \cos\mu}\left[(a_1 - a_2)^+ - (a_1 - a_2)^- - (R^+ - R^-)\right].$$

For μ small enough, note that $\mu \approx \frac{|\xi|}{2\lambda_\mu}$ and $\frac{1}{\cos\mu} = 1 + \frac{1}{2}\mu^2 + \mathscr{O}(\mu^4) \leq 1 + \mu^2$. Therefore,

$$|\theta \cdot \delta\hat{A}(\xi)| \leq (1+\frac{|\xi|^2}{\lambda^2})\big[|\frac{1}{2\lambda_\mu}(a_1-a_2)^+|+|\frac{1}{2\lambda_\mu}(a_1-a_2)^-|+\frac{1}{2\lambda_\mu}|R^+-R^-|\big] \leq (1+\frac{|\xi|^2}{\lambda_\mu^2})(\varepsilon+\frac{C}{\lambda_\mu^2})$$

where we used the fact that $\varepsilon = \sup\limits_{\substack{\omega,\theta,\lambda \\ 0<\lambda_0\leq\lambda}} \big|\frac{1}{\lambda}(a_1-a_2)\big|$ and $|R_j^{\pm}| \leq \frac{C}{\lambda}$.

The r.h.s of above inequality is independent of μ. Therefore, for any fixed ξ, taking the limit of the above inequality as $\mu \to 0$ establishes the following estimate

$$|\theta \cdot \delta\hat{A}(\xi)| \leq \varepsilon.$$

Similar to the proof of Theorem 4.2.1, for any $\alpha \in \mathbf{R}^3$, set $\theta = \frac{\alpha\times\xi}{|\alpha\times\xi|}$. One can find c_α such that $|\alpha \times \xi| \leq c_\alpha(1+|\xi|) = c_\alpha\langle\xi\rangle$. Therefore,

$$|\frac{\alpha\cdot(\xi\times\delta\hat{A}(\xi))}{\langle\xi\rangle}| \leq |\frac{(\alpha\times\xi)\cdot\delta\hat{A}(\xi)}{|\alpha\times\xi|}| \leq \varepsilon.$$

The vector α is arbitrary, so one can stably recover all the components of the $\operatorname{curl}\mathbf{A}$ with the following estimate

$$\sup_{\xi}|\frac{\widehat{\operatorname{curl}(\delta\mathbf{A})}(\xi)}{\langle\xi\rangle}| < \varepsilon.$$

To establish an estimate for $(2\delta\hat{V} - \mathrm{i}\xi\cdot\delta\hat{\mathbf{A}})(\xi)$, we use the second equation of (4.10). One has

$$|(2\delta\hat{V} - \mathrm{i}\xi\cdot\delta\hat{\mathbf{A}})(\xi)| \leq |(a_1-a_2)^+|+|(a_1-a_2)^-|+|R^++R^-| \leq 2\varepsilon\lambda_\mu + \frac{C}{\lambda_\mu}.$$

The r.h.s of above is minimized when $\lambda_\mu = \varepsilon^{-\frac{1}{2}}$. Therefore, the following estimate holds.

$$|(2\delta\hat{V} - \mathrm{i}\xi\cdot\delta\hat{\mathbf{A}})(\xi)| \leq C\varepsilon^{\frac{1}{2}}.$$

■

Remark 4.6.2 One can use interpolation between norm spaces and the a priori assumptions

$$\| A_j \|_{C^k} < C_0 \quad \text{and} \quad \| V_j \|_{C^k} < C_0,$$

to derive stability estimates with different norms for the magnetic field $\mathbf{A}$ using different norms of the scattering amplitude at the expense of getting Hölder estimates.

REAL-TIME HYBRID SIMULATION

*** This chapter concludes my original work: "Predictive stability indicator: a novel approach to configuring a real-time hybrid simulation." Earthquake Engineering and Structural Dynamics, Engng Struct. Dyn. 2016. https://doi.org/10.1002/eqe.2775.**

Real-time hybrid simulation (RTHS) is an effective and versatile tool for the examination of complex structural systems with rate dependent behaviors. To meet the objectives of such a test, appropriate consideration must be given to the partitioning of the system into physical and computational portions (i.e., the configuration of the RTHS). Predictive stability and performance indicators (PSI and PPI) were initially established for use with only single degree-of-freedom systems. These indicators allow researchers to plan a RTHS, to quantitatively examine the impact of partitioning choices on stability and performance, and to assess the sensitivity of an RTHS configuration to de-synchronization at the interface. In this study, PSI is extended to any linear multi-degree-of-freedom (MDOF) system. The PSI is obtained analytically and it is independent of the transfer system and controller dynamics, providing a relatively easy and extremely useful method to examine many partitioning choices. A novel matrix method is adopted to convert a delay differential equation to a generalized eigenvalue problem using a set of vectorization mappings, and then to analytically solve the delay differential equations in a computationally efficient way. Through two illustrative examples, the PSI is demonstrated and validated. Validation of the MDOF PSI also includes comparisons to a MDOF dynamic model that includes realistic models of the hydraulic actuators and the control-structure interaction effects. Results demonstrate that the proposed PSI can be used as an effective design tool for conducting successful RTHS.

5.1 Existing Results

Dynamic experimental assessment of structural elements is critical in structural engineering. It provides structural engineers a better understanding of structural integrity at both component and system levels. Taking the cost and availability of experimental resources into consideration, full-scale experimental evaluation of structures is a challenging proposition. The concept of *hybrid simulation* (HS) found its way into structural engineering in the late 1960s Hakuno, Shidawara, and Hara (1969) and has been refined over the past four decades Mahin, Shing, Thewalt, and Hanson (1989); Shing, Nakashima, and Bursi (1996); Takanashi and Nakashima (1987). HS provides the capability to isolate and experimentally evaluate critical structural components for which a reliable analytical model is unavailable (i.e., *physical substructure*) while the remainder of the structure (i.e., *numerical substructure*) is modeled numerically Chen, Ricles, Karavasilis, Chae, and Sause (2012). Coupling between the two substructures is achieved by enforcing equilibrium and compatibility at the interface using a *transfer system* Wallace, Sieber, Neild, Wagg, and Krauskopf (2005).

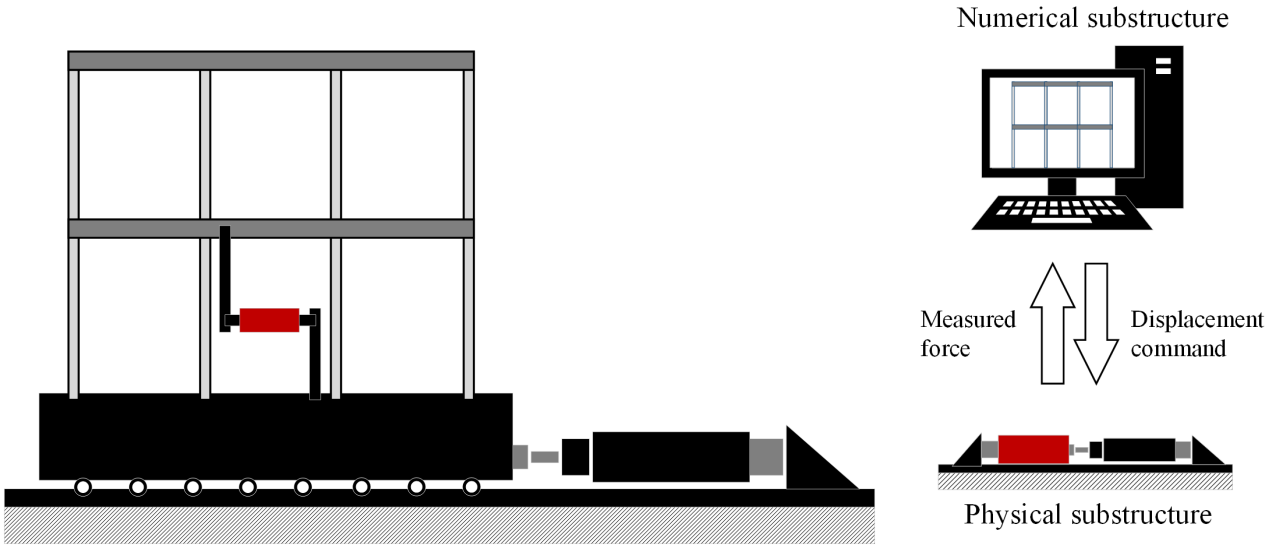

Figure 5.1. A typical real-time hybrid simulation of a civil structure.

In the field of structural dynamics and control, there is an increasing demand to enhance the current knowledge, evaluate the performance, and incorporate nonlinear rate-dependent energy dissipative devices into structural design. Also, structural engineers are currently confronting more challenging problems such as soil-structure-interaction, accurate estimation of structural damping Brewick and Smyth (2015), mitigation of blast effects on protective structures, and nonlinear hysteretic behavior due to significant cycling excitations (*e.g.,* earthquake, wind, and sea waves) Chatzi, Smyth, and Masri (2010). In most cases, due to rate-dependent nature of the new challenges, real-time execution of the experiment is necessary when hybrid simulation is adopted as an experimental method.

Real-time realization of HS (i.e., *real-time hybrid simulation*) is a powerful and cost-effective experimental technique to evaluate the dynamic performance of civil structures, especially, when rate-dependence plays a role. In RTHS, to enforce the interface equilibrium and compatibility conditions between the numerical and physical substructures, dynamic hydraulic actuators and/or shake tables are often used as transfer systems. Researchers have proposed control techniques for transfer systems to satisfy the interface boundary conditions in real-time, see Figure 5.1. Carrion and Spencer (2007) developed a model-based feedforward compensator for RTHS. Chen *et al.,* proposed an adaptive controller using an error tracking indicator Chen and Ricles (2010). Gao *et al.,* and Ou *et al.,* developed and validated H_∞ loop shaping designs for actuator motion control in RTHS Gao, Castaneda, and Dyke (2012); Ou, Ozdagli, Dyke, and Wu (2015). Phillips *et al.,* proposed a model-based feedforward control with the backward-difference method for hydraulic actuator control in RTHS Phillips, Takada, Spencer, and Fujino (2014).

RTHS has been successfully conducted to evaluate the seismic performance of structures and implement new structural control techniques. For example, magneto-rheological (MR) dampers have been found to be an effective type of semiactive control device Dyke, Spencer, Sain, and Carlson (1999). In the first large-scale RTHS on a complex frame system using multiple actuators, Friedman *et al.,* evaluated a control algorithm that utilizes overdriving and backdriving current control to increase the efficacy of MR control devices Friedman et al. (2015). Christenson *et al.,* verified the performance of MR fluid dampers for seismic protection of civil structures using large-scale RTHS Christenson, Lin, Emmons, and Bass (2008). Saouma *et al.,* conducted an RTHS study on a nonductile reinforced concrete frame and compared the results with shake table testing, see Saouma, Haussmann, Kang, Ghannoum, and Asce (2013). Cha *et al.,* evaluated the performances of four semiactive control algorithms for the control of a large-scale realistic moment-resisting frame using a large-scale 200-kN MR damper Cha et al. (2014). Mercan and Ricles studied structures with full-scale elastomeric dampers using RTHS Mercan and Ricles (2009). In the implementation of any RTHS, global stability must be given appropriate attention. Instability in RTHS stems from numerical and experimental sources. A major source of instability is incapability of the transfer and sensing systems to realize proper boundary conditions between the numerical and physical substructures.

Imperfect realization of boundary conditions by transfer system is inevitable because it is physically impossible for any transfer system to react instantaneously to a change of state as required by the numerical substructure. Wallace *et al.,* studied the effect of delay errors that are inherently present in RTHS Wallace et al. (2005). Kyrychko *et al.,* studied local and global stability analyses of RTHS in a coupled oscillator-pendulum system and identified the delay dependent stability boundaries for this type of system Kyrychko, Blyuss, Gonzalez-Buelga, Hogan, and Webb (2006).

Mercan and Ricles conducted a stability analysis for real-time pseudodynamic and hybrid pseudodynamic testing with multiple sources of delay Mercan and Ricles (2008). Zhu *et al.,* adopted a discrete-time root locus technique to investigate the delay-dependent stability in RTHS, see Zhu, Wang, Jin, Chi, and Gui (2015). In another study, Botelho and Christenson conducted a robust stability and performance analysis method for multi-actuator RTHS based on robust stability theory for multiple-input-multiple-output feedback control Botelho and Christenson (2015).

Predictive stability and *performance indicators* (PSI and PPI) were initially established for single-degree-of-freedom systems Maghareh, Dyke, Prakash, and Rhoads (2013, 2014). Prior to adopting a transfer system controller, the PSI and PPI assess the impact of partitioning choices on the stability and performance of a global RTHS response and enable RTHS users to quantitatively examine the sensitivity of an RTHS configuration to any de-synchronization at the interface.

These indicators assist the users to choose an appropriate control/compensation technique for any configuration choice. Furthermore, Maghareh *et al.,* developed a stability switch criterion for effective RTHS implementation, specified minimum transfer system performance requirement, minimum required sampling frequency, and effective methods to stabilize an unstable system due to the performance of transfer system Maghareh, Dyke, Prakash, and Bunting (2014).

In this study, the PSI is extended to any linear multi-degree-of-freedom system, irrespective of whether shake table(s) and/or hydraulic actuator(s) serve as the transfer system. Moreover, we demonstrate how PSI can be used as an effective design tool in implementation of successful RTHS. The design of partitioning choice is a primary and fundamental step in the implementation of a successful and safe RTHS. Also, the PSI sets the minimum transfer system performance. Based on the PSI and available transfer system performance, prior to conducting an experiment, alternative partitioning choices can be classified, on the basis of system instability as: extremely sensitive, moderately sensitive, and slightly sensitive choices.

5.2 Real-time hybrid simulation: stability

De-synchronization at the cyber-physical interface is a major source of system instability in RTHS. A typical real-time hybrid simulation framework, see Figure 5.2, includes: (i) a numerical model capable of being executed in real-time within the adopted time increment, (ii) a transfer system control strategy to obtain accurate tracking of desired trajectory at the interface in real-time, (iii) sensing system, and (iv) physical substructure.

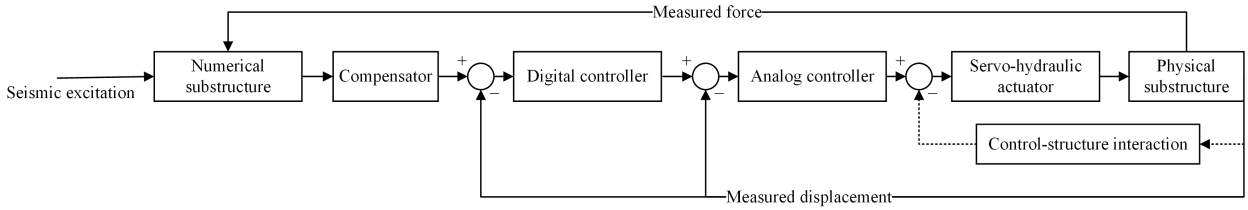

Figure 5.2. A typical real-time hybrid simulation block diagram.

It has also been demonstrated that the dynamical characteristics of the physical substructure affect the transfer system performance due to *control-structure-interaction* (CSI) Dyke, Spencer Jr., Quast, and Sain (1995). The transfer and sensing systems introduce de-synchronization at the interface which can be categorized into two groups: frequency-independent time delay (caused by communication delay, analog-to-digital and digital-to analog conversions, and computation delay) and frequency-dependent time lag (caused by transfer system dynamics and limitations) into the system.

In RTHS, system instability is a significant safety concern and it may damage physical specimens and/or the transfer system. Also, system instability causes some researchers to avoid using RTHS due the level of complexity in comparison with other alternatives. In RTHS, there are many transfer system parameters impacting the stability (and performance) of the system. These parameters include physical limitations of the available components (actuator speed, servo-valve speed, oil-column resonance, etc.) and user choices (analog controller's parameters, digital control strategy, etc.). To conduct a successful RTHS, it is absolutely necessary for a user to have a good understanding of these parameters and limitations.

How to partition a structure into numerical and physical is a significant user controlled factor which determines the stability of the experiment subject to the existing physical limitations of the transfers system. Each partitioning choice has a different set of stability requirements. It's also important to point out that the set of stability requirements can become extremely narrow as the partitioning choice gets more complex. This fact explains why conducting a multi-dimensional complex RTHS is still an existing challenge for researchers. Thus, one (or a set of) stability indicator(s) is required to assist users in *designing* a successful experiment. Herein, for a specific emulated structure, designing an experiment refers to selection of a proper partitioning choice (of numerical and physical substructures) and control strategy, subject to the existing transfer system limitations and interaction between the transfer system and the physical substructure (CSI).

5.3 Control-structure interaction in RTHS

In this section, control-structure interaction and its effect on the implementation of RTHS is discussed while hydraulically actuated systems are considered as the transfer system. In the case of hydraulic actuators, a significant coupling is present between the transfer system and the physical specimen. This phenomenon was initially explained by Dyke et al. (1995). Currently, RTHS is being implemented for complex MDOF systems in which control of multiple actuators are required. These multiple actuators are intrinsically coupled through the physical substructure. This phenomenon imposes a certain challenges and considerations in transfer system control for implementing a successful test. For a better understanding of this phenomenon, herein, we briefly explain CSI. More detailed explanations are provided in Dyke et al. (1995); Phillips (2012).

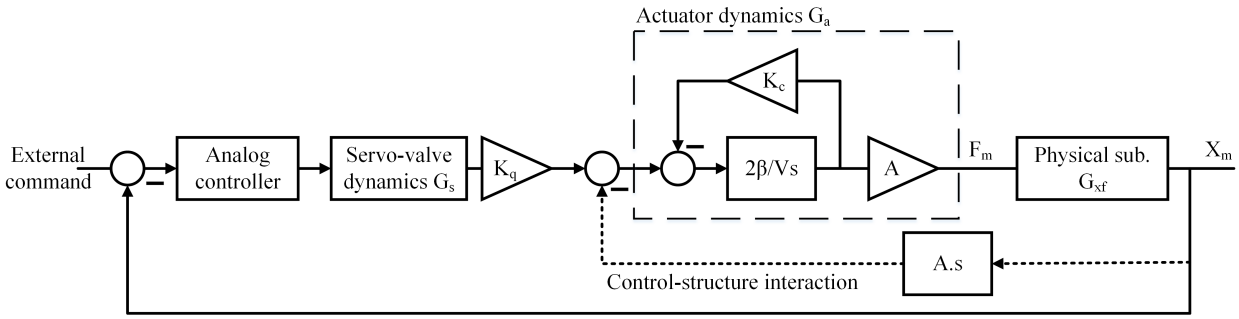

Figure 5.3. Transfer system coupled through the physical substructure.

In displacement control RTHS, an external command (command displacement) drives the transfer system attached to the physical substructure, see Figure 5.3. The hydraulic actuator is a part of the transfer system which is driven by valve input command and generates the force applied to the physical substructure. A block diagram representation of open-loop actuator model is provided in Figure 5.4. For RTHS and in the case of a hydraulically actuated system attached to a physical substructure, a velocity feedback exists between the actuated system and the valve input. In de Silva (2007), the fluid flow rate in an actuator is linearized about the origin to obtain the input to the actuator. Figure 5.4 is obtained based on the linearized equation of hydraulic flow rate in an actuator, which is

$$\dot{f} = \frac{2\beta}{V}(AK_q i - K_c f - A^2 \dot{x}) \tag{5.1}$$

where f, β, V, A, K_q, i, K_c, and x are actuator force, bulk modulus of the fluid, hydraulic fluid volume of actuator, cross-sectional area of actuator, system constant, valve input, system constant, and actuator displacement, respectively. Thus, the dynamics of the physical substructure directly impact the characteristics of the transfer system. Moreover, when the physical substructure undergoes structural changes or is replaced by a new substructure, the overall dynamics (and performance) of the transfer system change due to CSI and a new controller is required.

With a simple rearrangement in the block diagram shown in Figure 5.4, Figure 5.5a can be obtained. In this representation, actuator transfer function can be written as

$$G_a = \frac{A}{\frac{V}{2\beta}s + K_c} \tag{5.2}$$

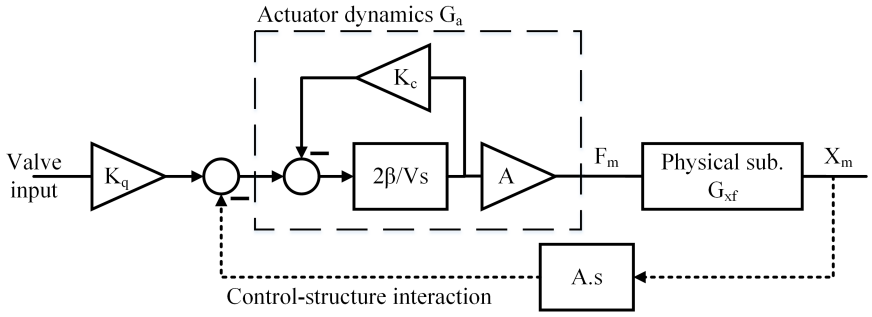

Figure 5.4. Actuator dynamics and the physical substructure.

and,

$$K_q G_a = \frac{AK_q}{\frac{V}{2\beta}s + K_c} = \frac{\frac{AK_q}{K_c}}{\frac{V}{2\beta K_c}s + 1}. \tag{5.3}$$

Next, we lump all the parameters into three new parameters: a_1, a_2, and a_3,

$$a_1 = \frac{2\beta K_q A}{V}; a_2 = \frac{2\beta A^2}{V}; a_3 = \frac{2\beta K_c}{V} \tag{5.4}$$

and rewrite Equation 5.3 as

$$K_q G_a = \frac{\frac{a_1}{a_3}}{\frac{1}{a_3}s + 1} = \frac{a_1}{s + a_3}. \tag{5.5}$$

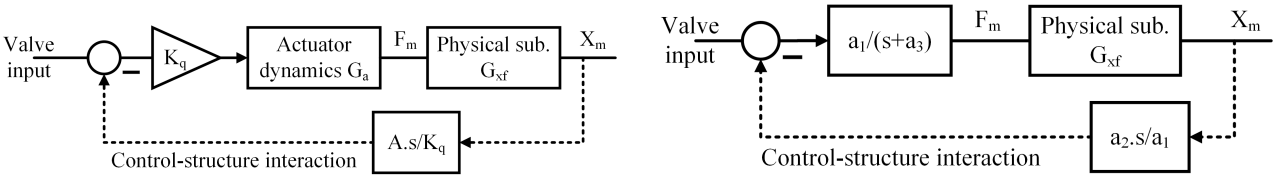

Figure 5.5. Equivalent actuator dynamics and the physical substructure.

The fact that a change in the structural properties of the physical substructure will change the dynamics of the transfer system and, consequently, the global RTHS response, imposes a challenge for studying the impact of partitioning choice on global stability and performance of an RTHS system. In the next section, we propose a new virtual framework in which the sensitivity of a partitioning choice to the interface de-synchronization will be studied prior to adopting a transfer system control strategy.

5.4 Predictive Stability Indicator

5.4.1 Framework

As a predictive (or pre-experiment) indicator for conducting successful and safe RTHS, the PSI was initially developed for single-degree-of-freedom systems Maghareh, Dyke, Prakash, and Rhoads (2014). In the current PSI framework, a virtual time delay is applied to the feedback force (interaction force) in order to assess the sensitivity and stability requirement of an RTHS partitioning choice subject to the interface de-synchronization. The PSI framework is shown in Figure 5.6. For linear systems, Figure 5.6 can be mathematically represented as either a neutral or retarded delay differential equation. In order to obtain *critical delay* of a partitioning choice, the delay differential equation is analytically solved using a novel computationally inexpensive method. Critical time delay refers to the time delay associated with occurrence of a stability switch in Figure 5.6.

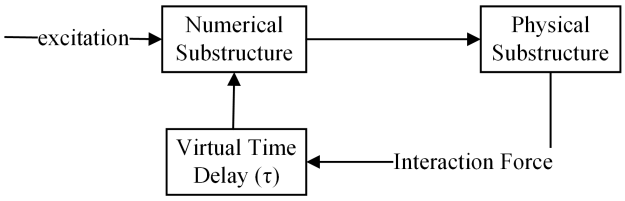

Figure 5.6. Predictive stability indicator's virtual framework.

Transfer system is used to apply the boundary condition and force equilibrium at the interface. Depending on how the emulated structure is partitioned into numerical and physical substructures, hydraulic actuator(s) and/or shake table(s) are used as the transfer system. The general formulation for linear RTHS method and substructuring techniques are provided by Shao *et al.,* Shao, Reinhorn, and Sivaselvan (2011).

Herein, to demonstrate the preliminary PSI formulations (obtaining *delay differential equations*), two partitioning choices are selected using shake table and hydraulic actuators as transfer system. It should be mentioned that the PSI formulations also apply to any other partitioning choices in which hydraulic actuators and/or shake tables are used. Moreover, the PSI formulation can be used for more challenging RTHS cases in which stability is more critical such as multi-directional multi-actuator RTHS configurations, multi-rate RTHS (mrRTHS) or geographically distributed RTHS.

5.4.2 PSI formulation for case I: RTHS using shake table

In this section, a multi-story structure ($n+p$ stories) is partitioned into n stories as numerical substructure and p stories as physical substructure shown in Figure 5.7. The numerical substructure can be modeled as a shear model or a finite element model (as long as Equation 5.6 still applies). In this partitioning procedure, the top p stories are mounted on a shake table while the bottom n stories are numerically modeled on a real-time operating system. In this case, the shake table serves as the transfer system to meet the boundary conditions at interface. Some implementations of RTHS with similar partitioning approach can be found in Franco, Botelho, and Christenson (2015); Mueller, Griffith, Shao, and Enyart (2013); Nakata and Stehman (2014); Shao et al. (2011). To assess the sensitivity of possible partitioning choices, the virtual PSI framework shown in Figure 5.6 is adopted. Thus the PSI equation of motion for the numerical substructure is

$$M_n\ddot{X}_n + C_n\dot{X}_n + K_nX_n = F(x_g,\dot{x}_g) - F_p(\tau) \tag{5.6}$$

where M_n, C_n, K_n, $F(x_g,\dot{x}_g)$, τ and F_p are numerical mass, damping, stiffness, input force, virtual time delay and interface force from the physical substructure, respectively. In this section, all states are absolute (or total) values. Because for linear systems, stability is an internal system characteristic and independent of the input, without loss of generality, the ground motion force in Equation 5.6 is dropped. The equation of motion for the numerical substructure becomes

$$M_n\ddot{X}_n + C_n\dot{X}_n + K_nX_n = -F_p(\tau). \tag{5.7}$$

For this type of partitioning choice, the interface force becomes

$$F_p = k_{n+1}(x_{n+1} - x_n) + c_{n+1}(\dot{x}_{n+1} - \dot{x}_n). \tag{5.8}$$

Equation 5.8 can be written in the state space form as follows

$$\begin{bmatrix} \dot{X}_n \\ \ddot{X}_n \end{bmatrix} = \overbrace{\begin{pmatrix} 0_{n\times n} & I_{n\times n} \\ -M_n^{-1}K_n & -M_n^{-1}C_n \end{pmatrix}}^{An} \overbrace{\begin{bmatrix} X_n \\ \dot{X}_n \end{bmatrix}}^{Yn} + \overbrace{\begin{pmatrix} 0_{n\times 1} \\ -M_n^{-1}R^T \end{pmatrix}}^{Bn} F_p(\tau) \tag{5.9}$$

$$\overbrace{\begin{bmatrix} x_n \\ \dot{x}_n \end{bmatrix}}^{Yi} = \overbrace{\begin{pmatrix} R & 0_{1\times n} \\ 0_{1\times n} & R \end{pmatrix}}^{Cn} \begin{bmatrix} X_n \\ \dot{X}_n \end{bmatrix} \tag{5.10}$$

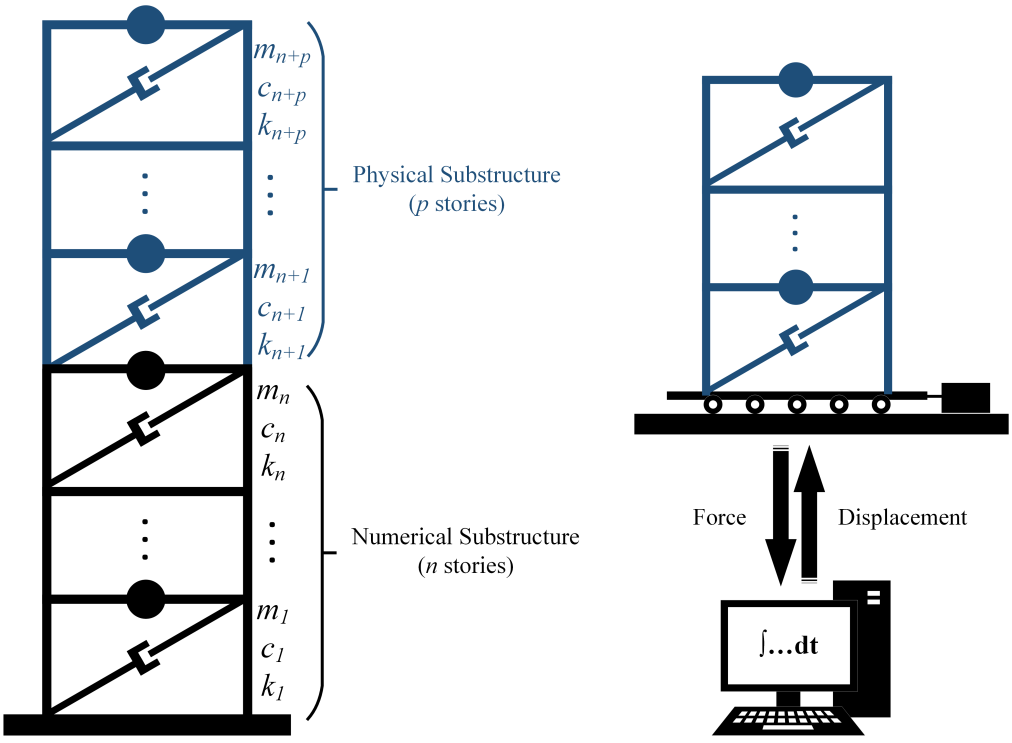

Figure 5.7. A typical real-time hybrid simulation using shake table as transfer system.

where R is interface vector $[0_{1\times n-1}1]^T$. The equation of motion for the physical substructure is

$$M_p\ddot{X}_p + C_p\dot{X}_p + K_pX_p = K_p\Gamma x_n + C_p\Gamma\dot{x}_n. \tag{5.11}$$

Equation 5.11 can also be written in the state space form as follows

$$\begin{bmatrix}\dot{X}_p\\ \ddot{X}_p\end{bmatrix} = \overbrace{\begin{pmatrix}0_{p\times p} & I_{p\times p}\\ -M_p^{-1}K_p & -M_p^{-1}C_p\end{pmatrix}}^{A_p}\overbrace{\begin{bmatrix}X_p\\ \dot{X}_p\end{bmatrix}}^{Y_p} + \overbrace{\begin{pmatrix}0_{p\times 1} & 0_{p\times 1}\\ -M_p^{-1}K_p\Gamma & -M_p^{-1}C_p\Gamma\end{pmatrix}}^{B_p}\begin{bmatrix}x_n\\ \dot{x}_n\end{bmatrix} \tag{5.12}$$

$$F_p = \overbrace{\begin{pmatrix}k_{n+1} & 0_{1\times p-1} & k_{n+1} & 0_{1\times p-1}\end{pmatrix}}^{C_p}\begin{bmatrix}X_p\\ \dot{X}_p\end{bmatrix} + \overbrace{\begin{pmatrix}-k_{n+1} & -c_{n+1}\end{pmatrix}}^{D_p}\begin{bmatrix}x_n\\ \dot{x}_n\end{bmatrix}. \tag{5.13}$$

Subject to virtual time-delay, Equation 5.13 becomes

$$F_p(\tau) = C_pY_p(\tau) + D_pY_i(\tau). \tag{5.14}$$

Using Equation 5.10, $F_p(\tau)$ can be written as

$$F_p(\tau) = C_pYp(\tau) + D_pC_nYn(\tau). \tag{5.15}$$

By substituting Equation 5.15 into Equation 5.9 and Equation 5.10 into Equation 5.12, respectively, dynamics of the numerical and physical substructures can be expressed as

$$\dot{Y}_n = A_nY_n + B_nD_pC_nY_n(\tau) + B_nC_pY_p(\tau) \tag{5.16}$$

$$\dot{Y}_p = B_pC_nY_n + A_pY_p. \tag{5.17}$$

Equations 5.16 and 5.17 can be expressed in the following *retarded delay differential equation* (RDDE) format

$$\begin{bmatrix} \dot{Y}_n \\ \dot{Y}_p \end{bmatrix} = \overbrace{\begin{pmatrix} A_n & 0_{n\times p} \\ B_p C_n & A_p \end{pmatrix}}^{A_0} \begin{bmatrix} Y_n \\ Y_p \end{bmatrix} + \overbrace{\begin{pmatrix} B_n D_p C_n & B_n C_p \\ 0_{n\times n} & 0_{n\times p} \end{pmatrix}}^{A_1} \begin{bmatrix} Y_n(\tau) \\ Y_p(\tau) \end{bmatrix}. \tag{5.18}$$

5.4.3 PSI formulation for case II: RTHS using hydraulic actuator(s)

In this section, a multi-story structure (n stories) is divided into $n-m$ stories as numerical substructure and m partitioned stories shown in Figure 5.8. The numerical substructure can be modeled as shear model or finite element model (as long as Equation 5.19 still applies). In this partitioning procedure, the bottom m partitioned stories are physically constructed and attached to hydraulic actuators as transfer system while the numerical substructure is being executed on a real-time operating system. Some implementations of RTHS with similar partitioning approach can be found in Cha et al. (2014); Chae, Ricles, and Sause (2012); Dong, Sause, and Ricles (2015); Friedman et al. (2015); Phillips and Spencer (2013). In this case, all states are relative values (relative to ground motion) and it is assumed that all the degrees of freedom has a non-zero numerical mass. To assess the sensitivity of possible partitioning choices, the virtual PSI framework shown in Figure 5.6 is applied. The PSI equation of motion for the system shown in Figure 5.8 is

$$M_n\ddot{X} + C_n\dot{X} + K_nX = F(\ddot{x}_g) - F_p(\tau). \tag{5.19}$$

As mentioned earlier, because for linear systems, stability is an internal system characteristic and independent of the input, without loss of generality, the ground motion force in Equation 5.19 is dropped and it becomes

$$M_n\ddot{X} + C_n\dot{X} + K_nX = -F_p(\tau). \tag{5.20}$$

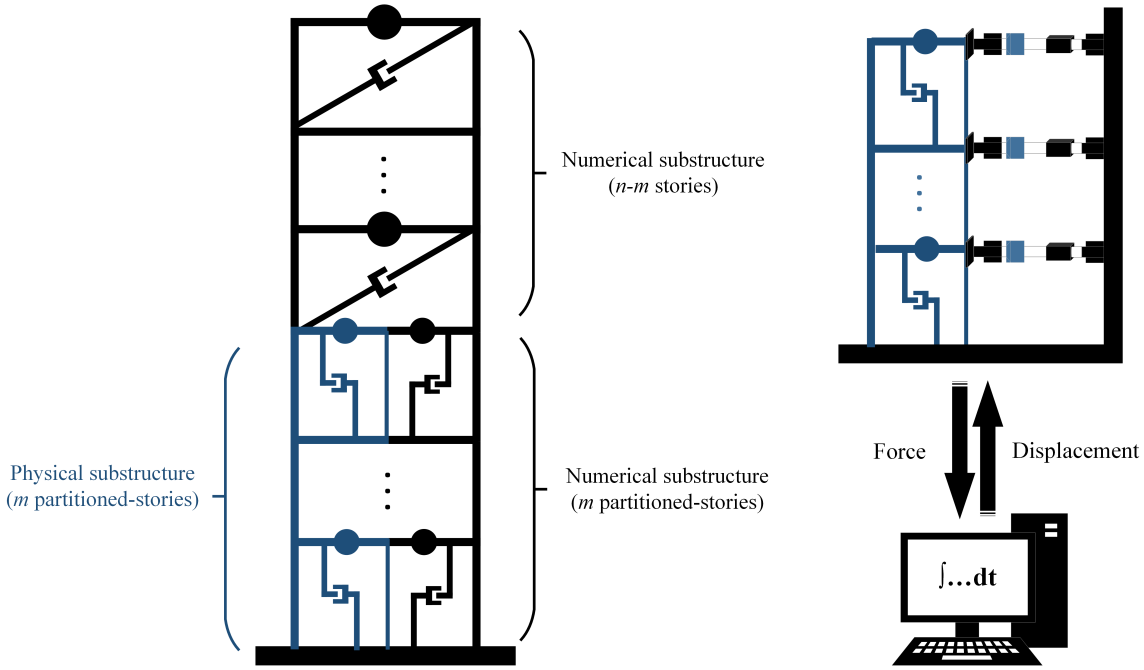

Figure 5.8. A typical real-time hybrid simulation using hydraulic actuator(s) as transfer system.

Equation 5.20 can also be written as

$$\begin{bmatrix} \dot{X} \\ \ddot{X} \end{bmatrix} = \begin{pmatrix} 0_{n\times n} & I_{n\times n} \\ -M_n^{-1}K_n & -M_n^{-1}C_n \end{pmatrix} \begin{bmatrix} X \\ \dot{X} \end{bmatrix} + \begin{pmatrix} 0_{n\times n} \\ -M_n^{-1} \end{pmatrix} F_p(\tau), \tag{5.21}$$

where F_p is

$$F_p = M_p\ddot{X} + C_p\dot{X} + K_pX. \tag{5.22}$$

The interface force can also be expressed as

$$F_p = \begin{pmatrix} K_p & \rho C_p \end{pmatrix} \begin{bmatrix} X \\ \dot{X} \end{bmatrix} + \begin{pmatrix} (1-\rho)C_p & M_p \end{pmatrix} \begin{bmatrix} \dot{X} \\ \ddot{X} \end{bmatrix} \tag{5.23}$$

where ρ can take any value between 0 to 1. Substituting Equation 5.23 into Equation 5.21, it becomes

$$\begin{bmatrix} \dot{X} \\ \ddot{X} \end{bmatrix} = \begin{pmatrix} 0_{n\times n} & I_{n\times n} \\ -M_n^{-1}K_n & -M_n^{-1}C_n \end{pmatrix} \begin{bmatrix} X \\ \dot{X} \end{bmatrix} + \begin{pmatrix} 0_{n\times n} & 0_{n\times n} \\ -M_n^{-1}K_p & -\rho M_n^{-1}C_p \end{pmatrix} \begin{bmatrix} X(\tau) \\ \dot{X}(\tau) \end{bmatrix} + \begin{pmatrix} 0_{n\times n} & 0_{n\times n} \\ -M_n^{-1}(1-\rho)C_p & -M_n^{-1}M_p \end{pmatrix} \begin{bmatrix} \dot{X}(\tau) \\ \ddot{X}(\tau) \end{bmatrix}. \quad (5.24)$$

Finally, Equation 5.24 can be rearranged and written in the following *neutral delay differential equation* (NDDE) format

$$\begin{bmatrix} \dot{X} \\ \ddot{X} \end{bmatrix} + \overbrace{\begin{pmatrix} 0_{n\times n} & 0_{n\times n} \\ -M_n^{-1}(1-\rho)C_p & -M_n^{-1}M_p \end{pmatrix}}^{B} \begin{bmatrix} \dot{X}(\tau) \\ \ddot{X}(\tau) \end{bmatrix} = \overbrace{\begin{pmatrix} 0_{n\times n} & I_{n\times n} \\ -M_n^{-1}K_n & -M_n^{-1}C_n \end{pmatrix}}^{A_0} \begin{bmatrix} X \\ \dot{X} \end{bmatrix} + \overbrace{\begin{pmatrix} 0_{n\times n} & 0_{n\times n} \\ -M_n^{-1}K_p & -\rho M_n^{-1}C_p \end{pmatrix}}^{A_1} \begin{bmatrix} X(\tau) \\ \dot{X}(\tau) \end{bmatrix}. \quad (5.25)$$

In the next section, we demonstrate how to solve these delay differential equations.

5.4.4 Conversion of delay differential equation to a generalized eigenvalue problem

In this section, we adopt a novel method to solve the delay differential equations obtained in the previous section in a computationally efficient way. To derive the PSI, we convert the delay differential equation to a generalized eigenvalue problem using a set of vectorization mappings. After obtaining *the critical time delay* for the neutral and retarded delay differential equations, we compute the PSI value to assess the sensitivity of the partitioning choice to de-synchronization of interface. First, note that RDDE (obtained for Case I) is a special case of NDDE in which the B matrix in Equation 5.26 becomes 0. Thus, without loss of generality, hereinafter, all the equations are based on the NDDE format. In general, a neutral delay differential equation takes the form of

$$\dot{X}(t) + B\dot{X}(t-\tau) = A_0X(t) + A_1X(t-\tau). \tag{5.26}$$

The characteristic equation of Equation 5.26 is

$$|s(I + Be^{-\tau s}) - A_0 - A_1e^{-\tau s}| = 0 \tag{5.27}$$

where $|.|$ denotes the determinant, I refers to identity matrix and $s \in \mathbb{C}$. For a linear dynamic system to be asymptotically stable about its fixed points, all roots of the characteristic equation (i.e., eigenvalues) must lie in the left half of the complex plane. Therefore, stability switching occurs when the rightmost eigenvalue goes from the left complex half-plane into the right complex half-plane by crossing the imaginary axis. So the appearance of an eigenvalue on the imaginary axis is the critical condition. Equation 5.27 can be rearranged as

$$|sI - A_0 + e^{-\tau s}(sB - A_1)| = 0. \tag{5.28}$$

Associated eigenvector (v) can be added to Equation 5.28

$$(sI - A_0)v = -e^{-\tau s}(sB - A_1)v, \tag{5.29}$$

conjugating and transposing Equation 5.29 yield

$$v^*(-sI - A_0^T) = -e^{\tau s} v^*(-sB^T - A_1^T). \tag{5.30}$$

Multiplying both sides of Equation 5.29 by minus Equation 5.30, we obtain

$$\overbrace{(sI - A_0)}^{O}\overbrace{vv^*}^{P}\overbrace{(sI + A_0^T)}^{Q} = (sB - A_1)vv^*(sB^T + A_1^T). \tag{5.31}$$

To solve Equation 5.31, we adopt the matrix method proposed by Louisell Louisell (2001). A brief overview of this matrix method is provided here. Let a vectorization operator $\xi : C^{n\times n} \longrightarrow C^{n^2}$ be defined as follows

$$\xi M = \begin{bmatrix} m_1^T \\ m_2^T \\ \cdots \\ m_n^T \end{bmatrix} \tag{5.32}$$

for any $M = \begin{bmatrix} m_1 \\ m_2 \\ \cdots \\ m_n \end{bmatrix}$. We particularly use an important identity of this operator which is

$$\xi(OPQ) = (O \otimes Q^T)\xi P \tag{5.33}$$

where O, P, and $Q \in C^{n\times n}$ and $\otimes$ refers to the Kronecker product. Using Equation 5.33, Equation 5.31 becomes

$$[(sI - A_0) \otimes (sI + A_0) - (sB - A_1) \otimes (sB + A_1)]V = 0 \tag{5.34}$$

or simply

$$\Lambda(s)V = 0 \tag{5.35}$$

where V and $\Lambda(s)$ are ξvv^* and $(sI-A_0)\otimes(sI+A_0)-(sB-A_1)\otimes(sB+A_1)$. Next, consider the following two ordinary differential equations

$$\dot{X}(t)+B\dot{Y}(t)=A_0X(t)+A_1Y(t) \tag{5.36}$$

$$\dot{X}(t)B^T+\dot{Y}(t)=-X(t)A_1^T-Y(t)A_0^T \tag{5.37}$$

where A_0, A_1, B, X, and $Y \in C^{n\times n}$. Herein, we define two new operators E and F by

$$E\begin{bmatrix}X\\Y\end{bmatrix}=\begin{bmatrix}X+BY\\XB^T+Y\end{bmatrix} \tag{5.38}$$

$$F\begin{bmatrix}X\\Y\end{bmatrix}=\begin{bmatrix}A_0X+A_1Y\\-XA_1^T-YA_0^T\end{bmatrix}. \tag{5.39}$$

If $Z(t)=\begin{bmatrix}X\\Y\end{bmatrix}$, then Equations 5.36 and 5.37 can be written in the matrix differential equation as

$$E\dot{Z}(t)=FZ(t). \tag{5.40}$$

Next, we write E and F in vector coordinates and apply the vectorization operator ξ to Z

$$E_0=\begin{bmatrix}I\otimes I & B\otimes I\\ I\otimes B & I\otimes I\end{bmatrix}, F_0=\begin{bmatrix}A_0\otimes I & A_1\otimes I\\ -I\otimes A_1 & -I\otimes A_0\end{bmatrix}, z=\xi Z=\begin{bmatrix}\xi X\\ \xi Y\end{bmatrix}=\begin{bmatrix}x\\y\end{bmatrix}. \tag{5.41}$$

Thus Equation 5.40 becomes

$$E_0\dot{z}(t)=F_0z(t) \tag{5.42}$$

and the corresponding characteristic equation becomes

$$(sE_0-F_0)z=0. \tag{5.43}$$

In the Laplace domain, Equations 5.36 and 5.37 become

$$(sI - A_0)X + (sB - A_1)Y = 0 \tag{5.44}$$

$$X(sB^T - A_1^T) + Y(sI + A_0^T)Y = 0. \tag{5.45}$$

Defining a new operator as $T = sE - F$

$$T \begin{bmatrix} X \\ Y \end{bmatrix} = \begin{bmatrix} (sI - A_0)X + (sB - A_1)Y \\ X(sB^T + A_1^T) + Y(sI + A_0^T) \end{bmatrix}, \tag{5.46}$$

Equations 5.44 and 5.45 become

$$T \begin{bmatrix} X \\ Y \end{bmatrix} = TZ = 0. \tag{5.47}$$

To understand the behavior of operator T, we attempt to solve

$$T \begin{bmatrix} X \\ Y \end{bmatrix} = \begin{bmatrix} X_0 \\ Y_0 \end{bmatrix}. \tag{5.48}$$

By multiplying the upper equation by $sI + A_0^T$, and the lower on the left by $sB - A_1$, then subtracting, we obtain

$$(sI - A_0)X(sI + A_0^T) - (sB - A_1)X(sB^T + A_1^T) = X_0(sI + A_0^T) - (sB - A_1)Y_0. \tag{5.49}$$

Similarly, by multiplying the upper equation by $sB^T + A_1^T$, and the lower on the left by $sI - A_0$, then subtracting, we obtain

$$(sI - A_0)Y(sI + A_0^T) - (sB - A_1)Y(sB^T + A_1^T) = (sI - A_0)Y_0 - X0(sB^T - A_1^T). \tag{5.50}$$

Here, we define another operator T^+ as

$$T^+ \begin{bmatrix} X \\ Y \end{bmatrix} = \begin{bmatrix} X(sI + A_0^T) - (sB - A_1)Y \\ -X(sB^T + A_1^T) + (sI - A_0)Y \end{bmatrix}. \tag{5.51}$$

Applying both operators T^+ and T on $\begin{bmatrix} X \\ Y \end{bmatrix}$, we obtain

$$T^+T \begin{bmatrix} X \\ Y \end{bmatrix} = \begin{bmatrix} \lambda X \\ \lambda Y \end{bmatrix} \tag{5.52}$$

where

$$\lambda X = (sI - A_0)X(sI + A_0^T) - (sB - A_1)X(sB^T + A_1^T) \tag{5.53}$$

$$\lambda Y = (sI - A_0)Y(sI + A_0^T) - (sB - A_1)Y(sB^T + A_1^T). \tag{5.54}$$

Next, we vectorize all the operators using the vectorization operator ξ. Therefore, $T \begin{bmatrix} X \\ Y \end{bmatrix}$, $T^+ \begin{bmatrix} X \\ Y \end{bmatrix}$, λX and λY map to $K \begin{bmatrix} x \\ y \end{bmatrix}$, $K^+ \begin{bmatrix} x \\ y \end{bmatrix}$, Λx and Λy, accordingly, where

$$K = \begin{bmatrix} (sI - A_0) \otimes I & (sB - A_1) \otimes I \\ I \otimes (sB + A_1) & I \otimes (sI + A_0) \end{bmatrix} = sE_0 - F_0 \tag{5.55}$$

$$K^+ = \begin{bmatrix} I \otimes (sI + A_0) & -(sB - A_1) \otimes I \\ -I \otimes (sB + A_1) & (sI - A_0) \otimes I \end{bmatrix} \tag{5.56}$$

$$\Lambda(s) = (sI - A_0) \otimes (sI + A_0) - (sB - A_1) \otimes (sB + A_1). \tag{5.57}$$

Notice, in Equations 5.57 and 5.34, $\Lambda(s)$ is identical. Applying the vectorization operation (ξ) on Equation 5.52, we obtain

$$K^+K \begin{bmatrix} x \\ y \end{bmatrix} = \begin{bmatrix} \Lambda x \\ \Lambda y \end{bmatrix} = \begin{bmatrix} \Lambda & 0 \\ 0 & \Lambda \end{bmatrix} \begin{bmatrix} x \\ y \end{bmatrix} \tag{5.58}$$

which means

$$K^+K = \begin{bmatrix} \Lambda & 0 \\ 0 & \Lambda \end{bmatrix} \tag{5.59}$$

and therefore,

$$|K^{+}K| = \begin{vmatrix} \Lambda & 0 \\ 0 & \Lambda \end{vmatrix} = |\Lambda|^2. \tag{5.60}$$

In a lemma, Louisell proved that $|K| = |K^{+}|$, see Louisell (2001). Thus we know

$$|K| = |\Lambda|. \tag{5.61}$$

To obtain the solution to Equation 5.26, we need to solve Equation 5.34. The solution to Equation 5.34 is

$$|\Lambda| = 0. \tag{5.62}$$

Using Equations 5.55 and 5.61, we know

$$|\Lambda| = |K| = |sE_0 - F_0| = 0. \tag{5.63}$$

Notice, Equation 5.63 is a generalized eigenvalue problem which can be simply solved. To find the corresponding critical time delay(s), we adopt the method proposed by Marshal *et al.,* Marshall, Gorecki, Korytowski, and Walton (1992). For the imaginary eigenvalues found from Equation 5.63 ($s = i\omega$), Equation 5.29 becomes singular

$$|(i\omega I - A_0) + e^{-\tau i\omega}(i\omega B - A_1)| = 0. \tag{5.64}$$

The solutions of Equation 5.64 are the solutions of the generalized eigenvalue of the pair matrix $A_0 - i\omega I$ and $i\omega B - A_1$ if and only if the magnitude of the eigenvalue solution is 1 as $|e^{\tau i\omega}| = 1$.

5.4.5 Predictive stability indicator: PSI value and stability categories

Designing an RTHS configuration becomes more meaningful if we realize that designing a transfer system controller is inherently characterized by a balance between tracking accuracy (performance) and robustness (stability). To conduct an accurate RTHS, while system stability is reliably held, a researcher needs to know the sensitivity of the partitioning choice to the interface de-synchronization from stability and performance perspectives. In the proposed PSI framework, by solving the neutral (or retarded) delay differential equations, we obtain a set of critical time delays. For a particular partitioning choice, the critical time delays correspond to the time delays at which stability switch occurs in the virtual PSI framework. In order to develop a stability indicator, the first occurrence of a stability switch (from a stable system to an unstable system) is the most meaningful one. Thus, hereinafter, the critical time delay (τ_{cr}) refers to the smallest critical time delay obtained by solving the delay differential equation. The PSI value can be computed as

$$PSI = \log_{10}[\tau_{cr}(msec)]. \tag{5.65}$$

Equation 5.65 maps $\tau_{cr} \in (0, \infty)$ to $PSI \in (-\infty, \infty)$. Figure 5.9 shows the relationship between critical time delay, predictive stability indicator and global stability for any partitioning choice. It should be noted that the proposed boundaries in Figure 5.9 are based on experience and the values may change based on transfer system controller design procedure and reasonableness of assumptions of transfer system linearity. It can be seen in Figure 5.9 that higher values of PSI refers to a partitioning choice with a greater stability margin.

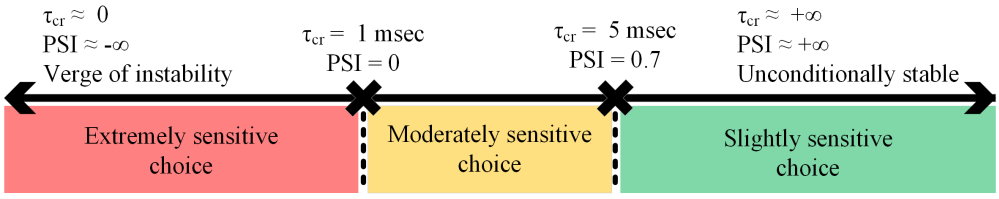

Figure 5.9. Relationship between PSI, critical time delay and RTHS stability due to interface de-synchronization.

The proposed predictive stability indicator can be applied to more complicated systems, such as multi-directional multi-actuator RTHS, multi-rate RTHS, distributed RTHS, and *piecewise linear* (PL) dynamical systems. From a stability point of view, researchers have shown that linear RTHS is more susceptible to interface de-synchronization than a partitioning choice with strain-softening nonlinearities or energy dissipating systems in the physical substructure.

With the recent scientific and engineering advances that extend the connectivity of cyber-physical systems, distributed RTHS can optimize the use of distributed computational and experimental resources and leverage multiple computational and experimental resources. However, the existence of substantial deterministic and random communication delays poses stability challenges which can be effectively addressed by the proposed stability framework.

5.5 Illustrative Examples

In this section, the objective is to demonstrate the effectiveness of using the PSI in designing a successful experiment. The term partitioning choice refers to various choices of partitioning a specific emulated structure into numerical and physical substructures. An alternative to the PSI is stability analysis of various detailed components of RTHS including transfer system dynamics, transfer system controller and control-structure-interaction.

In this alternative method, due to the presence of control-structure-interaction, any change in the physical substructure (new partitioning choice) yields change in transfer system performance which requires redesigning the control/compensation system. To conduct stability (or performance) analysis of many partitioning choices, it is unfeasible to design a new transfer system controller every time a change is made in the physical substructure. However, since PSI is obtained analytically and it is independent of transfer system and controller dynamics, generating a PSI plot for many partitioning choices is extremely easy, quick, and useful. Thus, to demonstrate the technique, and still make it possible to verify that PSI yields the same results as other techniques that include CSI and transfer system dynamics, the physical substructure is kept unchanged and the numerical substructure is varied.

5.5.1 MDOF RTHS with a single actuator

In the first illustrative example, we conduct a stability analysis of $2,500,000$ simulated RTHS cases and compare the results with the corresponding PSI values. Consider a linear three story shear building subjected to a one-dimensional seismic excitation partitioned in Figure 5.10. The physical substructure is a portion of the first story, and the remaining is the numerical part.

In this example, to avoid redesigning a control/compensation system for each case study, the physical substructure remains unchanged: $M_p = 2,924$ kg, $C_p = 15.8$ N.s/cm, $K_p = 13,895$ N/cm. However, to study various partitioning choices, the numerical substructure changes for each simulated case. Mass, stiffness, and damping of the numerical substructure are computed as follows

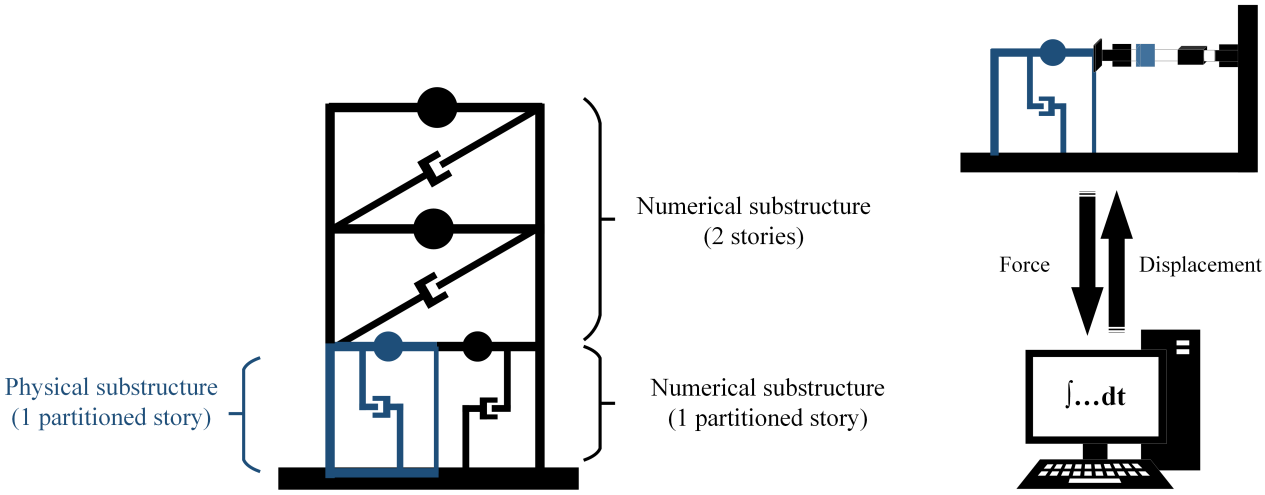

Figure 5.10. A typical real-time hybrid simulation using shake table as transfer system.

$$M_n = \begin{bmatrix} M_n^1 & 0 & 0 \\ 0 & M_n^2 & 0 \\ 0 & 0 & M_n^3 \end{bmatrix} \tag{5.66}$$

$$C_n = \begin{bmatrix} C_n^1 + C_n^2 & -C_n^2 & 0 \\ -C_n^2 & C_n^2 + C_n^3 & C_n^3 \\ 0 & -C_n^3 & C_n^3 \end{bmatrix} \tag{5.67}$$

$$K_n = \begin{bmatrix} K_n^1 + K_n^2 & -K_n^2 & 0 \\ -K_n^2 & K_n^2 + K_n^3 & K_n^3 \\ 0 & -K_n^3 & K_n^3 \end{bmatrix} \tag{5.68}$$

where, M_n^1 and K_n^1 are computed using partitioning parameters α_1 and γ_1

$$\alpha_1 = \frac{M_n^1}{M_n^1 + M_p}, \gamma_1 = \frac{K_n^1}{K_n^1 + K_p} \tag{5.69}$$

and

$$C_n^1 = C_p. \tag{5.70}$$

Mass, damping, and stiffness of the second and third floors are assigned as

$$M_n^2 = M_n^3 = M_n^1 + M_p \tag{5.71}$$

$$C_n^2 = C_n^3 = C_n^1 + C_p \tag{5.72}$$

$$K_n^2 = K_n^3 = K_n^1 + K_p. \tag{5.73}$$

For the simulated RTHS cases, a hydraulic actuator is modeled according to the block diagrams shown in Figures 5.3 and 5.5. The model parameters are selected using an identified actuator in Carrion and Spencer (2007) where $a_1 = 5.17 \times 10^5$ kN/(m.s), $a_2 = 7.77 \times 10^4$ kN/m, and $a_3 = 21.52$ 1/s. In Carrion and Spencer (2007), Carrion and Spencer also modeled the associated servo-valve dynamics as a first order transfer function

$$G_s = \frac{K_p}{\tau s + 1}, \tag{5.74}$$

where $K_p = 4.6$ and $\tau = 3.32$ ms are proportional gain and servo-valve time constant, respectively. Figure 5.12 depicts the block diagram of the simulated RTHS cases.

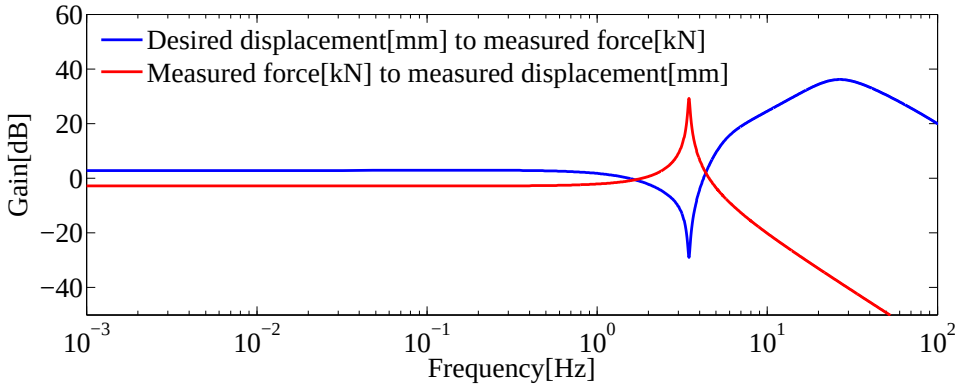

Figure 5.11. Frequency response functions demonstrating control-structure-interaction in RTHS.

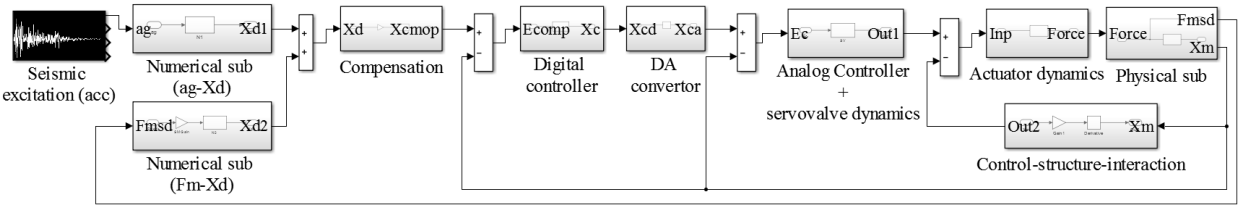

Figure 5.12. Block diagram of simulated RTHS.

In the simulated RTHS cases, control-structure interaction is also modeled. In Figure 5.11, the magnitude of frequency response functions of the physical substructure (force to displacement) and coupled actuator with the physical substructure (desired displacement to measured force) are demonstrated. This figure shows that because the physical substructure is lowly-damped (damping ratio: $\zeta = 1.24\%$), the actuator has a greatly limited ability to apply forces at the physical substructure's natural frequency. Next, five different compensation/control systems with various levels of performance are designed and stability of a total of $2,500,000$ ($=$ 5 control systems$\times 500,000$ partitioning choices) simulated cases are determined and showed in Figure 5.13. Simulated RTHS results in Figure 5.13 are categorized in 6 different stability cases: (i) 5 controllers stable - 0 controller unstable ($0U/5S$); (ii) 4 controllers stable - 1 controller unstable ($1U/4S$); (ii) 3 controllers stable - 2 controllers unstable ($2U/3S$); (ii) 2 controllers stable - 3 controllers unstable ($3U/2S$); (ii) 1 controller stable - 4 controllers unstable ($4U/1S$); (ii) 0 controller stable - 5 controllers unstable ($5U/0S$).

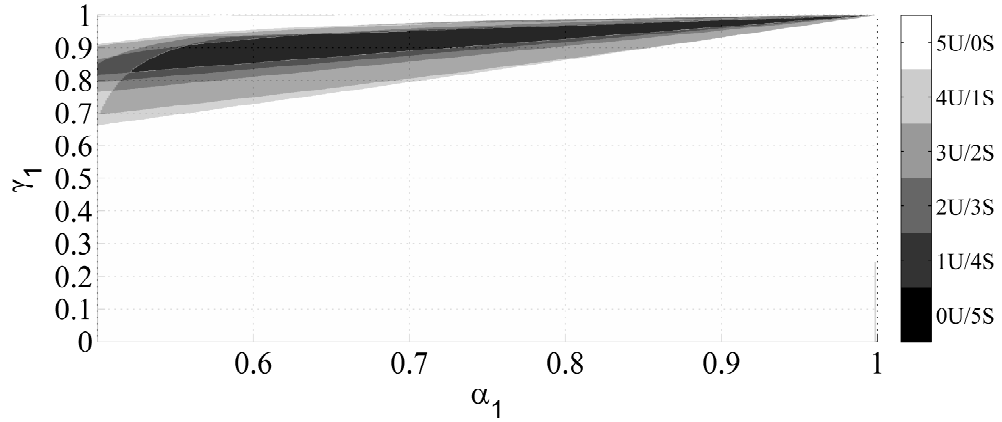

Figure 5.13. Stability of simulated cases (α_1 and γ_1 are defined as: Equation 5.69).

In the next step, the PSI values associated with each partitioning choice are computed using Equation 5.65 and depicted in Figure 5.14. By comparing Figures 5.13 and 5.14, we can see that

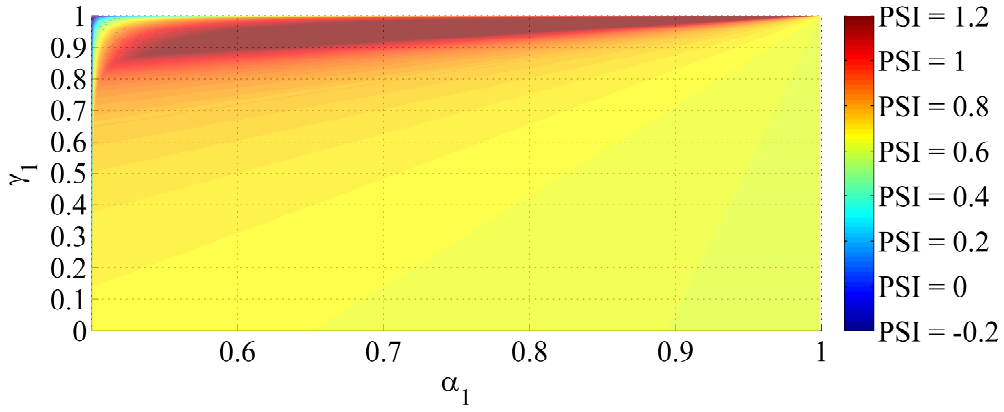

Figure 5.14. Predictive stability indicator (α_1 and γ_1 are defined as: Equation 5.69).

the PSI plot is able to capture the essential results of the global stability in RTHS. In other words, prior to conducting an experiment, the PSI value provides a researcher with relative measures associated with the sensitivity of alternative partitioning choices to interface de-synchronization. This information (the PSI plot) is extremely valuable for the design and configuration of RTHS experiment.

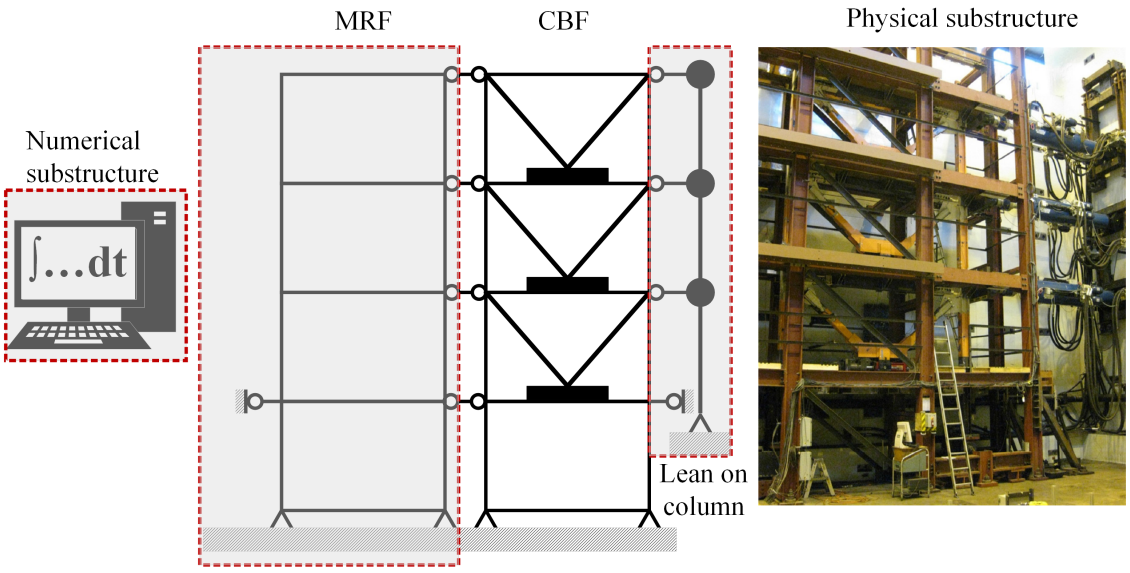

Figure 5.15. Large scale multi-actuator RTHS (NEES project ID: 648).

5.5.2 MDOF RTHS with multiple actuators

As discussed earlier, currently RTHS is being implemented for complex MDOF systems in which control of multiple actuators is required. The multiple actuators are inherently coupled through the physical substructure. This phenomenon imposes certain challenges and considerations in transfer system control for implementing a successful test. Here, the objective is to evaluate the effectiveness of the PSI for stability analysis of MDOF RTHS with multiple actuators while control-structure interaction is considered. In this study, stability of $9,000,000$ simulated RTHS are determined and the results are compared with the PSI plot to evaluate how effectively the PSI can capture the sensitivity of a partitioning choice to interface de-synchronization for MDOF RTHS with multiple actuators.

Here, to avoid redesigning a control/compensation system for each case study, the physical substructure is identified and kept unchanged for all simulations.

$$M_p = \begin{bmatrix} 3.147 & 0 & 0 \\ 0 & 3.147 & 0 \\ 0 & 0 & 3.147 \end{bmatrix} \; kN.s^2/m \tag{5.75}$$

$$C_p = \begin{bmatrix} 74.21 & -32.73 & 4.29 \\ -32.73 & 59.87 & -23.20 \\ 4.29 & -23.20 & 26.10 \end{bmatrix} \; kN.s/m \tag{5.76}$$

$$K_p = \begin{bmatrix} 5.49 & -3.35 & 0.76 \\ -3.35 & 4.32 & -1.83 \\ 0.76 & -1.83 & 1.21 \end{bmatrix} \times 10^4 \; kN/m. \tag{5.77}$$

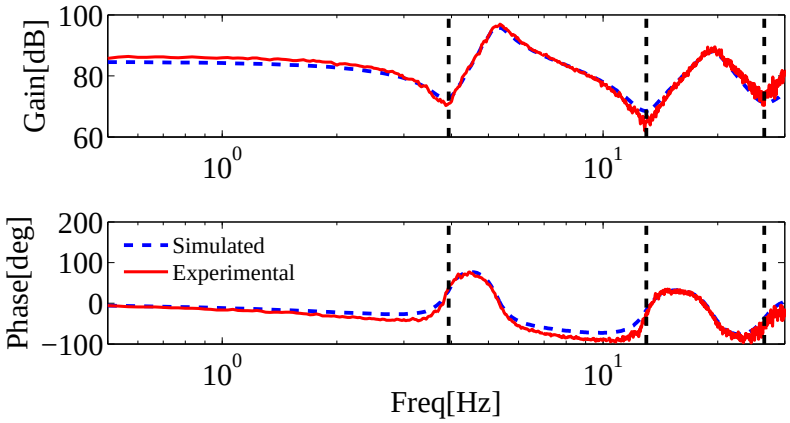

Figure 5.16. Validation of the actuator model.

The original numerical substructure is identified as

$$M_n = \begin{bmatrix} 98.9 & 0 & 0 \\ 0 & 98.9 & 0 \\ 0 & 0 & 70.8 \end{bmatrix} \; kN.s^2/m \tag{5.78}$$

$$C_n = \begin{bmatrix} 391.0 & -156.4 & 2.7 \\ -156.4 & 295.2 & -122.2 \\ 2.7 & -122.2 & 101.6 \end{bmatrix} \; kN.s/m \tag{5.79}$$

$$K_n = \begin{bmatrix} 1.17 & -0.73 & 0.16 \\ -0.73 & 0.89 & -0.34 \\ 0.16 & -0.34 & 0.20 \end{bmatrix} \times 10^5 \ \ kN/m. \tag{5.80}$$

which leads to $F_1 = 1.04$ Hz, $F_2 = 3.29$ Hz, $F_3 = 6.93$ Hz, $\zeta_1 = 2.71\%$, $\zeta_2 = 6.45\%$, and $\zeta_3 = 6.15\%$ where F_i and ζ_i are the i^{th} natural frequency and damping ratio, respectively. To investigate the stability of various partitioning choices, three sets of simulations were performed: Case I in which the first mode's natural frequency and damping between $[0.52 - 1.56]$Hz and $[0.54 - 3.25]\%$ while the second and third modes are kept unchanged; Case II in which the second mode's natural frequency and damping between $[1.65 - 4.94]$Hz and $[1.29 - 7.74]\%$ while the first and third modes are kept unchanged; Case III in which the third mode's natural frequency and damping between $[3.46 - 10.39]$Hz and $[1.23 - 7.38]\%$ while the first and second modes are kept unchanged. These varying parameters are provided in Table 5.1. It should be mentioned that in all the simulated cases, the modal mass and mode shapes remain unchanged.

Table 5.1. *Simulated case studies.*

	F_1 (Hz)	F_2 (Hz)	F_3 (Hz)	ζ_1 (%)	ζ_2 (%)	ζ_3 (%)
Case I	$\in$ [0.52 1.56]	3.29	6.93	$\in$ [0.54 3.25]	6.45	6.15
Case II	1.04	$\in$ [1.65 4.94]	6.93	2.71	$\in$ [1.29 7.74]	6.15
Case III	1.04	3.29	$\in$ [3.46 10.39]	2.71	6.45	$\in$ [1.23 7.38]

To capture the stability trend, three different compensation/control systems with various levels of performance are designed. Thus, in total, stability of $9,000,000$ ($=3$ control systems $\times 3$ variation cases $\times 1,000,000$ partitioning choices) simulated cases are determined.

In Figures 5.17-5.19, simulated RTHS results are categorized in four different stability groups: (i) 3 controllers stable - 0 controller unstable ($0U/3S$); (ii) 2 controllers stable - 1 controller unstable ($1U/2S$); (ii) 1 controller stable - 2 controllers unstable ($2U/1S$); (ii) 3 controllers stable - 0 controllers unstable ($3U/0S$). Next, the PSI plots corresponding to cases I-III are generated. Figures 5.17-5.19 provide comparisons between the stability results of all the simulated cases and the predictive stability analysis based on the PSI values.

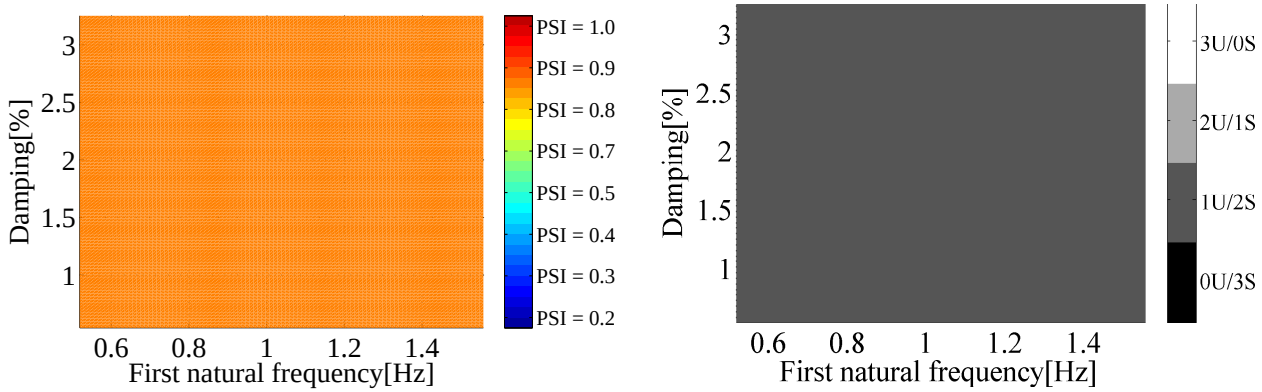

Figure 5.17. Sensitivity study of RTHS stability to the first mode of the numerical substructure.

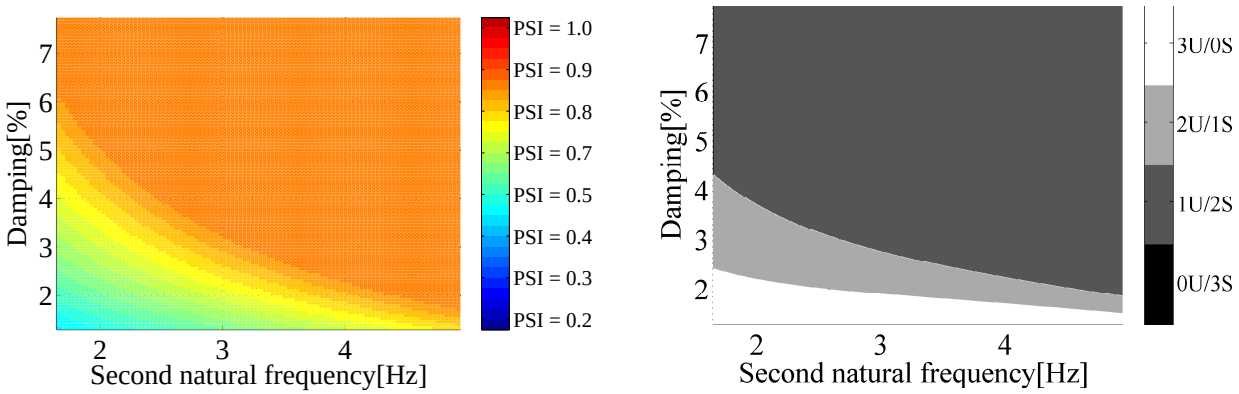

Figure 5.18. Sensitivity study of RTHS stability to the second mode of the numerical substructure.

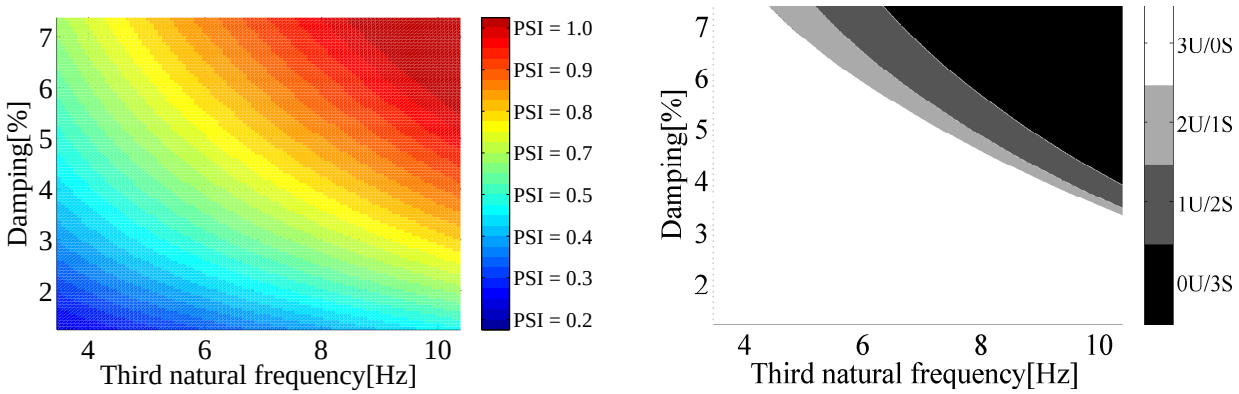

Figure 5.19. Sensitivity study of RTHS stability to the third mode of the numerical substructure.

The x and y axes in Figures 5.17-5.19 correspond to variations in the natural frequency and damping of the numerical substructure. Figures 5.17-5.19 show that there is significant agreement between the stability results and the PSI plots. Therefore, PSI plots are effective for designing a successful experiment. For this particular experiment, some observations can be made prior to conducting the experiment based on the PSI plots. There are some partitioning choices in which an almost perfect controller is required for the system to hold its stability. These partitioning choices are not always clear to a researcher. For instance, it's more likely that a numerical substructure with F_3 = 5 Hz and ζ_3 = 5% causes instability than the same numerical substructure with F_3 = 10 Hz and ζ_3 = 5%.

Global stability is highly sensitive to the higher modes of the numerical substructure and relatively insensitive to the lower modes of the numerical substructure. However, an effective control strategy might still be needed for certain partitioning choices. Adding damping in the numerical substructure can always improve stability in the system.

5.6 Conclusion

Currently, RTHS is being implemented to evaluate the performance of complex MDOF systems with rate dependent behaviors. For more complex experiments in this class, multiple actuators are required to enforce the boundary conditions at the interfaces, and with the need for more accuracy in RTHS, the challenges involved in configuring the test and designing highly accurate and robust controllers will increase. The particular RTHS configuration chosen for an experiment largely dictates the capabilities and accuracy requirements of the controller used. An RTHS can become unstable if de-synchronization at the boundaries occurs. Stability analysis with simulated RTHS requires that transfer system modeling and control be performed in advance. And due to control-structure interaction, any change in the physical substructure (a new partitioning choice) yields an associated change in the transfer system performance which requires redesign of the controller/compensator.

As the complexity of the test grows, such models require significant amounts of time to consider the large number of partitioning choices, and to search for a configuration with controller needs that are less sensitive to the partitioning choices. With large number of configurations, a pure simulation based approach is practically infeasible. Here the PSI has been extended to be applicable to any linear MDOF system. The PSI provides a quantitative tool to compare and contrast the configuration choices in terms of the challenge that will be involved in design of the actuator controller. Designing a transfer system controller is inherently characterized by a balance between tracking accuracy (performance) and robustness (stability).

For a partitioning choice with a non-sensitive interface, designing a more robust controller (which leads to larger stability margins for the transfer system) is more likely to ensure global stability in RTHS. However, for a partitioning choice with a sensitive interface, designing a transfer system controller with accurate tracking performance within the bandwidth of interest is an absolute requirement. To establish the PSI for MDOF systems, a delay differential equation is converted to a generalized eigenvalue problem using a set of vectorization mappings. This approach results in a computationally efficient method to solve the delay differential equations, thus yielding PSI values for a range of RTHS cases. Because it is independent of the transfer system and controller dynamics, the PSI is quite powerful for exploiting different configurations as well as designing a successful RTHS experiment.

REFERENCES

Aicha, I. B. (2015). Stability estimate for a hyperbolic inverse problem with time-dependent coefficient. *Inverse Problems*, *31*(12), 125010. Retrieved from http://stacks.iop.org/0266-5611/31/i=12/a=125010

Bellassoued, M., & Dos Santos Ferreira, D. (2011). Stability estimates for the anisotropic wave equation from the Dirichlet-to-Neumann map. *Inverse Probl. Imaging*, *5*(4), 745–773. Retrieved from http://dx.doi.org/10.3934/ipi.2011.5.745 doi: 10.3934/ipi.2011.5.745

Beylkin, G. (1984). The inversion problem and applications of the generalized radon transform. *Communications on pure and applied mathematics*, *37*(5), 579–599.

Boman, J. (1991). Helgason's support theorem for Radon transforms—a new proof and a generalization. In *Mathematical methods in tomography (oberwolfach, 1990)* (Vol. 1497, pp. 1–5). Berlin: Springer.

Boman, J., & Quinto, E. T. (1987). Support theorems for real-analytic Radon transforms. *Duke Math. J.*, *55*(4), 943–948. (x) doi: 10.1215/S0012-7094-87-05547-5

Boman, J., Quinto, E. T., et al. (1987). *Support theorems for real analytic radon transforms*. Stockholms Universitet. Matematiska Institutionen.

Bony, J.-M. (1977). Equivalence des diverses notions de spectre singulier analytique. *Séminaire Équations aux dérivées partielles (Polytechnique)*, 1–12.

Botelho, R. M., & Christenson, R. E. (2015). Robust Stability and Performance Analysis for Multi-actuator Real-Time Hybrid Substructuring. In (pp. 1–7). Retrieved from http://link.springer.com/10.1007/978-3-319-15209-7{_}1 doi: 10.1007/978-3-319-15209-7_1

Brewick, P. T., & Smyth, A. W. (2015). Exploration of the Impacts of Driving Frequencies on Damping Estimates. *Journal of Engineering Mechanics*, *141*(3), 04014130. Retrieved from http://ascelibrary.org/doi/10.1061/{\%}28ASCE{\%}29EM.1943-7889.0000847 doi: 10.1061/(ASCE)EM.1943-7889.0000847

Bros, J., & Iagolnitzer, D. (1975). Support essentiel et structure analytique des distributions. *Seminaire Goulaouic-Lions-Schwartz, exp*, *18*.

Carrion, J. E., & Spencer, B. F. (2007). Model-based Strategies for Real-time Hybrid Testing. (December).

Cha, Y., Agrawal, A. K., Friedman, A., Phillips, B., Ahn, R., Dong, B., ... Christenson, R. (2014). Performance Validations of Semiactive Controllers on Large-Scale Moment-Resisting Frame Equipped with 200-kN MR Damper Using Real-Time Hybrid Simulations. *Journal of Structural Engineering*, *140*(10), 04014066. Retrieved from `http://ascelibrary.org/doi/10.1061/{\%}28ASCE{\%}29ST.1943-541X.0000982` doi: 10.1061/(ASCE)ST.1943-541X.0000982

Chae, Y., Ricles, J. M., & Sause, R. (2012). Real-time hybrid simulations of a 3-story steel frame building with magneto-rheological dampers subject to strong ground motions. In F. Mazzolani & R. Herrera (Eds.), *Behaviour of steel structures in seismic areas: Stessa 2012*. CRC Press, Inc.

Chatzi, E. N., Smyth, A. W., & Masri, S. F. (2010). Experimental application of on-line parametric identification for nonlinear hysteretic systems with model uncertainty. *Structural Safety*, *32*(5), 326–337. doi: 10.1016/j.strusafe.2010.03.008

Chen, C., & Ricles, J. M. (2010). *Tracking Error-Based Servohydraulic Actuator Adaptive Compensation for Real-Time Hybrid Simulation* (Vol. 136) (No. 4). doi: 10.1061/(ASCE)ST.1943-541X.0000124

Chen, C., Ricles, J. M., Karavasilis, T. L., Chae, Y., & Sause, R. (2012, feb). Evaluation of a Real-time Hybrid Simulation System for Performance Evaluation of Structures with Rate Dependent Devices Subjected to Seismic Loading. *Engineering Structures*, *35*, 71–82. doi: 10.1016/j.engstruct.2011.10.006

Christenson, R., Lin, Y. Z., Emmons, A., & Bass, B. (2008). *Large-Scale Experimental Verification of Semiactive Control through Real-Time Hybrid Simulation1* (Vol. 134) (No. 4). doi: 10.1061/(ASCE)0733-9445(2008)134:4(522)

Crawford, C. R., King, K. F., Ritchie, C. J., & Godwin, J. D. (1996). Respiratory compensation in projection imaging using a magnification and displacement model. *IEEE transactions on medical imaging*, *15*(3), 327–332.

Denisjuk, A. (2006). Inversion of the x-ray transform for 3d symmetric tensor fields with sources on a curve. *Inverse problems*, *22*(2), 399.

Desbat, L., Roux, S., & Grangeat, P. (2007). Compensation of some time dependent deformations in tomography. *IEEE transactions on medical imaging*, *26*(2), 261–269.

de Silva, C. W. (2007). *Control Sensors and Actuators*. Broken Sound Parkway, NW: Taylor & Francis Group, LLC.

Dong, B., Sause, R., & Ricles, J. M. (2015, sep). Accurate real-time hybrid earthquake simulations on large-scale MDOF steel structure with nonlinear viscous dampers. *Earthquake Engineering & Structural Dynamics*, *44*(12), 2035–2055. Retrieved from http://doi.wiley.com/10.1002/eqe.2572 doi: 10.1002/eqe.2572

Duistermaat, J. J. (1996). *Fourier integral operators* (Vol. 130). Boston, MA: Birkhäuser Boston Inc.

Duistermaat, J. J., & Hörmander, L. (1972). Fourier integral operators. II. *Acta Math.*, *128*(3-4), 183–269.

Dyke, S. J., Spencer, B. F., Sain, M. K., & Carlson, J. D. (1999). *An experimental study of MR dampers for seismic protection* (Vol. 7) (No. 5). doi: 10.1088/0964-1726/7/5/012

Dyke, S. J., Spencer Jr., B. F., Quast, P., & Sain, M. K. (1995, feb). Role of Control-Structure Interaction in Protective System Design. *Journal of Engineering Mechanics*, *121*(2), 322–338. doi: 10.1061/(ASCE)0733-9399(1995)121:2(322)

Franco, J. A., Botelho, R. M., & Christenson, R. E. (2015). Effective Control of a Six Degree of Freedom Shake Table. In *Dynamics of coupled structures* (pp. 19–29). Springer International Publishing. Retrieved from http://link.springer.com/10.1007/978-3-319-15209-7{_}3 doi: 10.1007/978-3-319-15209-7_3

Friedman, A., Dyke, S. J., Phillips, B., Ahn, R., Dong, B., Chae, Y., ... Sause, R. (2015, jun). Large-Scale Real-Time Hybrid Simulation for Evaluation of Advanced Damping System Performance. *Journal of Structural Engineering*, *141*(6), 04014150. Retrieved from http://ascelibrary.org/doi/10.1061/{\%}28ASCE{\%}29ST.1943-541X.0001093 doi: 10.1061/(ASCE)ST.1943-541X.0001093

Frigyik, B., Stefanov, P., & Uhlmann, G. (2008). The X-ray transform for a generic family of curves and weights. *J. Geom. Anal.*, *18*(1), 89–108. doi: http://dx.doi.org/10.1007/s12220-007-9007-6

Gao, X., Castaneda, N., & Dyke, S. J. (2012). Real time hybrid simulation: from dynamic system, motion control to experimental error. *Earthquake Engineering & Structural Dynamics*, *42*, 815–832. Retrieved from http://onlinelibrary.wiley.com/doi/10.1002/eqe.2246/full doi: 10.1002/eqe

Gazzola, F., Grunau, H.-C., & Sweers, G. (2010). *Polyharmonic boundary value problems: positivity preserving and nonlinear higher order elliptic equations in bounded domains*. Springer Science & Business Media.

Guillemin, V. (1985). On some results of Gel'fand in integral geometry. In *Pseudodifferential operators and applications (Notre Dame, Ind., 1984)* (Vol. 43, pp. 149–155). Providence, RI: Amer. Math. Soc.

Guillemin, V., & Sternberg, S. (1977). *Geometric asymptotics*. Providence, R.I.: American Mathematical Society. (Mathematical Surveys, No. 14)

Guillemin, V., & Sternberg, S. (1979). Some problems in integral geometry and some related problems in micro-local analysis. *American Journal of Mathematics*, *101*(4), 915–955.

Hahn, B. (2014). Reconstruction of dynamic objects with affine deformations in computerized tomography. *Journal of Inverse and Ill-posed Problems*, *22*(3), 323–339.

Hahn, B., & Garrido, M. K. (2019). An efficient reconstruction approach for a class of dynamic imaging operators. *Inverse Problems*, *35*(9), 094005.

Hahn, B. N. (2014). Efficient algorithms for linear dynamic inverse problems with known motion. *Inverse Problems*, *30*(3), 035008.

Hahn, B. N., & Quinto, E. T. (2016). Detectable singularities from dynamic radon data. *SIAM Journal on Imaging Sciences*, *9*(3), 1195–1225.

Hakuno, M., Shidawara, M., & Hara, T. (1969). Dynamic destructive test of a cantilever beam, controlled by an analog-computer. *Trans. Japan Soc. Civil Eng.*, *171*, 1–9.

Holman, S., & Stefanov, P. (2010). The weighted Doppler transform. *Inverse Probl. Imaging*, *4*(1), 111–130. Retrieved from `http://dx.doi.org/10.3934/ipi.2010.4.111` doi: 10.3934/ipi.2010.4.111

Homan, A., & Zhou, H. (2017). Injectivity and stability for a generic class of generalized radon transforms. *The Journal of Geometric Analysis*, *27*(2), 1515–1529.

Hörmander, L. (1971). Uniqueness theorems and wave front sets for solutions of linear differential equations with analytic coefficients. *Communications on Pure and Applied Mathematics*, *24*(5), 671–704.

Hörmander, L. (1983a). *The analysis of linear partial differential operators. I* (Vol. 256). Berlin: Springer-Verlag. (Distribution theory and Fourier analysis)

Hörmander, L. (1983b). *The analysis of linear partial differential operators. II* (Vol. 257). Berlin: Springer-Verlag. (Differential operators with constant coefficients)

Hörmander, L. (1985). *The analysis of linear partial differential operators. III* (Vol. 274). Berlin: Springer-Verlag. (Pseudodifferential operators) doi: 10.1007/978-3-540-49938-1

Katchalov, A., Kurylev, Y., & Lassas, M. (2001). Inverse boundary spectral problems (monographs and surveys in pure and applied mathematics vol 123)(boca raton, fl: Crc).

Katsevich, A. (2006). Improved cone beam local tomography. *Inverse Problems*, *22*(2), 627.

Katsevich, A. (2008). Motion compensated local tomography. *Inverse Problems*, *24*(4), 045012.

Katsevich, A. (2010). An accurate approximate algorithm for motion compensation in two-dimensional tomography. *Inverse Problems*, *26*(6), 065007.

Katsevich, A., Silver, M., & Zamyatin, A. (2011). Local tomography and the motion estimation problem. *SIAM Journal on Imaging Sciences*, *4*(1), 200–219.

Katsevich, A. I. (1997). Local tomography for the limited-angle problem. *Journal of mathematical analysis and applications*, *213*(1), 160–182.

Kenig, C. E., Sjöstrand, J., & Uhlmann, G. (2007). The Calderón problem with partial data. *Ann. of Math. (2)*, *165*(2), 567–591.

Krishnan, V. P. (2009). A support theorem for the geodesic ray transform on functions. *J. Fourier Anal. Appl.*, *15*(4), 515–520. Retrieved from http://dx.doi.org/10.1007/s00041-009-9061-5 doi: 10.1007/s00041-009-9061-5

Krishnan, V. P., & Stefanov, P. (2009). A support theorem for the geodesic ray transform of symmetric tensor fields. *Inverse Probl. Imaging*, *3*(3), 453–464. Retrieved from http://dx.doi.org/10.3934/ipi.2009.3.453 doi: 10.3934/ipi.2009.3.453

Krupchyk, K., Lassas, M., & Uhlmann, G. (2012). Determining a first order perturbation of the biharmonic operator by partial boundary measurements. *Journal of Functional Analysis*, *262*(4), 1781–1801.

Kyrychko, Y. N., Blyuss, K. B., Gonzalez-Buelga, A., Hogan, S. J., & Webb, D. J. (2006). Real-time dynamic substructuring in a coupled oscillator-pendulum system. Retrieved from http://dx.doi.org/10.1098/rspa.2005.1624 doi: 10.1098/rspa.2005.1624

Lassas, M., Oksanen, L., Stefanov, P., & Uhlmann, G. (2018). On the Inverse Problem of Finding Cosmic Strings and Other Topological Defects. *Comm. Math. Phys.*, *357*(2), 569–595. Retrieved from https://doi.org/10.1007/s00220-017-3029-0

Lassas, M., Oksanen, L., Stefanov, P., & Uhlmann, G. (2019). The light ray transform on lorentzian manifolds. *arXiv preprint arXiv:1907.02210*.

Louisell, J. (2001). A matrix method for determining the imaginary axis eigenvalues of a delay system. *IEEE Transactions on Automatic Control*, *46*(12), 2008–2012. doi: 10.1109/9.975510

Maghareh, A., Dyke, S., Rabieniaharatbar, S., & Prakash, A. (2017). Predictive stability indicator: a novel approach to configuring a real-time hybrid simulation. *Earthquake Engineering & Structural Dynamics*, *46*(1), 95–116.

Maghareh, A., Dyke, S. J., Prakash, A., & Bunting, G. B. (2014, dec). Establishing a predictive performance indicator for real-time hybrid simulation. *Earthquake Engineering and Structural Dynamics*, *43*(15), 2299–2318. Retrieved from http://doi.wiley.com/10.1002/eqe.2448 doi: 10.1002/eqe.2448

Maghareh, A., Dyke, S. J., Prakash, A., & Rhoads, J. F. (2013). *Establishing Predictive Indicators for Stability and Performance of SDOF Real-time Hybrid Simulations* (Tech. Rep.). West Lafayette, IN: IISL.

Maghareh, A., Dyke, S. J., Prakash, A., & Rhoads, J. F. (2014). Establishing a stability switch criterion for effective implementation of real-time hybrid simulation. *Smart Structures and Systems*, *14*(6), 1221–1245. Retrieved from http://koreascience.or.kr/journal/view.jsp?kj=KJKHFZ{\&}py=2014{\&}vnc=v14n6{\&}sp=1221 doi: 10.12989/sss.2014.14.6.1221

Mahin, S. A., Shing, P. B., Thewalt, C. R., & Hanson, R. D. (1989, aug). Pseudodynamic Test Method—Current Status and Future Directions. *Journal of Structural Engineering*, *115*(8), 2113–2128. doi: 10.1061/(ASCE)0733-9445(1989)115:8(2113)

Marshall, J. E., Gorecki, H., Korytowski, A., & Walton, K. (1992). *Time-Delay Systems: Stability and Performance Criteria With Applications*. New York: Ellis Horwood.

Melrose, R. B. (1994). Spectral and scattering theory for the Laplacian on asymptotically Euclidian spaces. In *Spectral and scattering theory (Sanda, 1992)* (Vol. 161, pp. 85–130). Dekker, New York.

Mercan, O., & Ricles, J. M. (2008, aug). Stability analysis for real-time pseudodynamic and hybrid pseudodynamic testing with multiple sources of delay. *Earthquake Engineering & Structural Dynamics*, *37*(10), 1269–1293. Retrieved from http://doi.wiley.com/10.1002/eqe.814 doi: 10.1002/eqe.814

Mercan, O., & Ricles, J. M. (2009). *Experimental Studies on Real-Time Testing of Structures with Elastomeric Dampers* (Vol. 135) (No. 9). doi: 10.1061/(ASCE)0733-9445(2009)135:9(1124)

Montalto, C. (2014). Stable determination of a simple metric, a covector field and a potential from the hyperbolic Dirichlet-to-Neumann map. *Comm. Partial Differential Equations*, *39*(1), 120–145. Retrieved from http://dx.doi.org/10.1080/03605302.2013.843429 doi: 10.1080/03605302.2013.843429

Mueller, A., Griffith, C., Shao, X., & Enyart, G. (2013, apr). A Benchmark Testing System for Real-Time Hybrid Simulation Development. In *Structures congress 2013* (pp. 2370–2381). Reston, VA: American Society of Civil Engineers. Retrieved from http://ascelibrary.org/doi/abs/10.1061/9780784412848.207 doi: 10.1061/9780784412848.207

Nakamura, G., Sun, Z., & Uhlmann, G. (1995). Global identifiability for an inverse problem for the schrödinger equation in a magnetic field. *Mathematische Annalen*, *303*(1), 377–388.

Nakata, N., & Stehman, M. (2014, apr). Substructure Shake Table Testing with Force Controlled Actuators. In *Structures congress 2014* (pp. 1197–1208). Reston, VA: American Society of Civil Engineers. Retrieved from http://ascelibrary.org/doi/abs/10.1061/9780784413357.108 doi: 10.1061/9780784413357.108

Natterer, F. (1986). *The mathematics of computerized tomography*. Stuttgart: B. G. Teubner.

Ou, G., Ozdagli, A. I., Dyke, S. J., & Wu, B. (2015, mar). Robust integrated actuator control: experimental verification and real-time hybrid-simulation implementation. *Earthquake Engineering & Structural Dynamics*, *44*(3), 441–460. Retrieved from http://doi.wiley.com/10.1002/eqe.2479 doi: 10.1002/eqe.2479

Paternain, G. P., Salo, M., & Uhlmann, G. (2013). Tensor tomography on surfaces. *Invent. Math.*, *193*(1), 229–247. Retrieved from http://dx.doi.org/10.1007/s00222-012-0432-1 doi: 10.1007/s00222-012-0432-1

Pausader, B. (2010). Scattering for the defocusing beam equation in low dimensions. *Indiana University mathematics journal*, 791–822.

Peetre, J. (1959). Une caractérisation abstraite des opérateurs différentiels. *Mathematica scandinavica*, 211–218.

Pestov, L., & Uhlmann, G. (2005). Two dimensional compact simple Riemannian manifolds are boundary distance rigid. *Ann. of Math. (2)*, *161*(2), 1093–1110.

Phillips, B. M. (2012). Model-based Feedforward-feedback Control for Real-time Hybrid Simulation of Large-scale Structures. Retrieved from http://hdl.handle.net/2142/31052

Phillips, B. M., & Spencer, B. F. (2013, feb). Model-Based Multiactuator Control for Real-Time Hybrid Simulation. *Journal of Engineering Mechanics*, *139*(2), 219–228. Retrieved from http://ascelibrary.org/doi/10.1061/{\%}28ASCE{\%}29EM.1943-7889.0000493 doi: 10.1061/(ASCE)EM.1943-7889.0000493

Phillips, B. M., Takada, S., Spencer, B. F., & Fujino, Y. (2014). Feedforward actuator controller development using the backward-difference method for real-time hybrid simulation. *Smart Structures and Systems*, *14*(6), 1081–1103. Retrieved from http://koreascience.or.kr/journal/view.jsp?kj=KJKHFZ{\&}py=2014{\&}vnc=v14n6{\&}sp=1081 doi: 10.12989/sss.2014.14.6.1081

Quinto, E. T. (1993). Real analytic radon transforms on rank one symmetric spaces. *Proceedings of the American Mathematical Society*, *117*(1), 179–186.

RabieniaHaratbar, S. (2018). Support theorem for the light-ray transform of vector fields on minkowski spaces. *Inverse Problems & Imaging*, *12*(2), 293.

Rabieniaharatbar, S. (2019). Inverse scattering and stability estimates for the biharmonic operator.

RabieniaHaratbar, S. (2019). Invertibility and stability for a generic class of radon transforms with application to dynamic operators. *Journal of Inverse and Ill-posed Problems*, *27*(4), 469–486.

Ramm, A. G., & Rakesh. (1991). Property *C* and an inverse problem for a hyperbolic equation. *J. Math. Anal. Appl.*, *156*(1), 209–219. Retrieved from http://dx.doi.org/10.1016/0022-247X(91)90391-C doi: 10.1016/0022-247X(91)90391-C

Ramm, A. G., & Sjöstrand, J. (1991). An inverse problem of the wave equation. *Math. Z.*, *206*(1), 119–130. Retrieved from http://dx.doi.org/10.1007/BF02571330 doi: 10.1007/BF02571330

Roux, S., Desbat, L., Koenig, A., & Grangeat, P. (2004). Exact reconstruction in 2d dynamic ct: compensation of time-dependent affine deformations. *Physics in Medicine & Biology*, *49*(11), 2169.

Salazar, R. (2013). Determination of time-dependent coefficients for a hyperbolic inverse problem. *Inverse Problems*, *29*(9), 095015, 17. Retrieved from http://dx.doi.org/10.1088/0266-5611/29/9/095015 doi: 10.1088/0266-5611/29/9/095015

Saouma, V., Haussmann, G., Kang, D., Ghannoum, W., & Asce, A. M. (2013). Real-Time Hybrid Simulation of a Nonductile Reinforced Concrete Frame. *Journal of Structural Engineering*, 1–12. doi: 10.1061/(ASCE)ST

Sato, M. (1969). Hyperfunctions and partial differential equations. In *Proc. int. conf. on functional analysis, tokyo* (Vol. 9).

Sato, M., Kawai, T., & Kashiwara, M. (1973). Microfunctions and pseudo-differential equations. In *Hyperfunctions and pseudo-differential equations (proc. conf., katata, 1971; dedicated to the memory of andré martineau)* (pp. 265–529. Lecture Notes in Math., Vol. 287). Berlin: Springer.

Serov, V. (2017). *Fourier series, fourier transform and their applications to mathematical physics*. Springer.

Shao, X., Reinhorn, A. M., & Sivaselvan, M. V. (2011). *Real-Time Hybrid Simulation Using Shake Tables and Dynamic Actuators* (Vol. 137) (No. 7). doi: 10.1061/(ASCE)ST.1943-541X.0000314

Sharafutdinov, V. A. (n.d.). Integral geometry of tensor fields, inverse and ill-posed problems series, vsp, utrecht, 1994. *MR 97h*, *53077*.

Sharafutdinov, V. A. (1994). *Integral geometry of tensor fields*. Utrecht: VSP.

Shing, P. B., Nakashima, M., & Bursi, O. S. (1996). Application of Psuedodynamic Test Method to Structural Research. *Earthquake Spectra*, *12(1)*, 29–56.

Sjöstrand, J. (1982). Singularités analytiques microlocales. In *Astérisque, 95* (Vol. 95, pp. 1–166). Paris: Soc. Math. France.

Stefanov, P. (1989). Uniqueness of the multi-dimensional inverse scattering problem for time dependent potentials. *Math. Z.*, *201*(4), 541–559.

Stefanov, P. (2017). Support theorems for the light ray transform on analytic Lorentzian manifolds. *Proc. Amer. Math. Soc.*, *145*(3), 1259–1274. Retrieved from http://dx.doi.org/10.1090/proc/13117 doi: 10.1090/proc/13117

Stefanov, P., & Uhlmann, G. (2004). Stability estimates for the X-ray transform of tensor fields and boundary rigidity. *Duke Math. J.*, *123*(3), 445–467. doi: 10.1215/S0012-7094-04-12332-2

Stefanov, P., & Uhlmann, G. (2005). Boundary rigidity and stability for generic simple metrics. *J. Amer. Math. Soc.*, *18*(4), 975–1003. doi: 10.1090/S0894-0347-05-00494-7

Stefanov, P., & Uhlmann, G. (2008). Integral geometry on tensor fields on a class of non-simple Riemannian manifolds. *Amer. J. Math.*, *130*(1), 239–268. doi: 10.1353/ajm.2008.0003

Stefanov, P., & Yang, Y. (2018). The inverse problem for the dirichlet-to-neumann map on lorentzian manifolds. *Analysis & PDE*, *11*(6), 1381–1414.

Stefanov, P. D. (1989). Uniqueness of the multi-dimensional inverse scattering problem for time dependent potentials. *Mathematische Zeitschrift*, *201*(4), 541–559.

Sun, Z. Q. (1993). An inverse boundary value problem for schrödinger operators with vector potentials. *Transactions of the American Mathematical Society*, *338*(2), 953–969.

Takanashi, K., & Nakashima, M. (1987, jul). Japanese Activities on On-Line Testing. *Journal of Engineering Mechanics*, *113*(7), 1014–1032. doi: 10.1061/(ASCE)0733-9399(1987)113:7(1014)

Taylor, M. E. (1981). *Pseudodifferential operators* (Vol. 34). Princeton, N.J.: Princeton University Press.

Trèves, F. (1980). *Introduction to pseudodifferential and Fourier integral operators. Vol. 1*. New York: Plenum Press. (Pseudodifferential operators, The University Series in Mathematics)

Tyni, T., & Harju, M. (2017). Inverse backscattering problem for perturbations of biharmonic operator. *Inverse Problems*, *33*(10), 105002.

Tyni, T., & Serov, V. (2017). Scattering problems for perturbations of the multidimensional biharmonic operator. *Inverse Problems & Imaging*, *12*(1), 205.

Uhlmann, G., & Vasy, A. (2016a). The inverse problem for the local geodesic ray transform. *Invent. Math.*, *205*(1), 83–120. Retrieved from `https://doi.org/10.1007/s00222-015-0631-7`

Uhlmann, G., & Vasy, A. (2016b). The inverse problem for the local geodesic ray transform. *Inventiones mathematicae*, *205*(1), 83–120.

Wallace, M. I., Sieber, J., Neild, S. A., Wagg, D. J., & Krauskopf, B. (2005, dec). Stability Analysis of Real-time Dynamic Substructuring Using Delay Differential Equation Models. *Earthquake Engineering & Structural Dynamics*, *34*(15), 1817–1832. doi: 10.1002/eqe.513

Waters, A. (2014). Stable determination of X-Ray transforms of time dependent potentials from partial boundary data. *Comm. Partial Differential Equations*, *39*(12), 2169–2197.

Waters, A., & Salazar, R. (2013). Global stability for time dependent X-ray transforms on simple manifolds and applications. *arXiv:1311.1591*.

Zhu, F., Wang, J., Jin, F., Chi, F., & Gui, Y. (2015). Stability analysis of MDOF real-time dynamic hybrid testing systems using the discrete-time root locus technique. *Earthquake Engineering & Structural Dynamics*, *44*(2), 221–241. Retrieved from `http://doi.wiley.com/10.1002/eqe.2467` doi: 10.1002/eqe.2467